MAX-PLANCK-INSTITUT FÜR PLASMAPHYSIK

GARCHING BEI MÜNCHEN

DATA ON LOW ENERGY LIGHT ION SPUTTERING

J. Roth, J. Bohdansky, W. Ottenberger

IPP 9/26 May 1979

Die nachstehende Arbeit wurde im Rahmen des Vertrages zwischen dem Max-Planck-Institut für Plasmaphysik und der Europäischen Atomgemeinschaft über die Zusammenarbeit auf dem Gebiete der Plasmaphysik durchgeführt.

IPP 9/26

J. Roth,
J. Bohdansky,
W. Ottenberger

Data on Low Energy Light Ion Sputtering

May, 1979

ABSTRACT

Sputtering yield data for light ions H, D, and He in the energy range of 60 to 8000 keV are presented for 13 different elements and 13 compounds. Data for heavier projectile ions are given for Ni and W.

For normal incidence the energy dependence of the sputtering solid for all materials can be normalised and an empirical universal sputtering formula describes the measured data within a factor of 2.

For the materials Au, Mo, Ni, W and TaC the dependence of the sputtering yield of the angle of incidence has been measured. The distribution of sputtered particles is given for Ni, W and TaC for different angles of incidence.

CONTENT

PAGE

INTRODUCTION 1

EXPERIMENTAL 2

RESULTS 5

1) Energy dependence of the sputtering yield for normal incidence 5

Elements 5 - 35
Compounds 36 - 61

2) Angular dependence of the sputtering yield 63

3) Angular distribution of the sputtered particles 74

DISCUSSION 82

REFERENCE 90

INTRODUCTION

This report describes the results on light ion sputtering of a variety of materials at energies between 50 eV and 50 keV obtained in the years 1974 to 1978. In this energy range very little data on sputtering was available for helium and hydrogen isotopes. There was, however, an urgent need for these data as impurity problems in fusion research became important and one main impurity source was supposed to be sputtering. Some data obtained for heavy ions and selfsputtering are also included.

Most of the data presented have been published in condensed form in a variety of journals and conference proceedings but it was felt that a complete presentation of these data may be helpful. In the course of the work, many scientists have contributed and will be quoted in the list of original publications.

The data are presented in three different forms:

1) The bulk of the data is presented as sputtering yield versus energy of the sputtering ions at normal incidence. The data for elemental materials are listed in alphabetic order. Separated from the elemental materials are also data for different compounds as carbides and oxides are listed again alphabetically. In addition to tables the results are presented in graphical form.

2) The angular dependence of the sputtering yield is given for a small number of material. The data are plotted as sputtering yield versus the angle of incidence with the energy of the sputtering ions as parameter. Again tables are added for convenience.

3) The angular distribution of the sputtered particles is also given for some materials. The data are presented in a polar plot as sputtering yield per steradian versus angle of emergence of the sputtered particles. The angle of incidence of the ion beam and the ion energy are parameters.

The data for normal incidence for the different materials are compared. The observed similarities at lower ion energy are used to deduce an empirical formula for the energy dependence of the sputtering yield in this energy regime. The plots for normal incidence show curves obtained from this formula to extrapolate the data to near threshold energies. No comparison of the presented data obtained during the course of this work with published results of other groups will be made.

Before presenting the results, the experimental set up will be discussed shortly.

EXPERIMENTAL

Most of the measurements were performed on a 15 keV ion accelerator, which has been described in /1/. A schematic of the main features is shown in fig. 1. A high current injector /2/ of the Oak Ridge type was used as an ion source. The central part of this beam was magnetically analysed and entered a viton sealed stainless steel target chamber. As the ion source operates at rather high gas pressure ($\sim 10^{-1}$ Torr) effective differential pumping is necessary to prevent excessive neutralization of the beam as well as a high partial pressure of the working gas in the target chamber. The differential pumping stage was therefore equipped with a turbomolecular pump (LEYBOLD 500) together with a roots pump (LEYBOLD Z 05). The pressure in the differential pumping stage was about 8×10^{-5} Torr. The target chamber was evacuated by a turbomolecular pump with 400 l/sec pumping speed. A pressure $< 10^{-7}$ Torr could be reached. During bombardment it rose to $2\text{-}3 \times 10^{-6}$ Torr, mainly due to the partial pressure of the working gas.

At extraction voltages below 2 keV the current density falls rapidly causing inconveniently long irradiation times. Therefore, in the cases of low energy irradiation, a 4 keV ion beam was extracted from the ion source and magnetically analyzed. Directly in front of the target the beam passed through a collimator system and was decellerated by a positive target bias (Fig. 1). This collimeter system has been described in more detail in /3/ as well as difficulties arising from neutral particles, which are not decelerated by this retarding field. As the neutralized fraction of the beam is very important at low energies, where the sputtering yield by the ions is strongly decreased, it has been measured carefully /3, 4/ to 2.6, 1.3 and 1.6 % for 4 keV He^+, D_3^+ and H_3^+ ion beams respectively. The presented data have been corrected for the amount sputtered by the 4 keV neutrals.

The amount of sputtered material was determined by the weight loss of the target measured by a Mettler ME 22 microbalance with a sensitivity < 1 μg. The weight loss Δm was usually 30 - 100 μg. The weight change due to the implanted ions has been neglected in determining the sputtering yield. The yield has been calculated using the equation

$$Y = \frac{\Delta m}{M_2 N_1} N_o \qquad (1)$$

where N_o is avogadro's number, M_2 the atomic weight of the target atoms and N_1 the total number of incoming ions. For selfsputtering, however, the implanted ions are identical with the target atoms and have been taken into account /6/. Hence the self-sputtering yields were calculated from

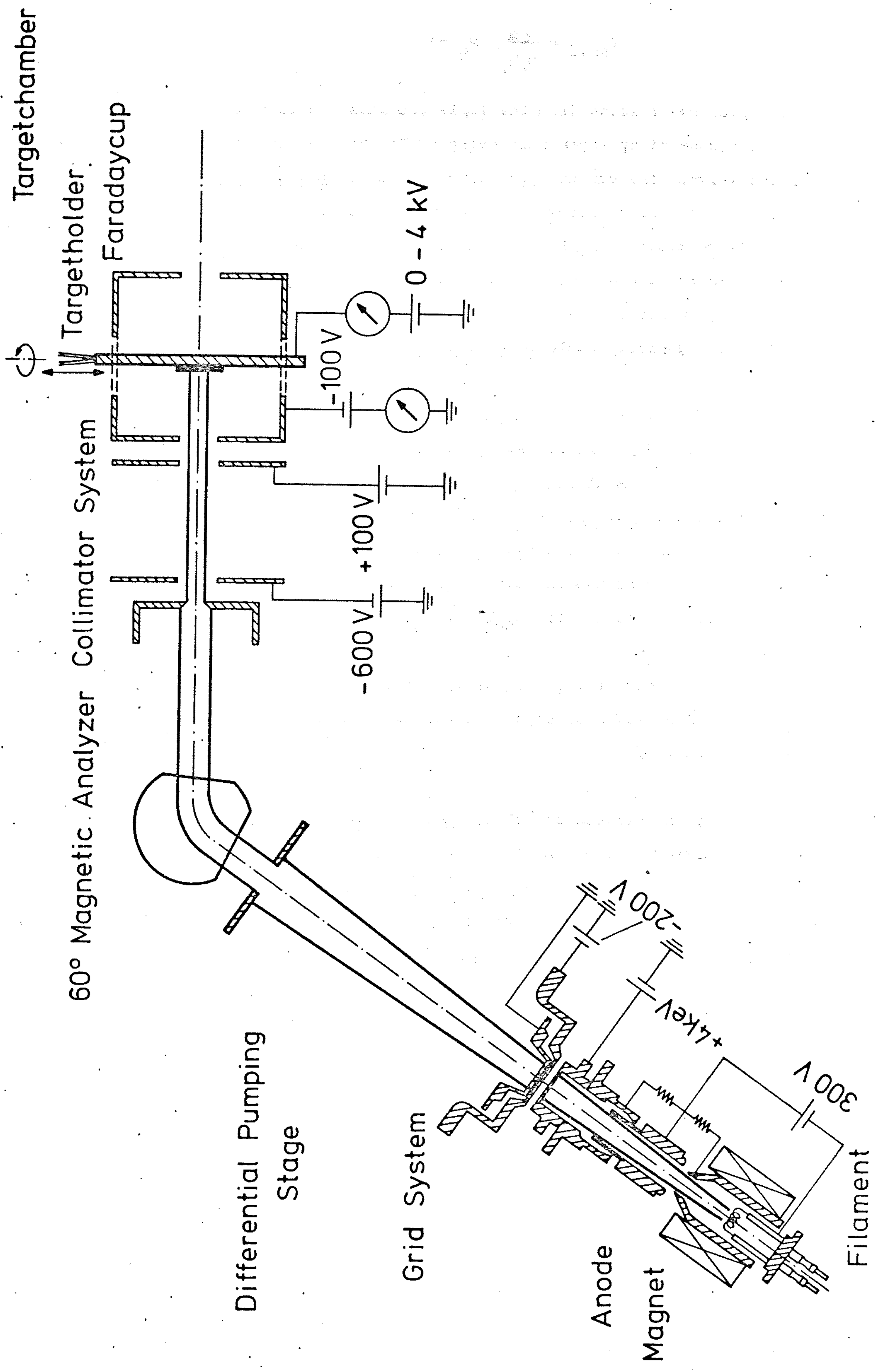

Fig. 1: Experimental set up

$$Y_{self} = \frac{\Delta m}{M_2 N_i} N_o - 1 \qquad (2)$$

The problems arising from the implanted ions has been discussed in /1/ and /3/. In the case of hydrogen sputtering of Ta the trapped amount of hydrogen exceeds the weight loss due to sputtering at room temperature. Therefore these measurements have been performed at 400° C, where it is known, that all trapped hydrogen is reemitted /5/. For Ti and Zr the sputtered particles have been collected on a Si collector and analysed with Rutherford backscattering. By comparison with He sputtering, where the weight loss can be used to measure the sputtering yield, the collection geometry could be calibrated.

A similar collection method has been used to determine the angular distribution of sputtered particles. The particles were collected on an organic foil, which had about 2000 Å Al film evaporated. The collector was analysed with RBS or nuclear reaction techniques /7,8/. To obtain absolute data the method has been calibrated assuming that at normal incidence the observed distributions has a rotational symmetry around the beam direction. The method is described in /32/. The angular resolution was limited by the size of the beamspot and was about ± 5°.

For measurements at energies above 8 keV the 150 keV ion accelerator PHARAO was used /9/. A 20 keV mass separator was used to determine the sputtering yield by heavier ions /10/.

Routinely the surface structure of the samples before and after sputtering have been observed in the SEM /11/. Typical surface structures are normally shown in the original publications. As in no case, neither for normal nor for grazing incidence, an influence of the surface structure on the yield data could be found, no SEM micrographs are presented here.

RESULT

1.) Energy dependence of the sputtering yield for normal incidence.

Data for the sputtering yield versus ion energy is given for the following ion target combinations.

Table I

elements	H	D	^{3}He	^{4}He	O	Ne	Ar	Ni	Kr	Xe
Al	x	x		x						
Au	x	x	x	x						
Be	x	x		x						
C	x	x		x						
Fe	x	x		x						
Mo	x	x	x	x						
Ni	x	x		x	x	x	x	x	x	x
Si	x	x		x						
Ta	x	x		x						
Ti	x			x						
V	x			x						
W	x	x		x	x	x	x		x	x
Zr	x			x						
compounds										
Al_2O_3	x	x		x						
B_4C	x	x		x						
BeO	x	x		x						
Ni-alloys	x	x		x						
SAP	x	x		x						
SiC	x	x		x						
SiO_2	x	x		x						
SS	x	x		x						
TaC	x	x		x						
Ta_2O_5	x	x		x						
TiC	x	x		x						
WC	x	x		x						
ZrC	x	x		x						

These results are presented in Figs.2-27 and table 2 to 27. References to the original publications are given in the figure captions.

Table 2 Al

Energy (eV)	H^+	D^+	$^4He^+$
70		$2.29 \cdot 10^{-3}$	
100		$6.74 \cdot 10^{-3}$	
200	$3.0 \cdot 10^{-3}$	$2.55 \cdot 10^{-2}$	$1.31 \cdot 10^{-1}$
210			$1.74 \cdot 10^{-1}$
300	$6.1 \cdot 10^{-3}$		
500	$6.8 \cdot 10^{-3}$	$3.44 \cdot 10^{-2}$	$2.25 \cdot 10^{-1}$
500			$2.05 \cdot 10^{-1}$
1000	$9.3 \cdot 10^{-3}$	$4.15 \cdot 10^{-2}$	
2000	$1.6 \cdot 10^{-2}$		$1.44 \cdot 10^{-1}$
2000			$1.90 \cdot 10^{-1}$
3000		$2.61 \cdot 10^{-2}$	
4000	$1.13 \cdot 10^{-2}$		
8000	$2.7 \cdot 10^{-3}$	$6.22 \cdot 10^{-3}$	$7.86 \cdot 10^{-2}$

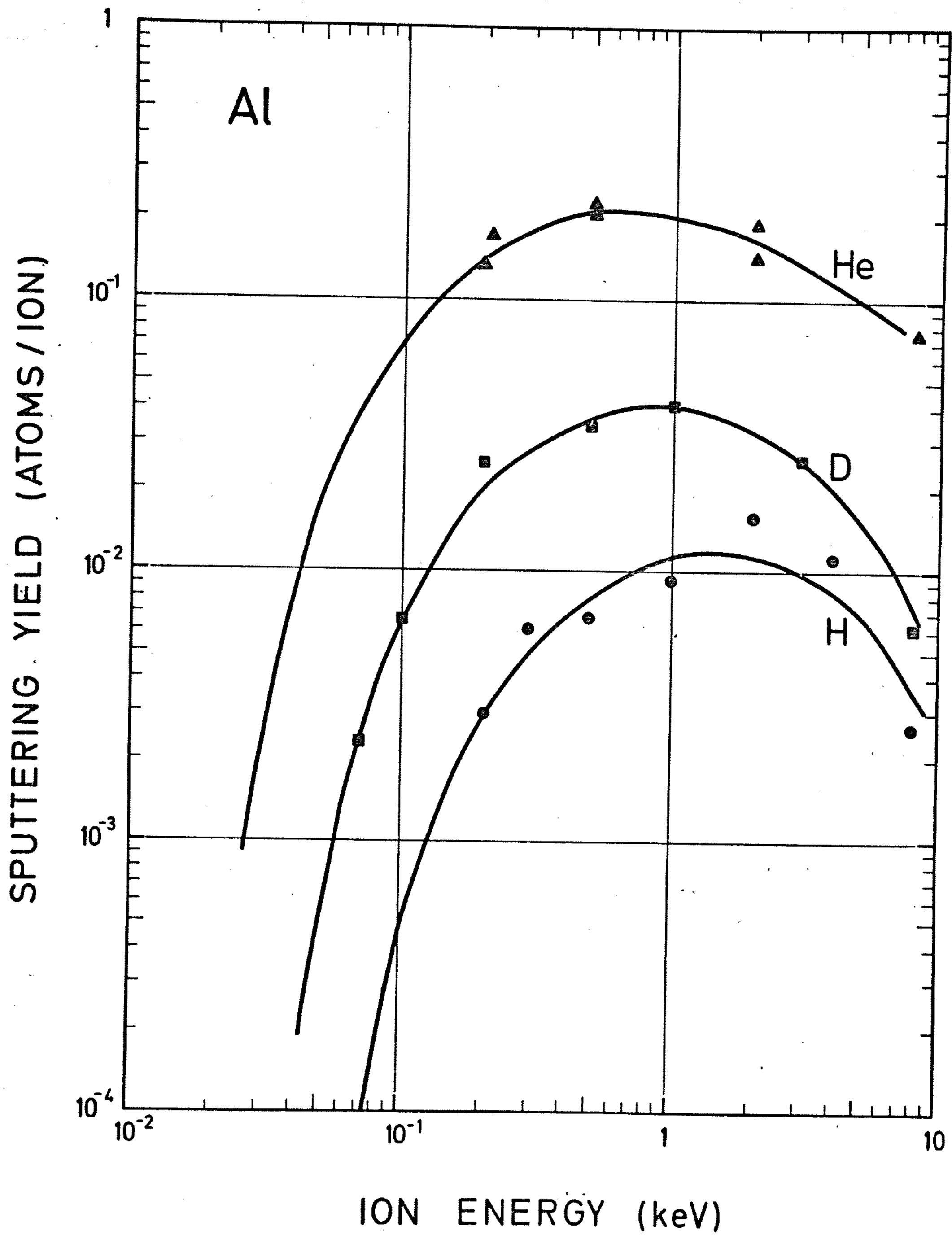

Fig. 2: Energy dependence of the sputtering yield of Al with H, D, He. The solid curves are a fit of the empiric formula eq. (7) to the measured points for energies up to 1 keV. The data will be published /12/. A comparison with fig. 15 shows a strong similarity between Al_2O_3 and Al. This might be due to oxide formation during sputtering of Al.

Table 3 Au

Energy (eV)	Yields H^+	Yields D^+	Yields $^3He^+$	Yields $^4He^+$
110		$1 \cdot 10^{-4}$		
150		$6 \cdot 10^{-4}$		$3.0 \cdot 10^{-2}$
200		$2.3 \cdot 10^{-3}$		
250	$8.0 \cdot 10^{-5}$	$3.9 \cdot 10^{-3}$		$4.8 \cdot 10^{-2}$
300	$3.85 \cdot 10^{-4}$			
400	$7.26 \cdot 10^{-4}$		$4.71 \cdot 10^{-2}$	
500	$1.57 \cdot 10^{-3}$	$1.5 \cdot 10^{-2}$		$9.28 \cdot 10^{-2}$
1000	$7.13 \cdot 10^{-3}$	$3.02 \cdot 10^{-2}$		
1000	$7.27 \cdot 10^{-3}$	$2.66 \cdot 10^{-2}$		$1.45 \cdot 10^{-1}$
1000	$5.77 \cdot 10^{-3}$			
2000	$9.50 \cdot 10^{-3}$	$3.81 \cdot 10^{-2}$	$1.08 \cdot 10^{-1}$	$1.95 \cdot 10^{-1}$
2000	$1.00 \cdot 10^{-2}$			$1.76 \cdot 10^{-1}$
2000	$1.12 \cdot 10^{-2}$			
4000	$1.60 \cdot 10^{-2}$	$4.28 \cdot 10^{-2}$		$1.92 \cdot 10^{-1}$
8000	$1.44 \cdot 10^{-2}$			
8000	$1.76 \cdot 10^{-2}$	$3.97 \cdot 10^{-2}$	$1.28 \cdot 10^{-1}$	$1.66 \cdot 10^{-1}$
8000	$1.36 \cdot 10^{-2}$			
10000	$1.02 \cdot 10^{-2}$			
20000	$8.14 \cdot 10^{-3}$	$2.7 \cdot 10^{-2}$		
20000	$8.68 \cdot 10^{-3}$			
20000	$8.59 \cdot 10^{-3}$			

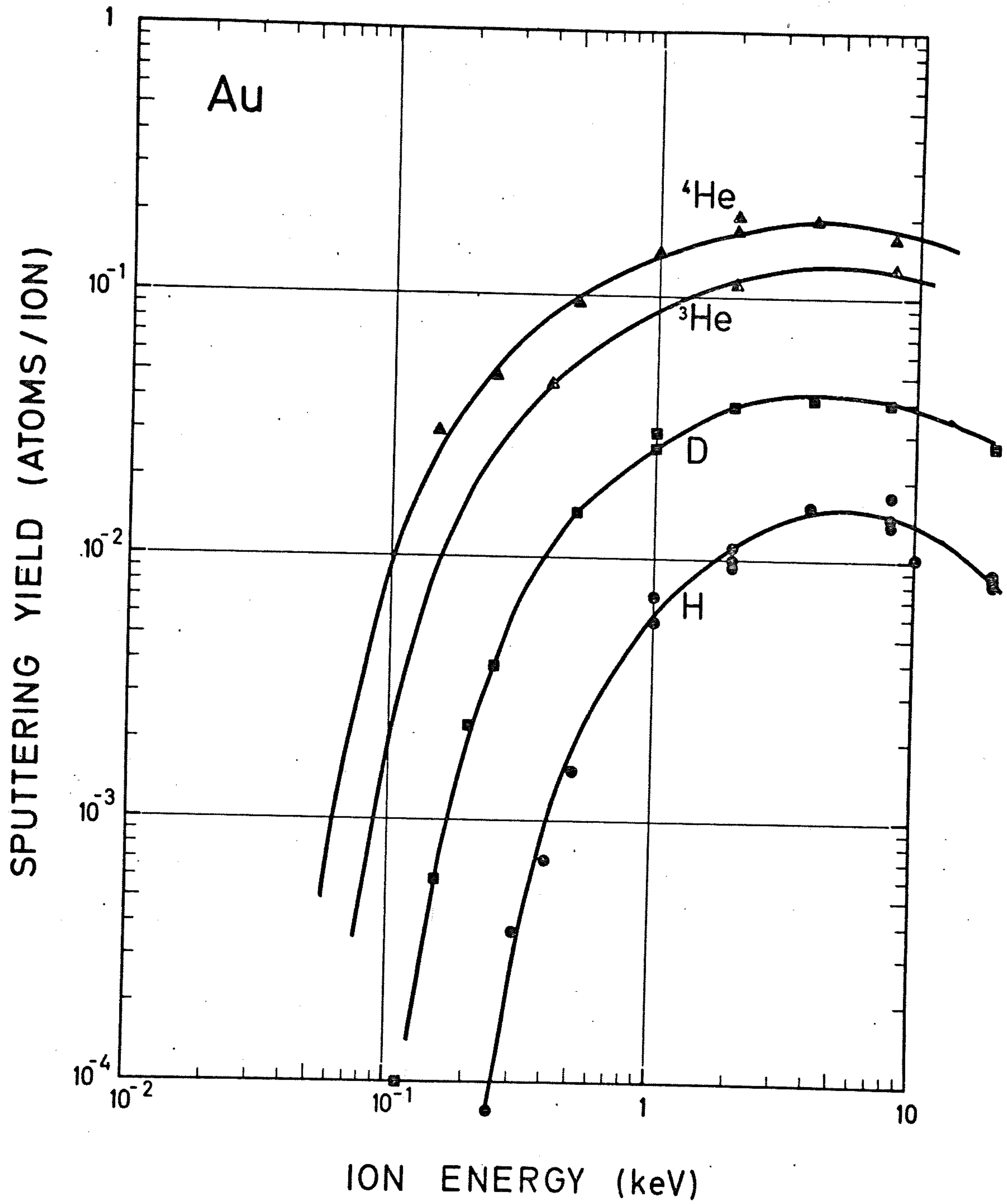

Fig. 3: Energy dependence of the sputtering yield of Au with H, D, ^{3}He and ^{4}He. The solid curves are given by eq. (7) for energies up to 5 keV. The data are partly published in /3/.

Table 4 Be

Energy (eV)	Yields H	D	He
50		$5.8 \cdot 10^{-3}$	
70	$2.06 \cdot 10^{-3}$		
90		$7.2 \cdot 10^{-3}$	
110		$3.9 \cdot 10^{-2}$	
130			$2.8 \cdot 10^{-2}$
150	$3.4 \cdot 10^{-3}$	$1.14 \cdot 10^{-2}$	
150	$3.99 \cdot 10^{-3}$		
250		$1.88 \cdot 10^{-2}$	
300			$5.67 \cdot 10^{-2}$
330	$1.6 \cdot 10^{-2}$	$3.5 \cdot 10^{-2}$	
500			$6.42 \cdot 10^{-2}$
750			$2.04 \cdot 10^{-1}$
1000	$1.82 \cdot 10^{-2}$	$2.8 \cdot 10^{-2}$	
1500			$1.52 \cdot 10^{-1}$
2670	$1.28 \cdot 10^{-2}$	$2.04 \cdot 10^{-2}$	
4000			$8.1 \cdot 10^{-2}$

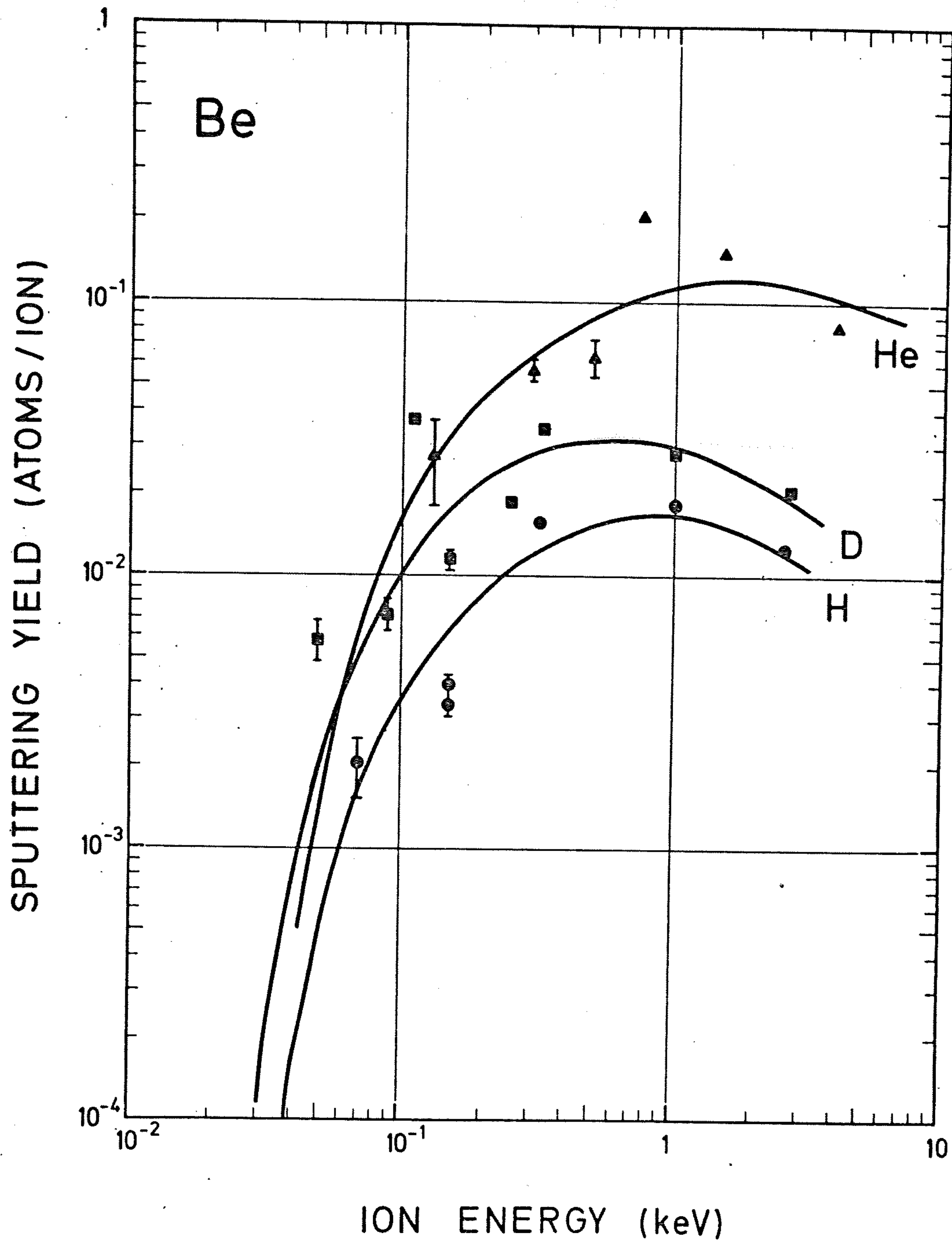

Fig. 4: Energy dependence of the sputtering yield of Be with H, D, ^4He. The solid curves are calculated from eq. (7) to extrapolate to low energies. The data will be published /13/. The similarity of the results with the results obtained for BeO indicates, that possible ion induced oxidation occurred during sputtering.

Table 5 C

Energy (eV)	yields H	D	He
50	$4.75 \cdot 10^{-3}$		
120	$8.61 \cdot 10^{-3}$	$1.78 \cdot 10^{-2}$	
150			$5.69 \cdot 10^{-2}$
250	$9.0 \cdot 10^{-3}$	$2.67 \cdot 10^{-2}$	
330	$9.4 \cdot 10^{-3}$		
360			$8.08 \cdot 10^{-2}$
500		$2.23 \cdot 10^{-2}$	
670	$7.8 \cdot 10^{-3}$		
670	$8.05 \cdot 10^{-3}$		
750			$8.62 \cdot 10^{-2}$
1000	$6.1 \cdot 10^{-3}$	$1.87 \cdot 10^{-2}$	
2000	$4.8 \cdot 10^{-3}$	$1.14 \cdot 10^{-2}$	$7.78 \cdot 10^{-2}$
2000	$4.9 \cdot 10^{-3}$		
2000	$5.6 \cdot 10^{-3}$		
4000	$3.37 \cdot 10^{-3}$	$7.77 \cdot 10^{-3}$	$8.2 \cdot 10^{-2}$
5000			
6000			$7.76 \cdot 10^{-2}$
8000			$6.1 \cdot 10^{-2}$

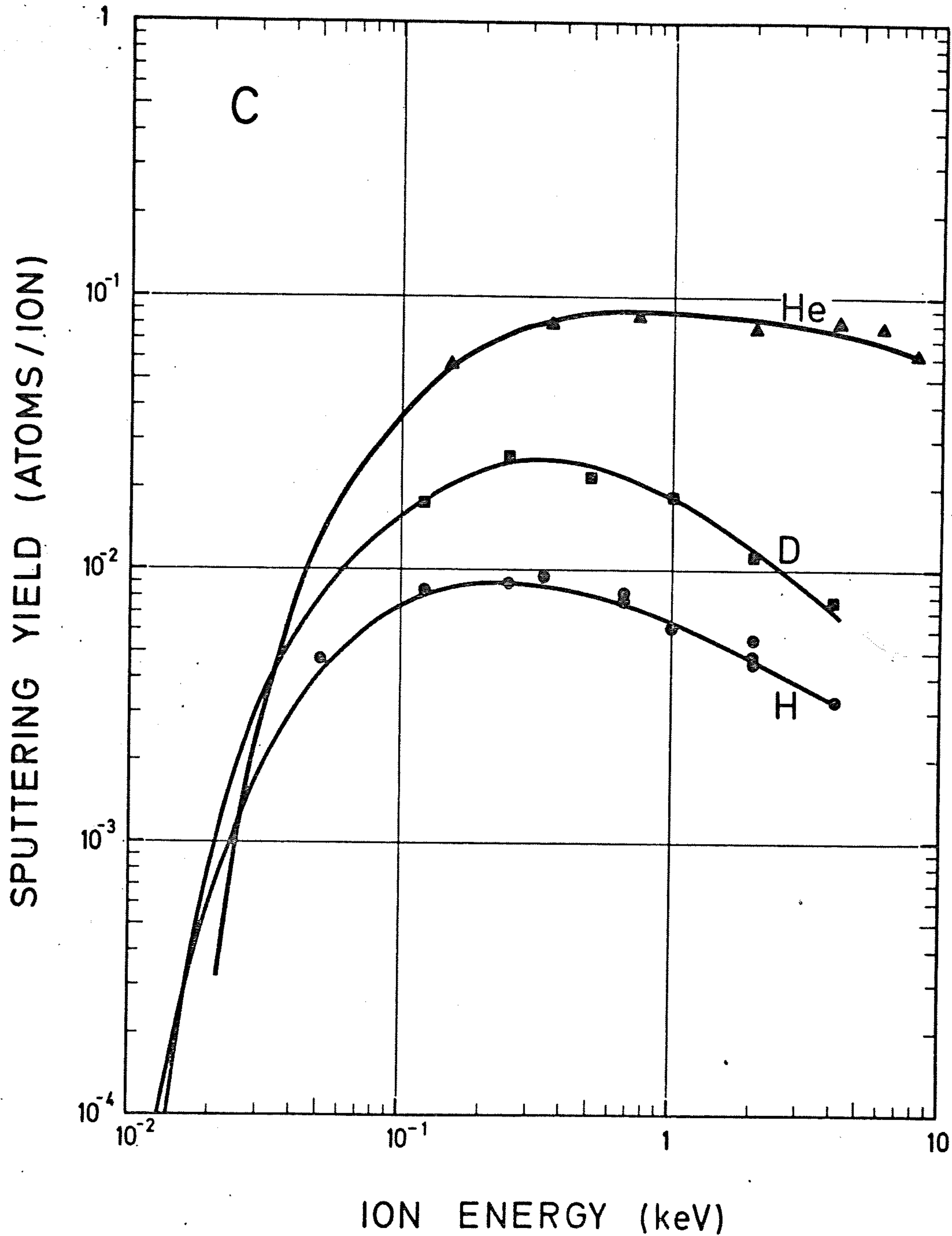

Fig. 5: Energy dependence of the sputtering yield of C with H, D, He. The sputtering yield for different kinds of graphite vary widely /1, 14/ according to their structure and orientation. Here only data for pyrolytic carbon (Union Graphite) are reported. These results are published in /1, 14, 15/. Data reported in /1, 14/ with total weight changes less than 10 μg are omitted. The solid curves are a best fit to the data taking eq. (7) for energies below 300 eV. For sputtering with D and H, an increase of the sputtering yield at elevated temperatures ($\sim$ 500°C) due to chemical effects has been observed and is published in /14/.

Table 6 Fe

Energy (eV)	Yields H	Yields D	Yields He
90		$3.25 \cdot 10^{-3}$	
100	$3.55 \cdot 10^{-4}$		$1.08 \cdot 10^{-2}$
200	$2.75 \cdot 10^{-3}$		
200	$3.4 \cdot 10^{-3}$	$1.58 \cdot 10^{-2}$	$5.1 \cdot 10^{-2}$
240	$4.6 \cdot 10^{-3}$		
300	$6.5 \cdot 10^{-3}$		
380	$8.7 \cdot 10^{-3}$		
500	$1.2 \cdot 10^{-2}$		
500	$1.18 \cdot 10^{-2}$	$3.18 \cdot 10^{-2}$	$1.08 \cdot 10^{-1}$
500	$1.0 \cdot 10^{-2}$		
640	$1.3 \cdot 10^{-2}$		
750	$1.1 \cdot 10^{-2}$		
1000	$1.1 \cdot 10^{-2}$		
1000	$1.4 \cdot 10^{-2}$		
1000	$1.45 \cdot 10^{-2}$		
1350	$1.28 \cdot 10^{-2}$		
2000	$9.2 \cdot 10^{-3}$	$3.69 \cdot 10^{-2}$	$1.75 \cdot 10^{-1}$
2000	$1.06 \cdot 10^{-2}$		
2000	$1.25 \cdot 10^{-2}$		
2000	$1.44 \cdot 10^{-2}$		
2000	$1.57 \cdot 10^{-2}$		
2000	$1.75 \cdot 10^{-2}$		
2700	$1.32 \cdot 10^{-2}$		
3000	$1.62 \cdot 10^{-2}$		
3000	$1.78 \cdot 10^{-2}$		
4000	$1.06 \cdot 10^{-2}$		
4000	$1.5 \cdot 10^{-2}$		
4000	$1.57 \cdot 10^{-2}$		
6000	$1.06 \cdot 10^{-2}$		
8000	$5.6 \cdot 10^{-3}$		
8000	$6.72 \cdot 10^{-3}$	$2.57 \cdot 10^{-2}$	$1.16 \cdot 10^{-1}$
8000	$8.9 \cdot 10^{-3}$		

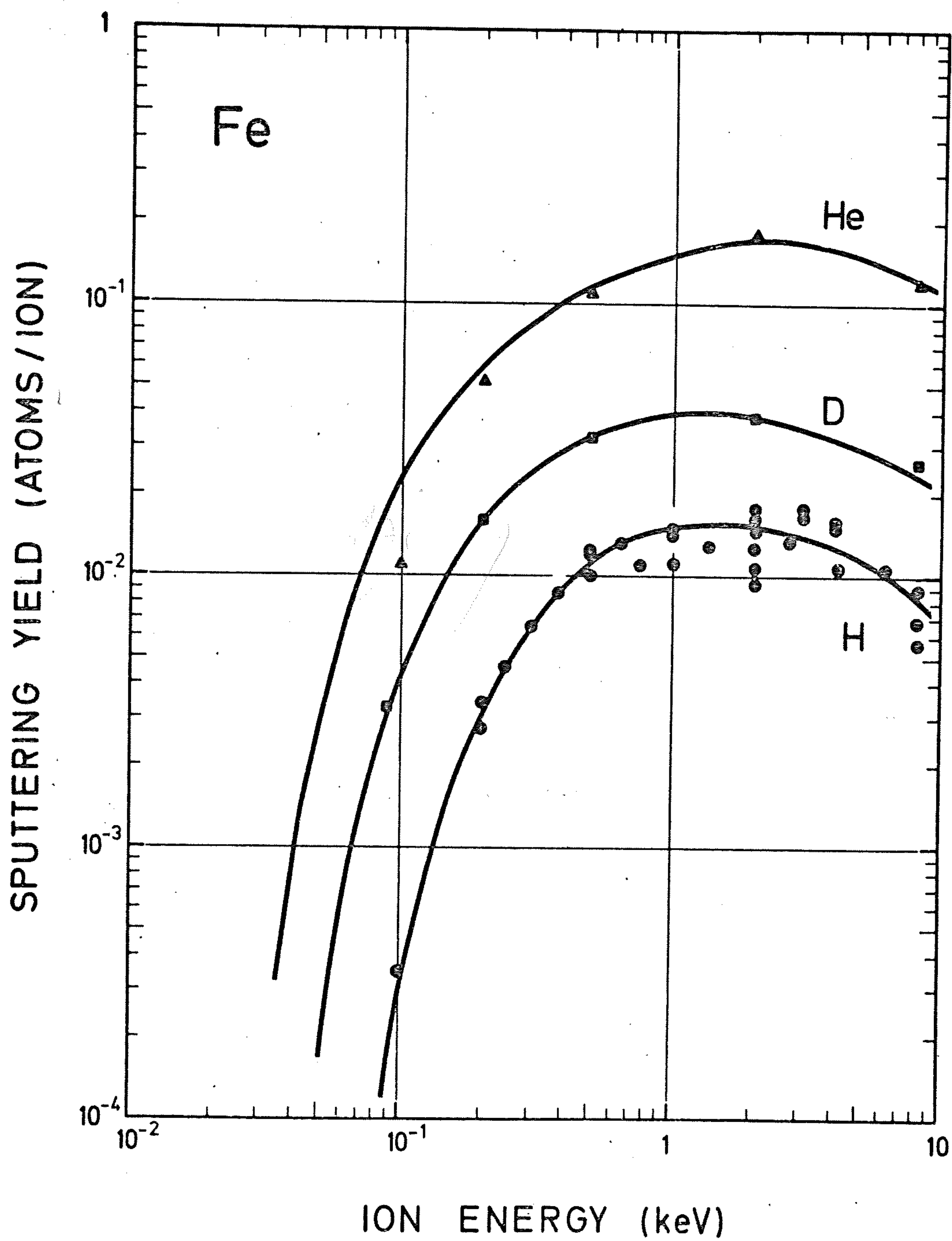

Fig. 6: Energy dependence of the sputtering yield of Fe with H, D and He. The solid curve is a fit to the data using the energy dependence of eq. (7). The data for H have been measured using the Laser fluorescence signal of the sputtered particles. This technique will be published /34/. The data are calibrated using the weight loss method.

Table 7 Mo

Energy (eV)	Yields H	D	^3He	^4He
150		$3 \cdot 10^{-4}$		$1.1 \cdot 10^{-2}$
170				$1.5 \cdot 10^{-2}$
200				$2.15 \cdot 10^{-2}$
250			$9.5 \cdot 10^{-3}$	
300	$9.8 \cdot 10^{-5}$	$1.8 \cdot 10^{-3}$		$2.4 \cdot 10^{-2}$
500	$4.3 \cdot 10^{-4}$	$3.5 \cdot 10^{-3}$	$1.8 \cdot 10^{-2}$	$3.6 \cdot 10^{-2}$
500	$2.8 \cdot 10^{-4}$	$3.55 \cdot 10^{-3}$		
670	$7.8 \cdot 10^{-4}$			
1000	$1.1 \cdot 10^{-3}$	$6.2 \cdot 10^{-3}$	$2.7 \cdot 10^{-2}$	$4.8 \cdot 10^{-2}$
1000		$5.7 \cdot 10^{-3}$		
2000	$2.0 \cdot 10^{-3}$	$7.8 \cdot 10^{-3}$	$3.1 \cdot 10^{-2}$	$5.2 \cdot 10^{-2}$
2000	$2.2 \cdot 10^{-3}$	$8.0 \cdot 10^{-3}$		$3.9 \cdot 10^{-2}$
2000		$9.3 \cdot 10^{-3}$		
4000	$2.1 \cdot 10^{-3}$	$7.7 \cdot 10^{-3}$		$4.9 \cdot 10^{-2}$
4000				$5.65 \cdot 10^{-2}$
6000	$1.8 \cdot 10^{-3}$			$5.2 \cdot 10^{-2}$
6000				$4.3 \cdot 10^{-2}$
8000	$1.7 \cdot 10^{-3}$	$4.8 \cdot 10^{-3}$	$2.5 \cdot 10^{-2}$	$4.2 \cdot 10^{-2}$
9000				$4.1 \cdot 10^{-2}$

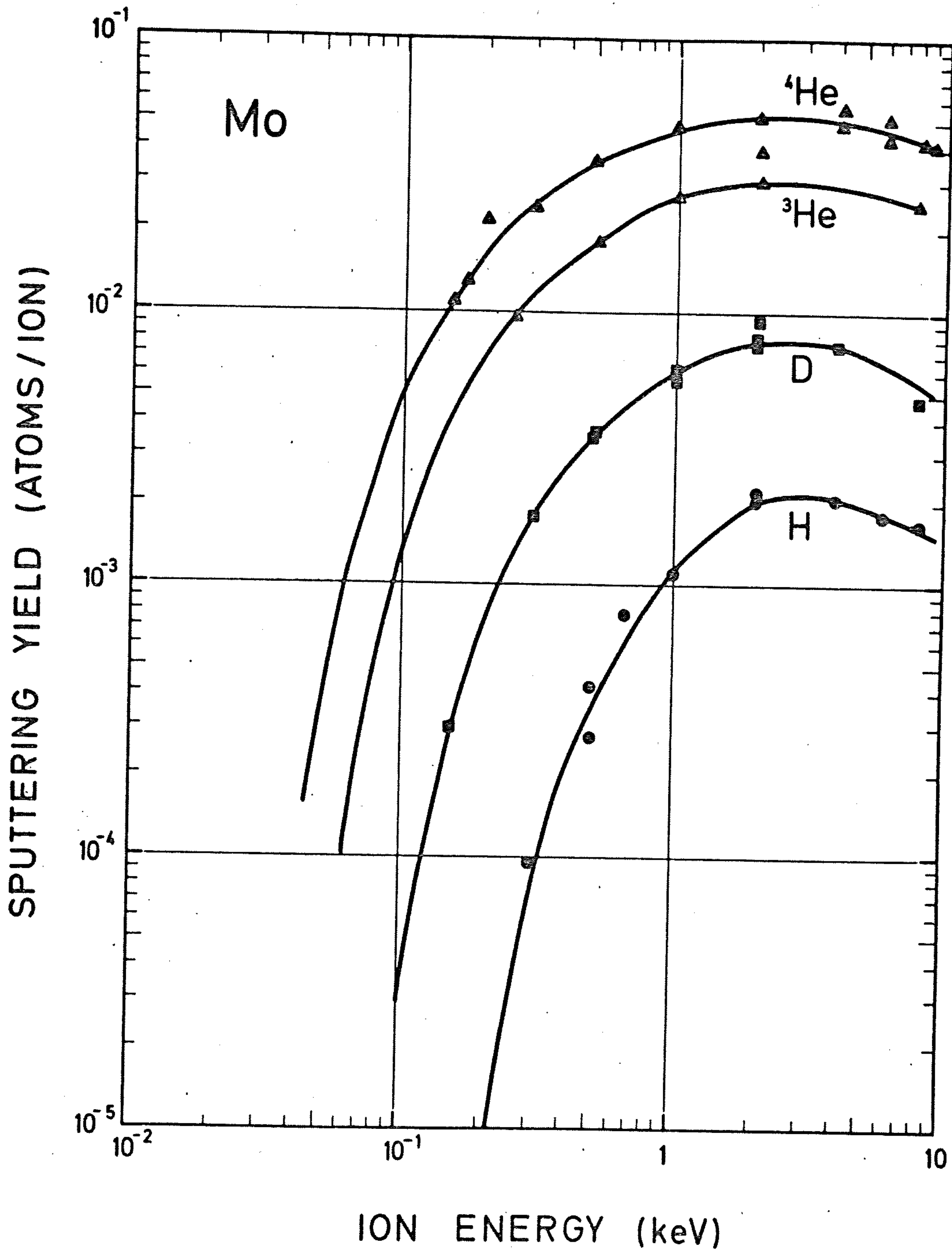

Fig. 7: Energy dependence of the sputtering yield of Mo with H, D, ^{3}He, ^{4}He. Most of the data have been published in /3/. The solid curves are the best fit to the data of the energy dependence in eq. (7).

Table 8 Ni

Energy (eV)	H	D	^{4}He	Ne	O	Ar	Ni	Kr	Xe
75							$8.2 \cdot 10^{-2}$		
80	$3.77 \cdot 10^{-4}$	$4.18 \cdot 10^{-2}$							
100	$8.4 \cdot 10^{-4}$				$2.4 \cdot 10^{-2}$		$1.87 \cdot 10^{-1}$		
120							$2.12 \cdot 10^{-1}$		
150	$2.4 \cdot 10^{-3}$	$1.34 \cdot 10^{-2}$	$8.14 \cdot 10^{-2}$	$4.38 \cdot 10^{-1}$	$6.20 \cdot 10^{-1}$	$4.5 \cdot 10^{-1}$	$3.46 \cdot 10^{-1}$	$2.2 \cdot 10^{-1}$	$2.07 \cdot 10^{-1}$
150							$3.8 \cdot 10^{-1}$		$1.13 \cdot 10^{-1}$
150							$4.04 \cdot 10^{-1}$		$1.28 \cdot 10^{-1}$
200					$1 \cdot 10^{-1}$		$5.7 \cdot 10^{-1}$		
200							$5.02 \cdot 10^{-1}$		
250	$5.33 \cdot 10^{-3}$	$2.58 \cdot 10^{-2}$	$1.25 \cdot 10^{-1}$						
300							$6.8 \cdot 10^{-1}$		
300							$7.4 \cdot 10^{-1}$		
350					$1.7 \cdot 10^{-1}$		$7.56 \cdot 10^{-1}$		
400							$8.6 \cdot 10^{-1}$		
450							1.00		
500	$1.13 \cdot 10^{-2}$		$1.16 \cdot 10^{-1}$		$2 \cdot 10^{-1}$		1.04		
500			$1.74 \cdot 10^{-1}$		$2.8 \cdot 10^{-1}$		1.11		
600				$9.7 \cdot 10^{-1}$		1.33	1.25	1.19	$8.9 \cdot 10^{-1}$
600						1.40			
800		$4.18 \cdot 10^{-2}$							
1000	$1.36 \cdot 10^{-2}$	$4.25 \cdot 10^{-2}$	$1.08 \cdot 10^{-1}$		$3.6 \cdot 10^{-1}$		1.72		
1000	$1.48 \cdot 10^{-2}$		$1.44 \cdot 10^{-1}$						
1000	$1.69 \cdot 10^{-2}$		$2.04 \cdot 10^{-1}$						
1000	$1.55 \cdot 10^{-2}$		$1.76 \cdot 10^{-1}$						
1000			$1.70 \cdot 10^{-1}$						
1000			$1.67 \cdot 10^{-1}$						
1000			$1.80 \cdot 10^{-1}$						
2000	$1.38 \cdot 10^{-2}$	$4.02 \cdot 10^{-2}$	$1.96 \cdot 10^{-1}$						
2000			$2.14 \cdot 10^{-1}$						
3000				1.67	$5.8 \cdot 10^{-1}$	2.56	3.02	3.07	3.07
3000						2.45			
4000	$1.22 \cdot 10^{-2}$	$3 \cdot 10^{-2}$	$1.97 \cdot 10^{-1}$						
4000	$1.36 \cdot 10^{-2}$		$2.08 \cdot 10^{-1}$						
4000			$1.8 \cdot 10^{-1}$						
5000			$1.9 \cdot 10^{-1}$						
8000	$8.22 \cdot 10^{-3}$	$2.28 \cdot 10^{-2}$	$1.73 \cdot 10^{-1}$						

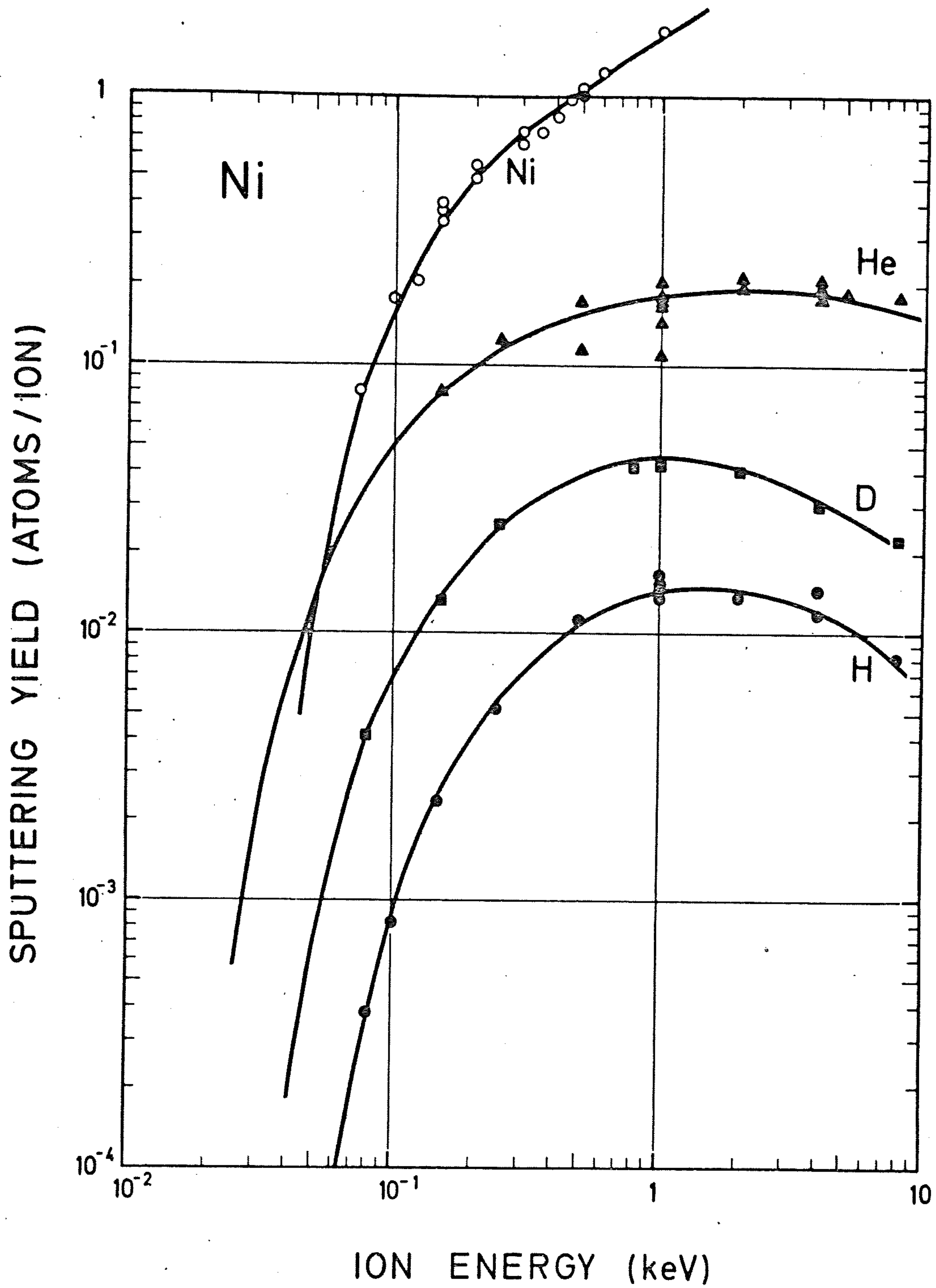

Fig. 8a: Energy dependence of the sputtering yield of Ni with H, D, He and Ni. The solid curves are fits to the experimental points taking the energy dependence of eq. (7).
The data are mostly published in /16/ and /6/.

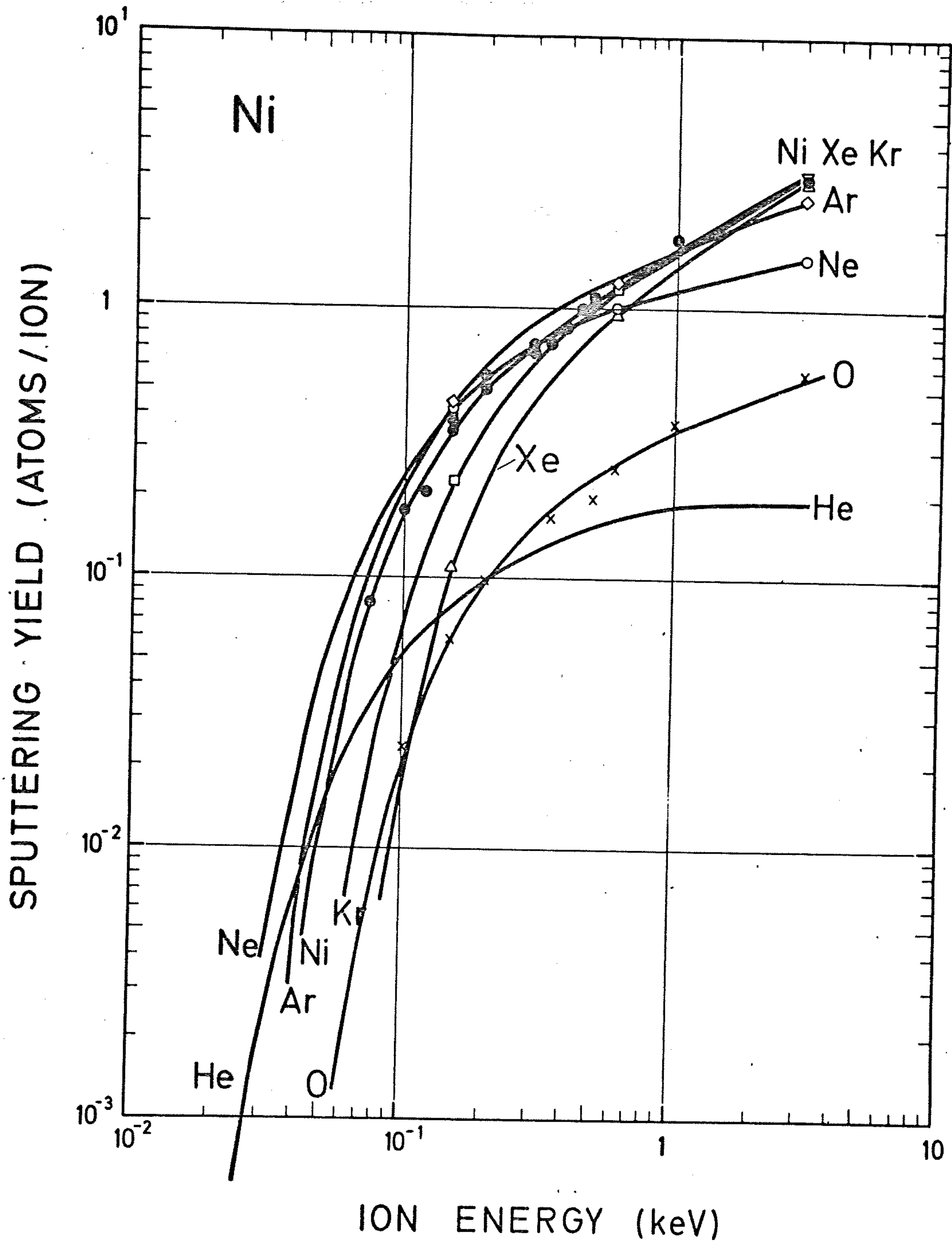

Fig. 8b: Energy dependence of the sputtering yield of Ni with Ne, O, Ar, Kr and Xe. The solid curves are fits to the experimental points and to published values from /22,23/, taking the energy dependence of eq. (7) to extrapolate to lower energies.
The data are mostly published in /17,18/.

Table 9 Si

Energy (eV)	Yields H	D	^{4}He
70		$8.7 \cdot 10^{-3}$	
100	$2.11 \cdot 10^{-3}$	$1.05 \cdot 10^{-2}$	
200			$6.7 \cdot 10^{-2}$
300	$5.59 \cdot 10^{-3}$	$1.9 \cdot 10^{-2}$	
500			$9.7 \cdot 10^{-2}$
700	$8.7 \cdot 10^{-3}$	$1.9 \cdot 10^{-2}$	
800			$9.73 \cdot 10^{-2}$
1000	$7.24 \cdot 10^{-3}$		
2000	$7.6 \cdot 10^{-3}$	$1.9 \cdot 10^{-2}$	$8.6 \cdot 10^{-2}$
8000			$9.46 \cdot 10^{-2}$

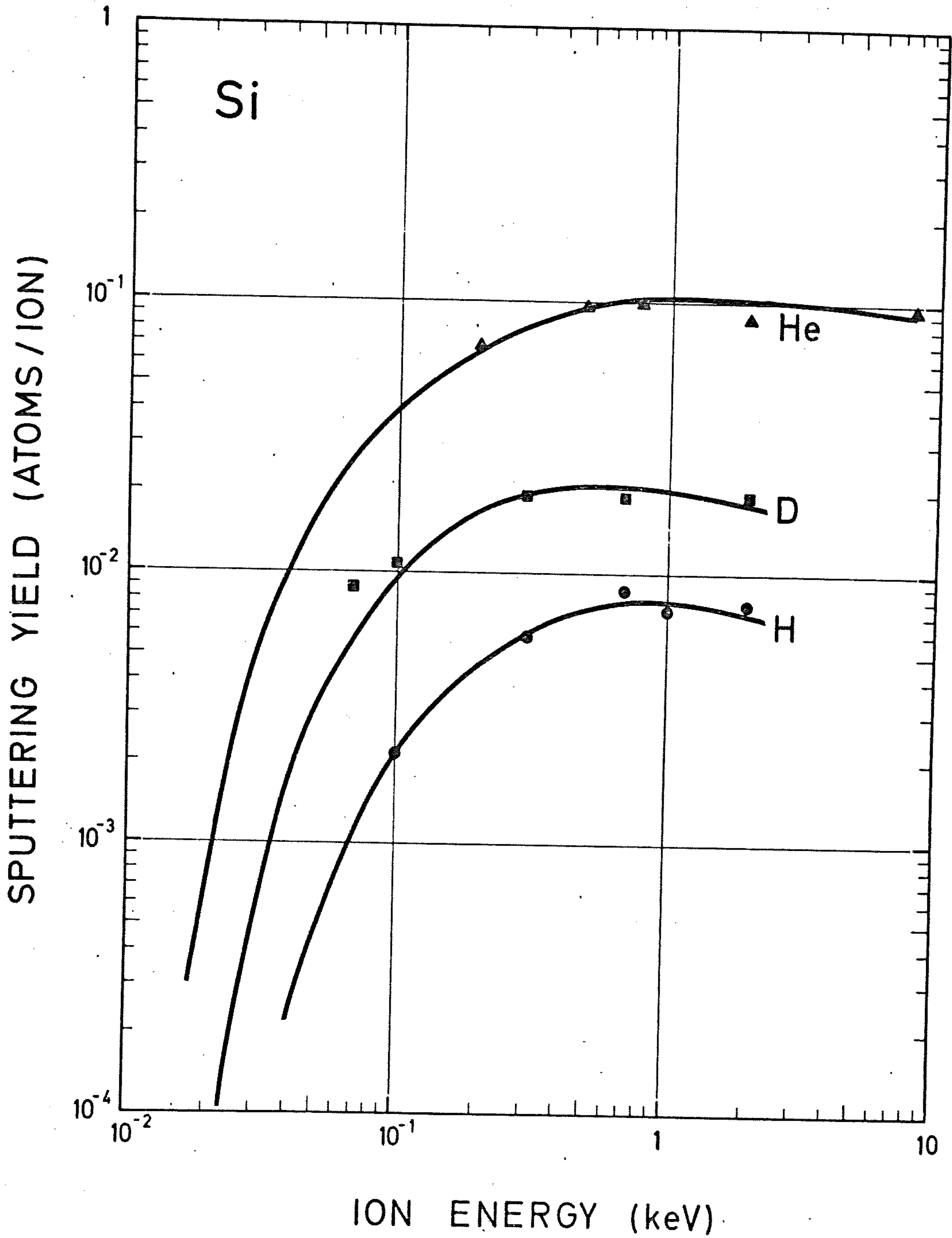

Fig. 9: Energy dependence of the sputtering yield of Si with H, D, ^{4}He. The solid curves are a fit to the data using the energy dependence of eq. (7). The data are published in /15/. For sputtering with D and H, an increase of the sputtering yield at elevated temperatures (150 to 500° C) due to chemical effects has been observed and will be published /19/.

Table 10 Ta

Energy (eV)	Yields H	D	^4He
200			$1.9 \cdot 10^{-3}$
200			$2.9 \cdot 10^{-3}$
300			$4.9 \cdot 10^{-3}$
500		$2.45 \cdot 10^{-4}$	$9.1 \cdot 10^{-3}$
600		$4.9 \cdot 10^{-4}$	
1000		$1.76 \cdot 10^{-3}$	$1.54 \cdot 10^{-2}$
2000	$6.1 \cdot 10^{-4}$		
2000	$6.8 \cdot 10^{-4}$		
3000	$9.7 \cdot 10^{-4}$		$2.4 \cdot 10^{-2}$
4000	$1.14 \cdot 10^{-3}$		
4000	$1.52 \cdot 10^{-3}$		
6000		$6.4 \cdot 10^{-3}$	$2.7 \cdot 10^{-2}$
6000			$2.8 \cdot 10^{-2}$
8000	$1.77 \cdot 10^{-3}$	$6.6 \cdot 10^{-3}$	$2.35 \cdot 10^{-2}$
8000			$3.05 \cdot 10^{-2}$
8000			$3.25 \cdot 10^{-2}$
8000			$3.8 \cdot 10^{-2}$

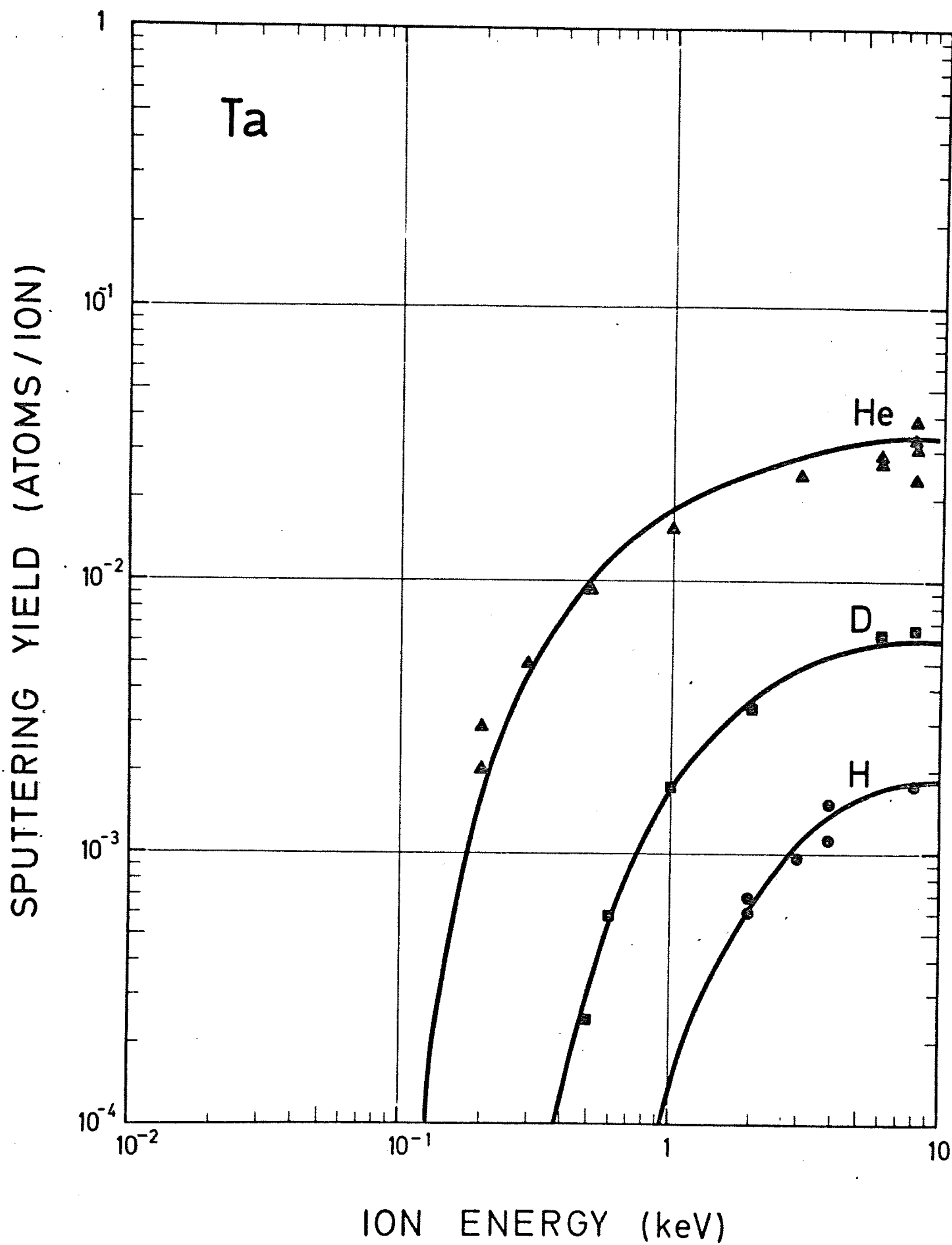

Fig. 10: Energy dependence of the sputtering yield of Ta with H, D and ^4He. The data for H and D have been measured partly with a collector technique, partly at 400° C as described in the experimental part. The solid curves are a fit to the data using the energy dependence of eq. (7).

The data are published in /15/.

Table 11 Ti

Energy (eV)	Yields H	Yields ^4He
150		$1.3 \cdot 10^{-2}$
200		$1.7 \cdot 10^{-2}$
300	$1.7 \cdot 10^{-3}$	
500		$3.75 \cdot 10^{-2}$
500		$3.0 \cdot 10^{-2}$
1000		$6.9 \cdot 10^{-2}$
1000		$6.5 \cdot 10^{-2}$
2000	$3.3 \cdot 10^{-3}$	
3000		$6.7 \cdot 10^{-2}$
4000		$6.5 \cdot 10^{-2}$
6000	$1.5 \cdot 10^{-3}$	$4.0 \cdot 10^{-2}$

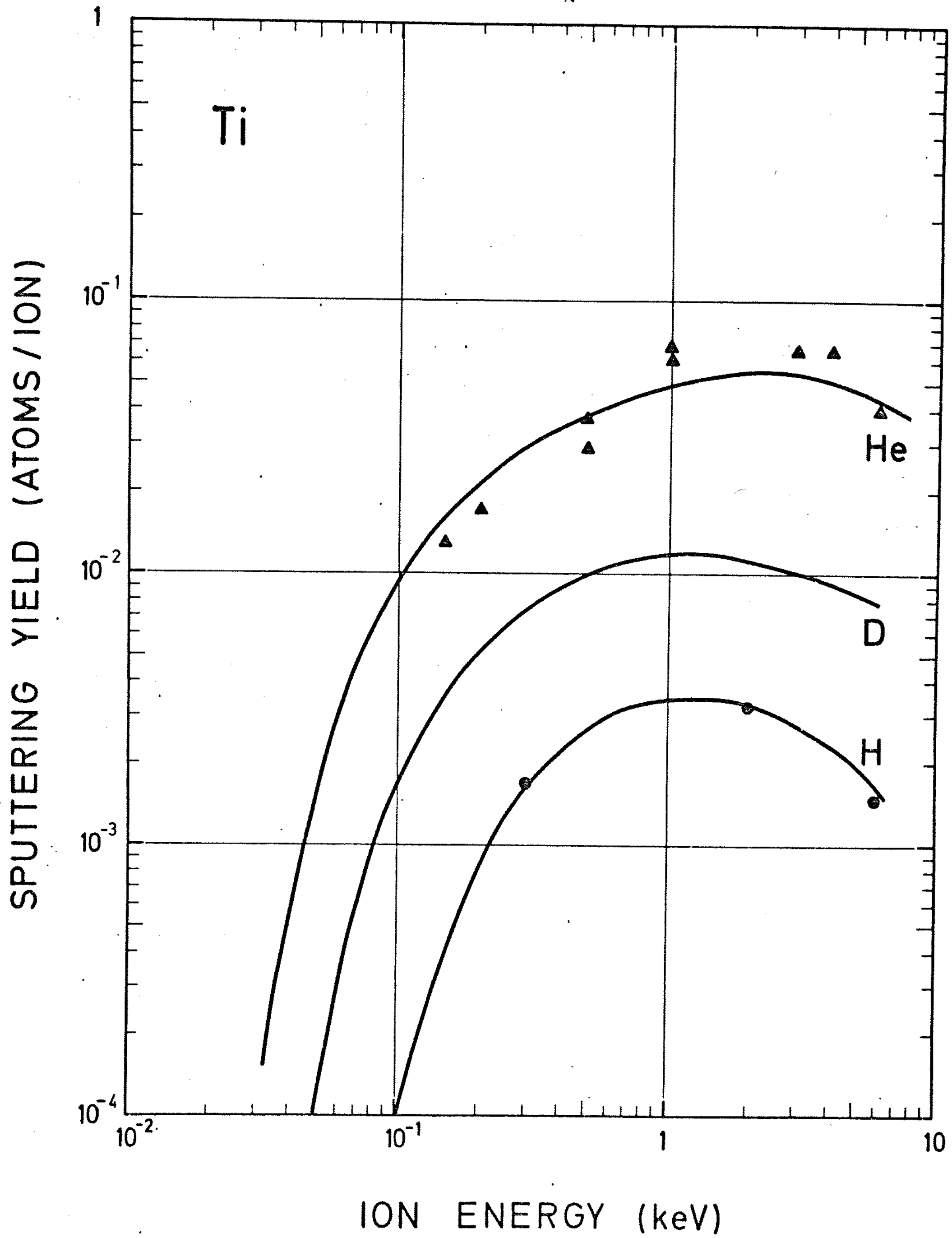

Fig. 11: Energy dependence of the sputtering yield of Ti with H and ^{4}He. The data for H have been obtained using the collector technique described in the experimental part. The solid curves for H and ^{4}He are fits to the data using the energy dependence of eq. (7). The curve for D is interpolated using eq. (7). The data are published in /15, 20/.

Table 12 V

Energy (eV)	H	^{4}He
250		$2.53 \cdot 10^{-2}$
500	$3.08 \cdot 10^{-3}$	$3.4 \cdot 10^{-2}$
500	$3.87 \cdot 10^{-3}$	$4.09 \cdot 10^{-2}$
500		$3.9 \cdot 10^{-2}$
1000		$6.1 \cdot 10^{-2}$
2000	$4.53 \cdot 10^{-3}$	$8.52 \cdot 10^{-2}$
2000	$4.8 \cdot 10^{-3}$	$9.54 \cdot 10^{-2}$
2000	$4.25 \cdot 10^{-3}$	$1.11 \cdot 10^{-2}$
4000		$1.02 \cdot 10^{-1}$
4000		$1.12 \cdot 10^{-1}$
8000		$7.62 \cdot 10^{-2}$

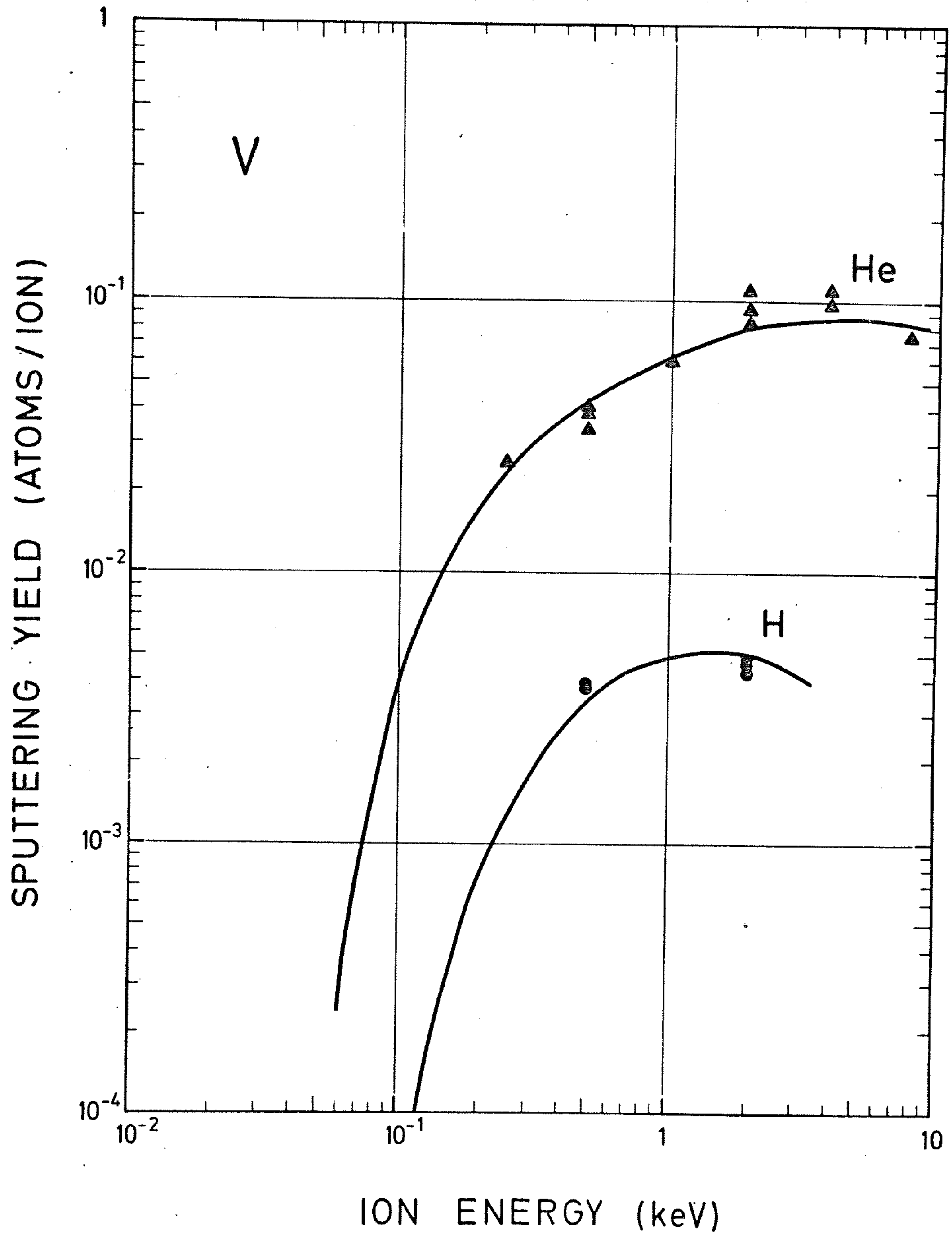

Fig. 12: Energy dependence of the sputtering yield of V with H and ^{4}He. The data for H have been measured at temperatures between 350 and 640° C. In this temperature range no influence on gas trapping has been found for H. For He, there is no change of the sputtering yield measured at room temperature compared to 560° C. The solid curves for H and ^{4}He are fits to the data using the energy dependence of eq. (7).
The data are unpublished /21/.

Table 13 W

Energies (eV)	Yields H	D	^{4}He	O	Ne	Ar	Kr	Xe
150			$4.5 \cdot 10^{-4}$	$8 \cdot 10^{-3}$	$8.6 \cdot 10^{-2}$	$2.2 \cdot 10^{-1}$	$1.42 \cdot 10^{-1}$	$1.19 \cdot 10^{-1}$
150						$1.2 \cdot 10^{-1}$		
200				$1.16 \cdot 10^{-2}$				
250		$1.52 \cdot 10^{-4}$	$3.81 \cdot 10^{-3}$					
300			$4.0 \cdot 10^{-3}$	$1.57 \cdot 10^{-2}$				
350		$3.12 \cdot 10^{-4}$						
400				$2.14 \cdot 10^{-2}$				
500		$7.05 \cdot 10^{-4}$	$8.89 \cdot 10^{-3}$	$3.46 \cdot 10^{-2}$				
550				$3.43 \cdot 10^{-2}$				
600				$3.74 \cdot 10^{-2}$	$2.72 \cdot 10^{-1}$	$5.5 \cdot 10^{-1}$	$7.88 \cdot 10^{-1}$	$7.05 \cdot 10^{-1}$
650				$4.58 \cdot 10^{-2}$				
650				$1.0 \cdot 10^{-1}$				
700	$1.09 \cdot 10^{-4}$			$1.22 \cdot 10^{-1}$				
1000	$3.26 \cdot 10^{-4}$	$2.12 \cdot 10^{-3}$	$2.32 \cdot 10^{-2}$	$2.0 \cdot 10^{-1}$				
1000				$2.0 \cdot 10^{-1}$				
2000	$9.48 \cdot 10^{-4}$	$4.6 \cdot 10^{-3}$	$2.89 \cdot 10^{-2}$					
3000				$4.06 \cdot 10^{-1}$	$7.47 \cdot 10^{-1}$	1.46	1.89	2.16
3000						1.53		
4000	$1.87 \cdot 10^{-3}$	$6.37 \cdot 10^{-3}$	$3.38 \cdot 10^{-2}$					
4000	$2.09 \cdot 10^{-3}$							
8000	$2.06 \cdot 10^{-3}$	$6.39 \cdot 10^{-3}$	$4.3 \cdot 10^{-2}$					
15000		$4.7 \cdot 10^{-3}$						
20000			$3.7 \cdot 10^{-2}$					
30000		$4.15 \cdot 10^{-3}$						
50000		$2.4 \cdot 10^{-3}$						

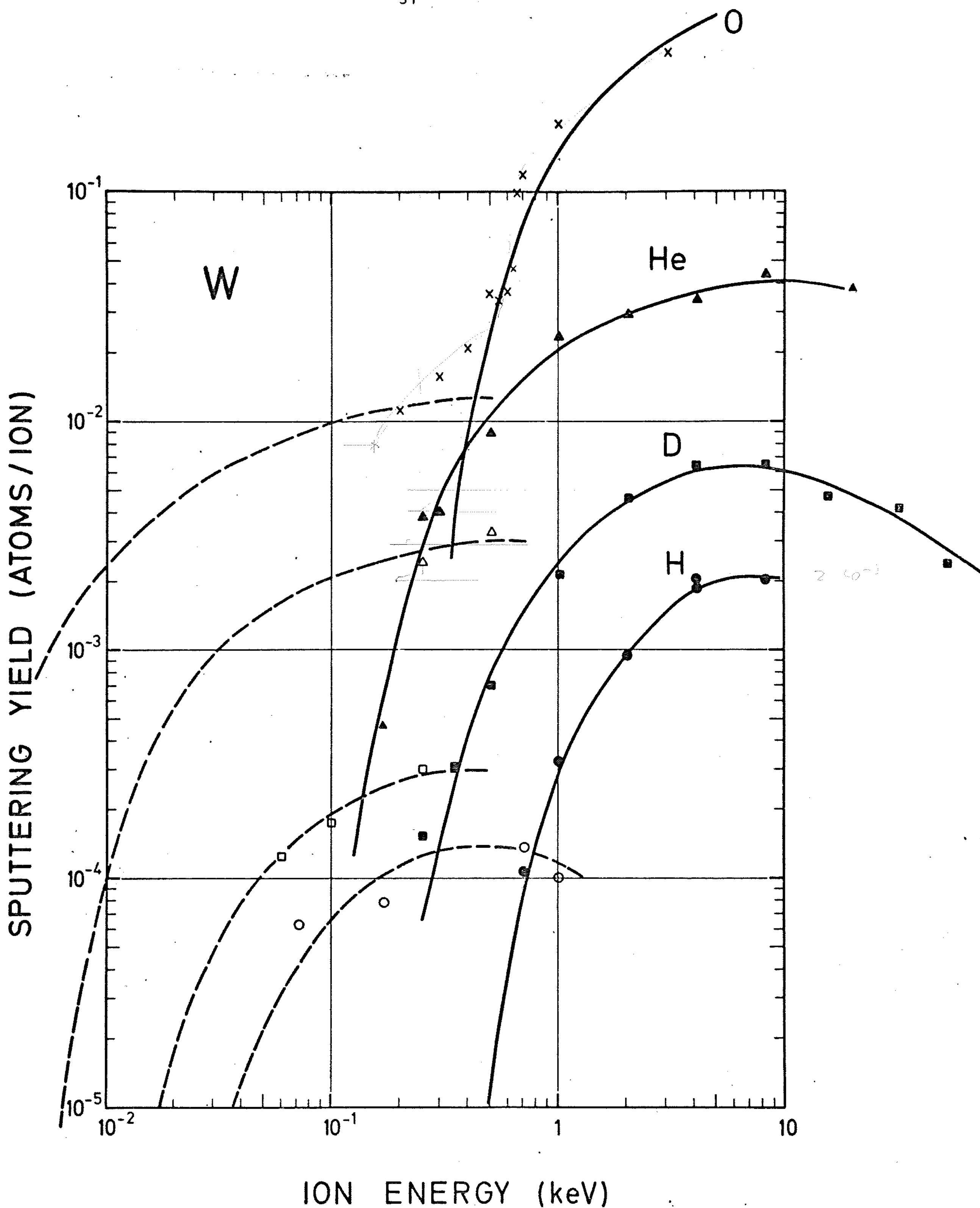

Fig. 13a: Energy dependence of the sputtering yield of W with H, D, He and O. The solid curves are a fit to the data using the energy dependence of eq. (7) for energies below the maximum of the sputtering yield. The data for H, D and He are published in /15/.
The dashed curves indicate an additional sputtering mechanism at low energies for O sputtering and for sputtering with H, D and He in a background pressure of $8 \cdot 10^{-5}$ Torr O_2. This mechanism might be due to sputtering of tungsten oxide molecules with lower surface binding energy than tungsten atoms. Taking the energy dependence of eq. (7) a binding energy of about 0.3 eV can be deduced.

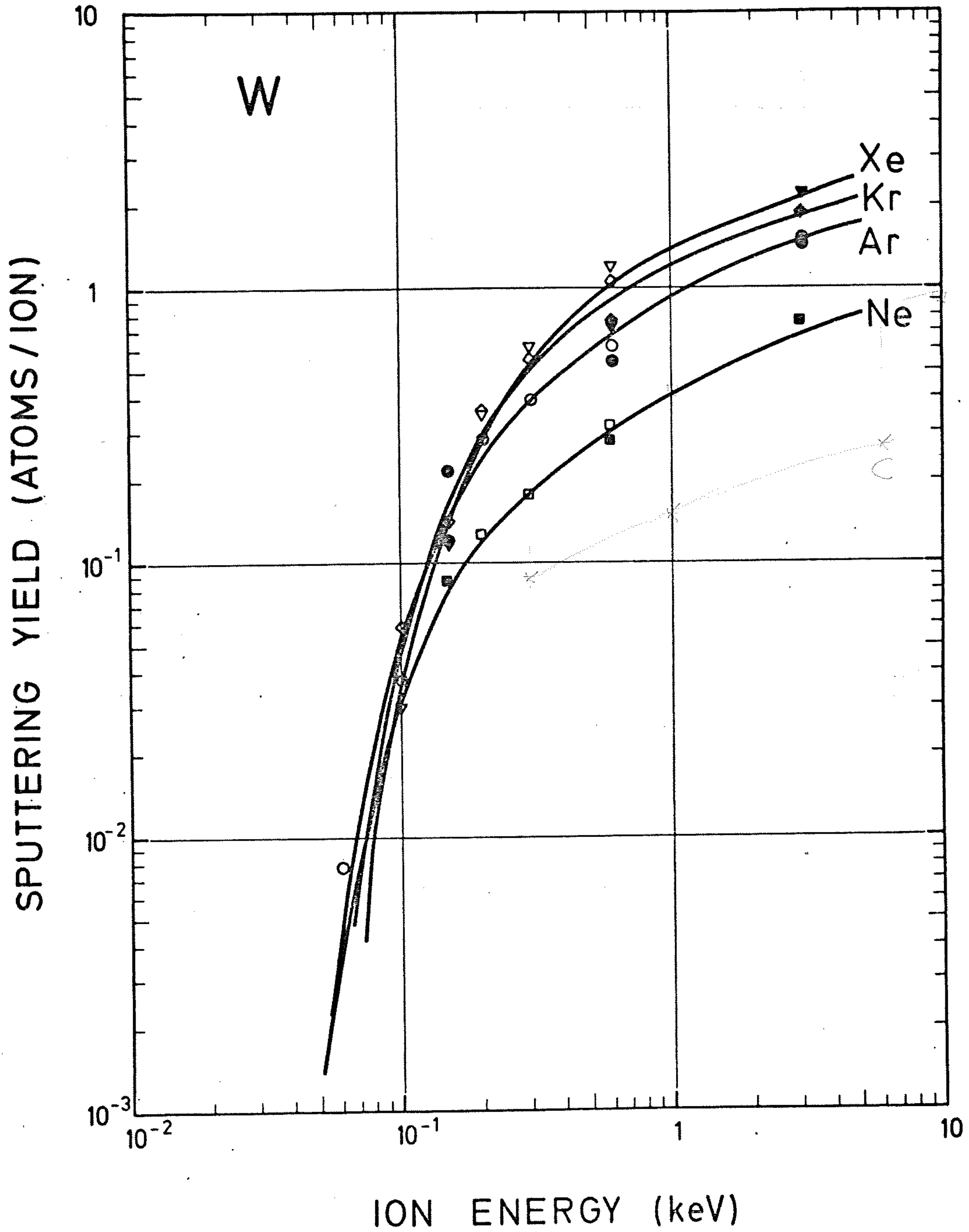

Fig. 13b: Energy dependence of the sputtering yield of W with Ne, Ar, Kr and Xe. For comparison values taken from /22, 23/ are included. The solid curves are a fit to the data using the energy dependence of eq. (7). These data as well as the data for O are unpublished /24/.

Table 14 Zr

Energy (eV)	Yields H	Yields He
200		$7.8 \cdot 10^{-3}$
500		$2.75 \cdot 10^{-2}$
2000		$4.43 \cdot 10^{-2}$
3000	$8.05 \cdot 10^{-4}$	
3000	$7.0 \cdot 10^{-4}$	
6000		$2.9 \cdot 10^{-2}$
6000		$3.9 \cdot 10^{-2}$

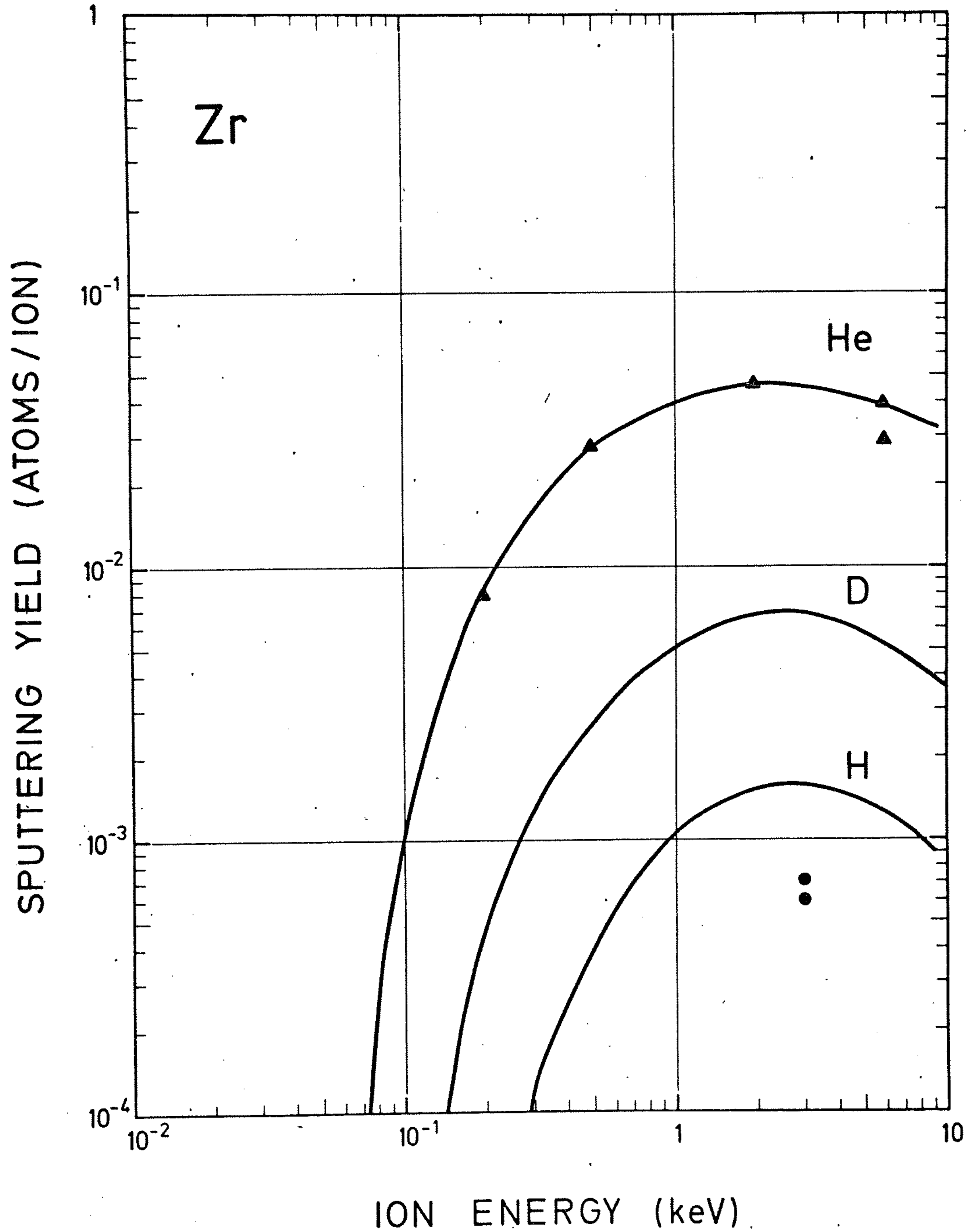

Fig. 14: Energy dependence of the sputtering yield of Zr with H and He. The solid curve for He is a fit to the data using the energy dependence of eq. (7). The interpolation to D and H has been done by comparison with the results of ZrC. This procedure has been described in /15/.
The sputtering yield for H has been measured using the collector method and is published in /25/. The He data are unpublished /26/.

<u>Table 15</u> Al_2O_3

Energy (eV)	Yields H	Yields D	Yields He
100	$1.1 \cdot 10^{-3}$	$2.4 . 10^{-3}$	
170		$5 \cdot 10^{-3}$	
200	$3.7 \cdot 10^{-3}$		$2 \cdot 10^{-2}$
250		$1.95 \cdot 10^{-2}$	$2.7 \cdot 10^{-2}$
300		$2.3 \cdot 10^{-2}$	
400	$1.45 \cdot 10^{-2}$		
500		$1.9 \cdot 10^{-2}$	$9.4 \cdot 10^{-2}$
900			$1.62 \cdot 10^{-1}$
1000	$2.03 \cdot 10^{-2}$	$3.89 \cdot 10^{-2}$	
2000	$1.65 \cdot 10^{-2}$	$4.7 \ 10^{-2}$	$2.22 \cdot 10^{-2}$
4000	$1.13 \cdot 10^{-2}$	$2.86 \cdot 10^{-2}$	$1.58 \cdot 10^{-1}$
6000			$1.21 \cdot 10^{-1}$
8000	$4.9 \cdot 10^{-3}$	$1.4 \cdot 10^{-1}$	$8.0 \cdot 10^{-2}$

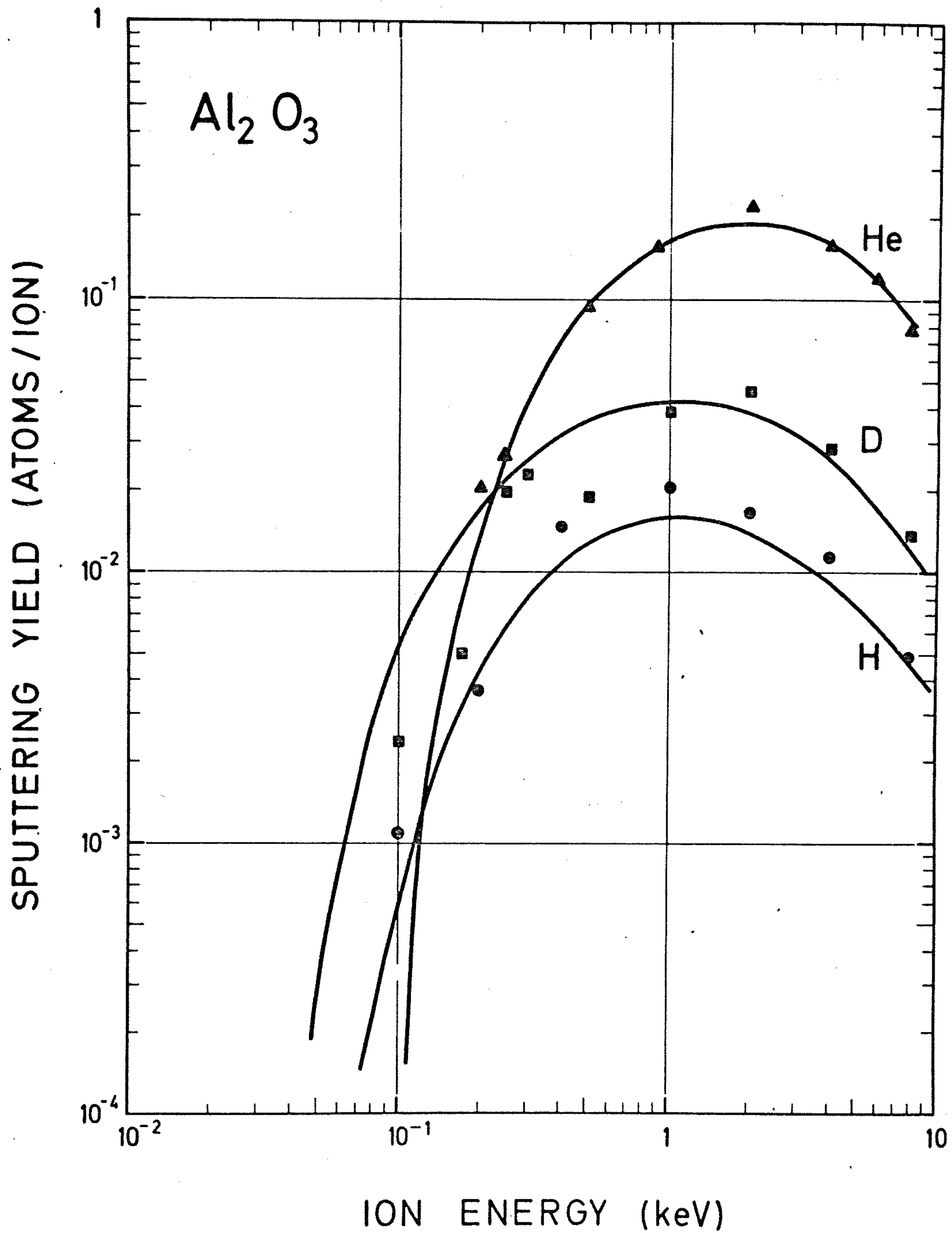

Fig. 15: Energy dependence of the sputtering yield of Al_2O_3 with H, D and ^4He. The solid curves for H and D are the curves obtained using eq. (7) for pure aluminium metal. This curves lead to a surface binding energy of about 3.5 eV. The curve for He is a fit to the data using eq. (7) at energies below the maximum of the sputtering yield. The surface binding energy obtained is about 8.5 eV, which is characteristic for Al_2O_3.
The data will be published in /12/.

Table 16 B_4C

Energy (eV)	Yields H	Yields D	Yields He
100	$8.3 \cdot 10^{-3}$	$2.9 \cdot 10^{-2}$	
100	$1.2 \cdot 10^{-2}$		
200	$1.45 \cdot 10^{-2}$	$3.68 \cdot 10^{-2}$	
200		$3.61 \cdot 10^{-2}$	
250			$1.11 \cdot 10^{-1}$
330	$1.67 \cdot 10^{-2}$		
330	$1.87 \cdot 10^{-2}$		
500		$2.83 \cdot 10^{-2}$	$1.34 \cdot 10^{-1}$
500		$3.24 \cdot 10^{-2}$	
530	$1.51 \cdot 10^{-2}$		
670	$1.13 \cdot 10^{-2}$		
1000	$1.1 \cdot 10^{-2}$	$2.13 \cdot 10^{-2}$	$1.32 \cdot 10^{-1}$
1500	$1.03 \cdot 10^{-2}$		
2000	$8.71 \cdot 10^{-3}$	$2.04 \cdot 10^{-2}$	$1.1 \cdot 10^{-1}$
2000	$9.58 \cdot 10^{-3}$		
4000	$5.17 \cdot 10^{-3}$	$1.21 \cdot 10^{-2}$	$6.8 \cdot 10^{-2}$
4000	$3.7 \cdot 10^{-3}$		
8000			$7.5 \cdot 10^{-2}$

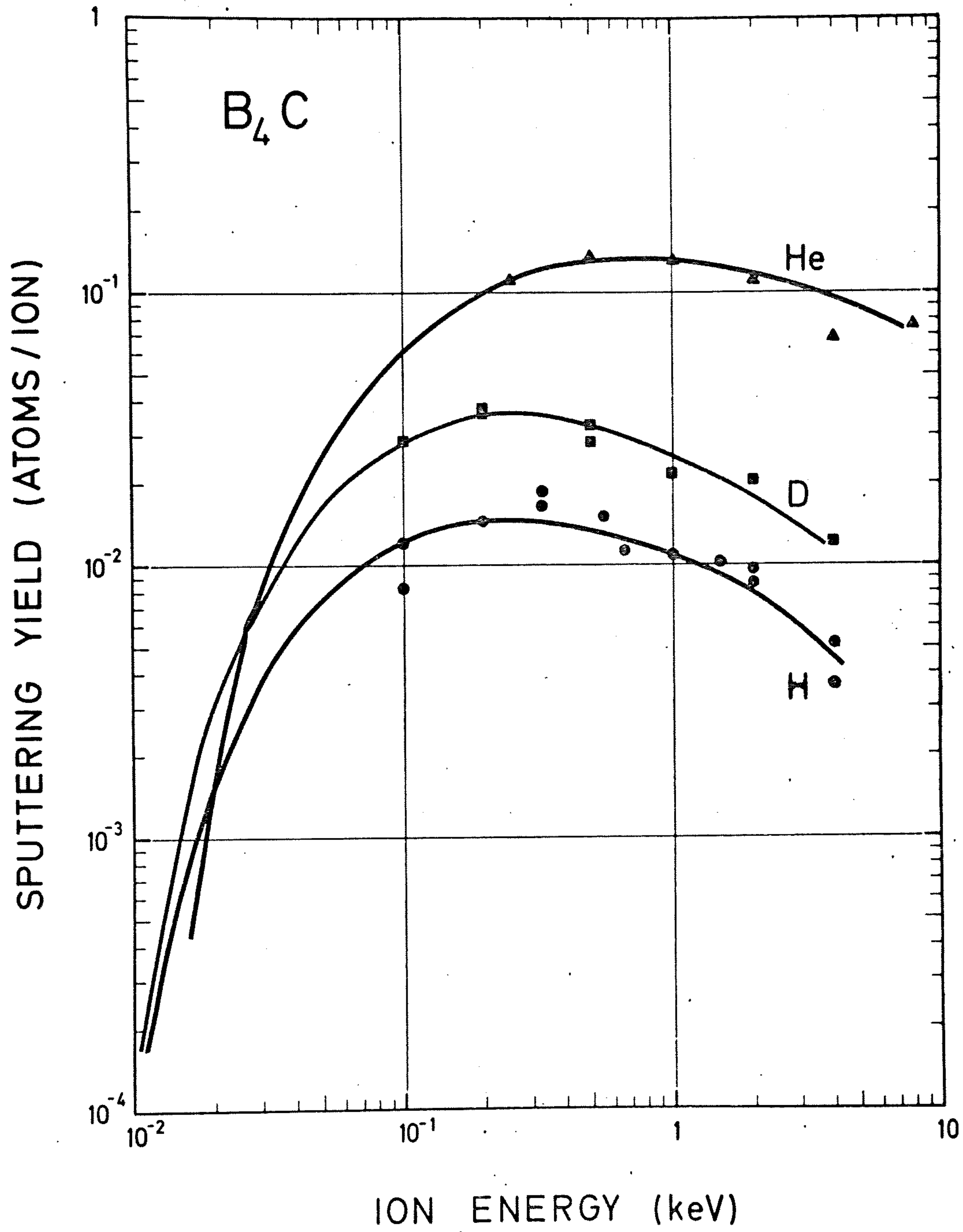

Fig. 16: Energy dependence of the sputtering yield of B_4C with H, D and ^4He. The solid curves are fits to the experimental points using the energy dependence of eq. (7). The data are published in /27/ and /15/.

Table 17 BeO

Energy (eV)	Yields H	Yields D	Yields He
60		$5.27 \cdot 10^{-3}$	
80	$1.5 \cdot 10^{-3}$		
150	$7.1 \cdot 10^{-3}$	$1.72 \cdot 10^{-2}$	
180			$3.71 \cdot 10^{-2}$
300			$6.7 \cdot 10^{-2}$
350	$1.83 \cdot 10^{-2}$		
500		$3.6 \cdot 10^{-2}$	
750			$1.53 \cdot 10^{-1}$
1000	$2.08 \cdot 10^{-2}$		
1250		$3.52 \cdot 10^{-2}$	
1500			$1.57 \cdot 10^{-1}$
2660		$3.95 \cdot 10^{-2}$	
4000	$1.34 \cdot 10^{-2}$		
4500			$1.43 \cdot 10^{-1}$

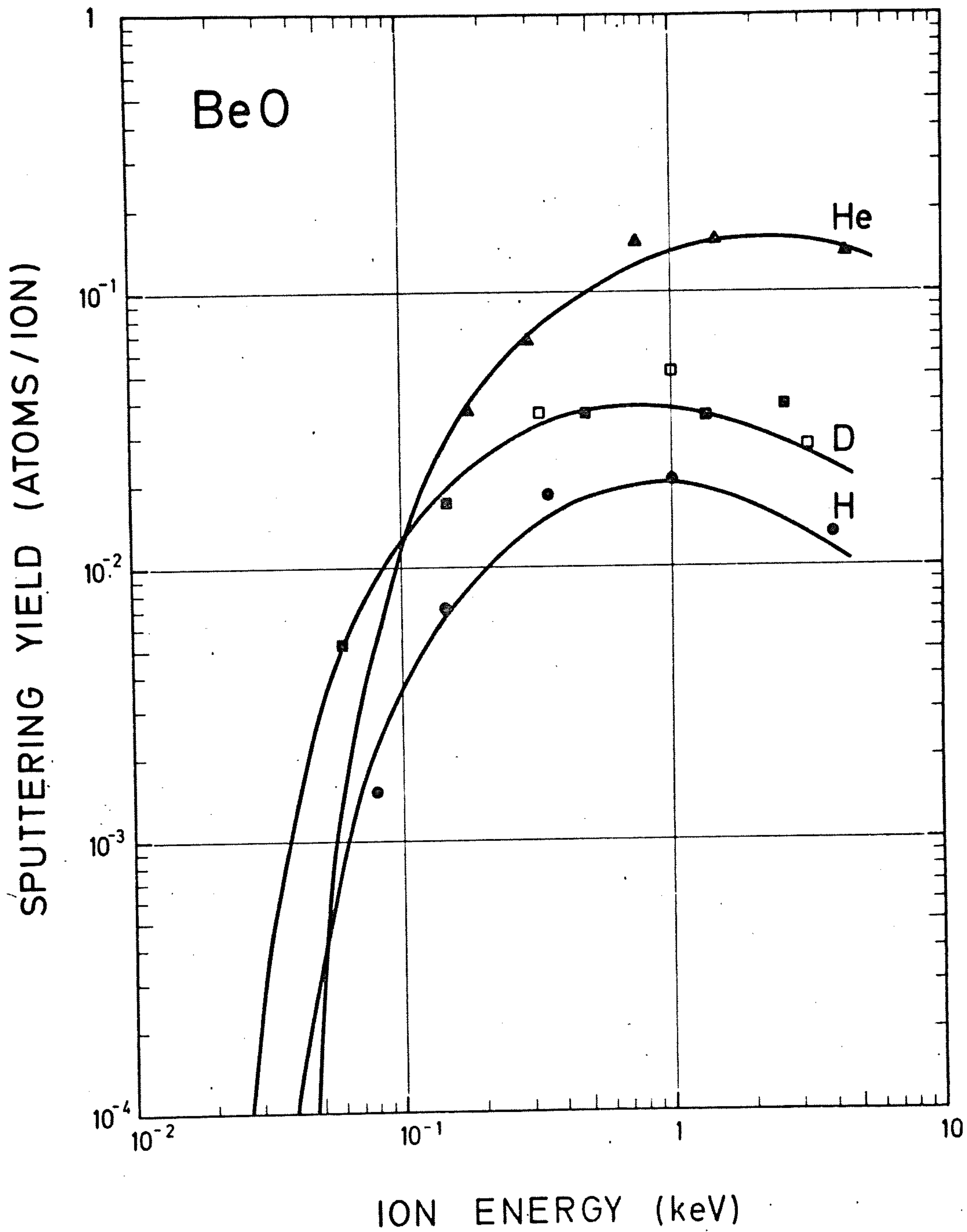

Fig. 17: Energy dependence of the sputtering yield of BeO with H, D and He. The solid curves are fits to the data using the energy dependence of eq. (7). From these curves an effective surface binding energy E_B $\sim$ 6 eV can be obtained which compares to $\sim$ 5 eV from the JANAF tables /38/. The open data points for D are taken from /43/. The data are published in /13/.

Table 18 Inconel & Nicrofer

Energy (eV)	Yields H	Yields D	Yields He
70		$2.19 \cdot 10^{-3}$	
100	$5.2 \cdot 10^{-4}$	$5.66 \cdot 10^{-3}$	
150	$1.48 \cdot 10^{-3}$	$1.16 \cdot 10^{-2}$	$8.2 \cdot 10^{-2}$
250	$4.87 \cdot 10^{-3}$	$1.87 \cdot 10^{-2}$	$1.08 \cdot 10^{-1}$
400			$1.35 \cdot 10^{-1}$
500	$9.16 \cdot 10^{-3}$	$2.95 \cdot 10^{-2}$	
500		$2.84 \cdot 10^{-2}$	
750			$1.78 \cdot 10^{-1}$
1000	$1.13 \cdot 10^{-2}$	$3.83 \cdot 10^{-2}$	
1500			$1.1 \cdot 10^{-1}$
2000	$1.46 \cdot 10^{-2}$	$3.43 \cdot 10^{-2}$	$1.75 \cdot 10^{-1}$
2000	$1.1 \cdot 10^{-2}$	$3.99 \cdot 10^{-2}$	$1.83 \cdot 10^{-1}$
2000	$1.27 \cdot 10^{-2}$		
4000	$1.2 \cdot 10^{-2}$	$2.97 \cdot 10^{-2}$	$1.91 \cdot 10^{-1}$
4000	$1.18 \cdot 10^{-2}$	$3.55 \cdot 10^{-2}$	$1.67 \cdot 10^{-1}$
6000			$1.9 \cdot 10^{-1}$
6000			$1.7 \cdot 10^{-1}$
6000			$1.38 \cdot 10^{-1}$
8000	$4.66 \cdot 10^{-3}$	$2.27 \cdot 10^{-2}$	$1.28 \cdot 10^{-1}$
8000	$6.17 \cdot 10^{-3}$		

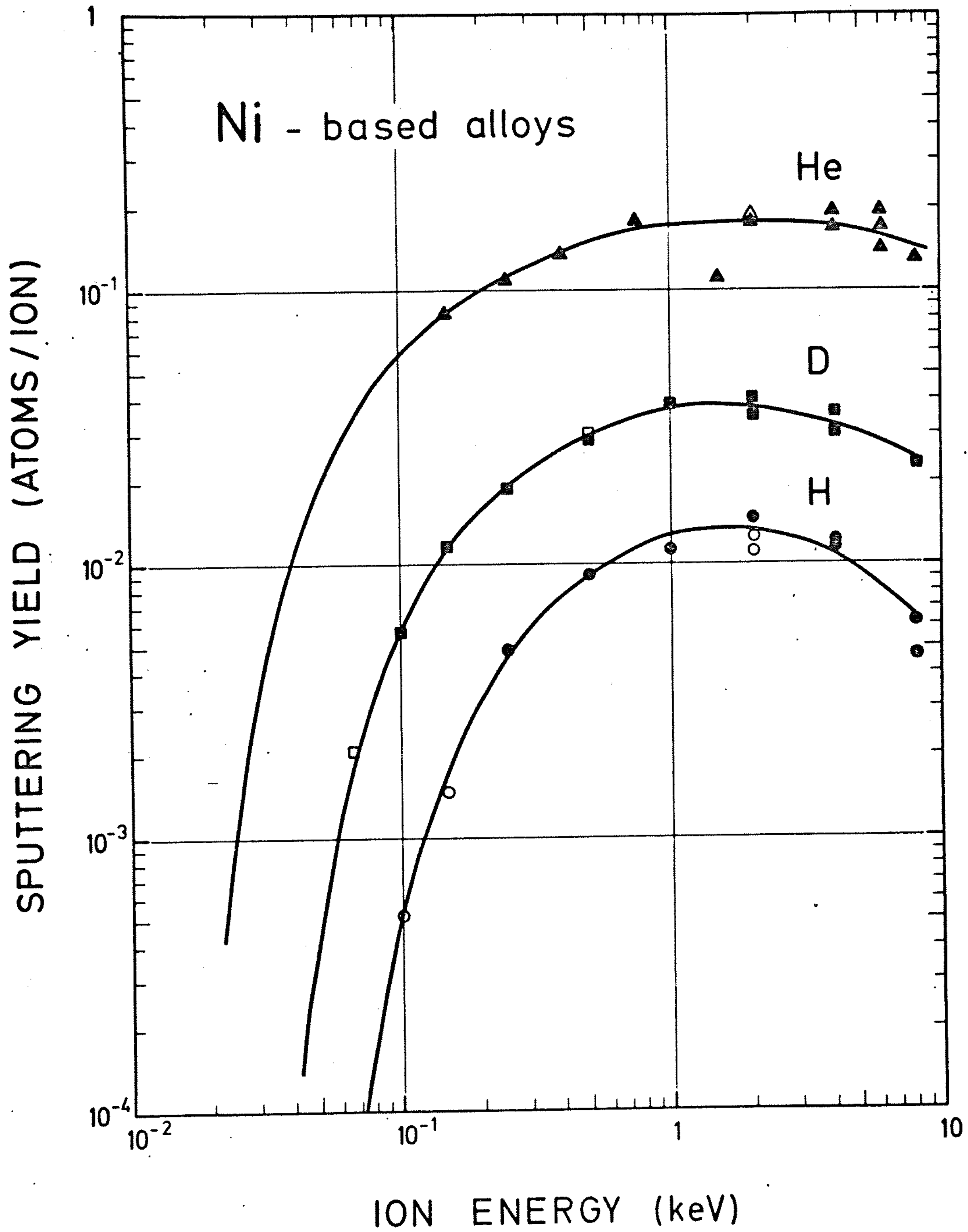

Fig. 18: Energy dependence of the sputtering yield of Ni based alloys with H, D and ^{4}He. Solid points are for Inconel, open points of Nicrofer. The solid curves are fits to the data using the energy dependence of eq. (7) for energies below the maximum. These results are published in /16/.

Table 19 SAP

Energy (eV)	Yields H	D	He
250	$1.15 \cdot 10^{-2}$	$1.82 \cdot 10^{-2}$	
300			$1.78 \cdot 10^{-1}$
500	$1.5 \cdot 10^{-2}$	$4.4 \cdot 10^{-2}$	$2.0 \cdot 10^{-1}$
1000	$1.2 \cdot 10^{-2}$	$4.1 \cdot 10^{-2}$	$2.21 \cdot 10^{-1}$
1300		$3.9 \cdot 10^{-2}$	
2000	$1.18 \cdot 10^{-2}$	$3.34 \cdot 10^{-2}$	$2.01 \cdot 10^{-1}$
2000	$1.22 \cdot 10^{-2}$	$3.77 \cdot 10^{-2}$	
2000		$3.26 \cdot 10^{-2}$	
2600		$2.7 \cdot 10^{-2}$	
4000	$8.46 \cdot 10^{-3}$	$3.38 \cdot 10^{-2}$	$1.17 \cdot 10^{-1}$
4000			$1.65 \cdot 10^{-1}$
8000	$8.75 \cdot 10^{-3}$	$1.12 \cdot 10^{-2}$	$8.5 \cdot 10^{-2}$

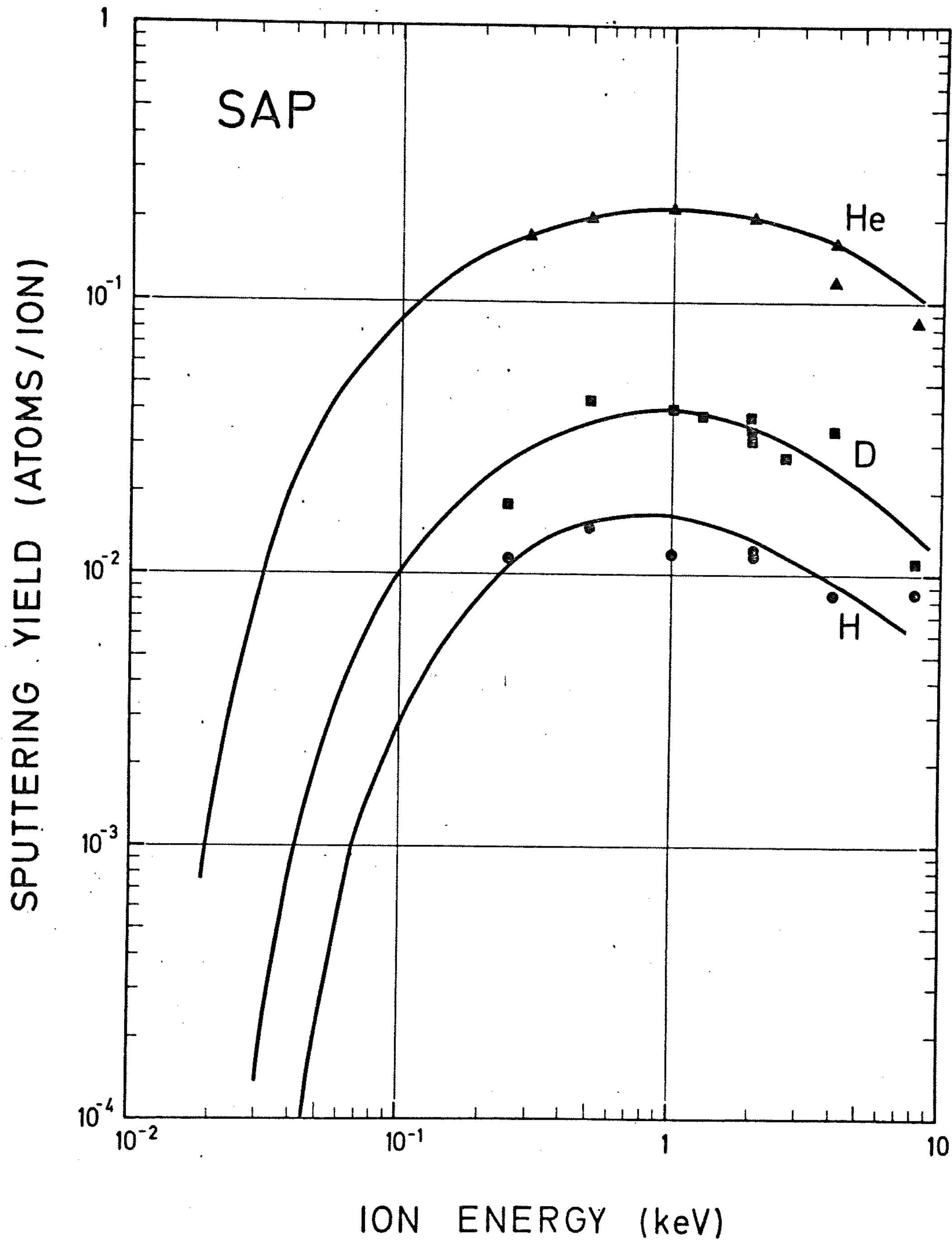

Fig. 19: Energy dependence of the sputtering yield of SAP (sintered aluminium powder) with H, D and ^{4}He. The solid curves are curves taken from pure Al metal using the energy dependence of eq. (7) for energies below the maximum.

The data will be published in /12/.

Table 20 SiC

Energy (eV)	Yields H	D	He
100	$3.07 \cdot 10^{-3}$	$1.27 \cdot 10^{-2}$	
120		$1.56 \cdot 10^{-2}$	
250	$7.0 \cdot 10^{-3}$	$2.3 \cdot 10^{-2}$	$9.5 \cdot 10^{-2}$
500	$1.27 \cdot 10^{-2}$	$3.0 \cdot 10^{-2}$	$1.26 \cdot 10^{-1}$
1000		$2.79 \cdot 10^{-2}$	$1.25 \cdot 10^{-1}$
1200			$1.4 \cdot 10^{-1}$
1500	$1.19 \cdot 10^{-2}$		
2000		$2.58 \cdot 10^{-2}$	$1.37 \cdot 10^{-1}$
4000	$4.86 \cdot 10^{-3}$	$2.12 \cdot 10^{-2}$	$1.05 \cdot 10^{-1}$
8000		$6.44 \cdot 10^{-3}$	$5.7 \cdot 10^{-2}$

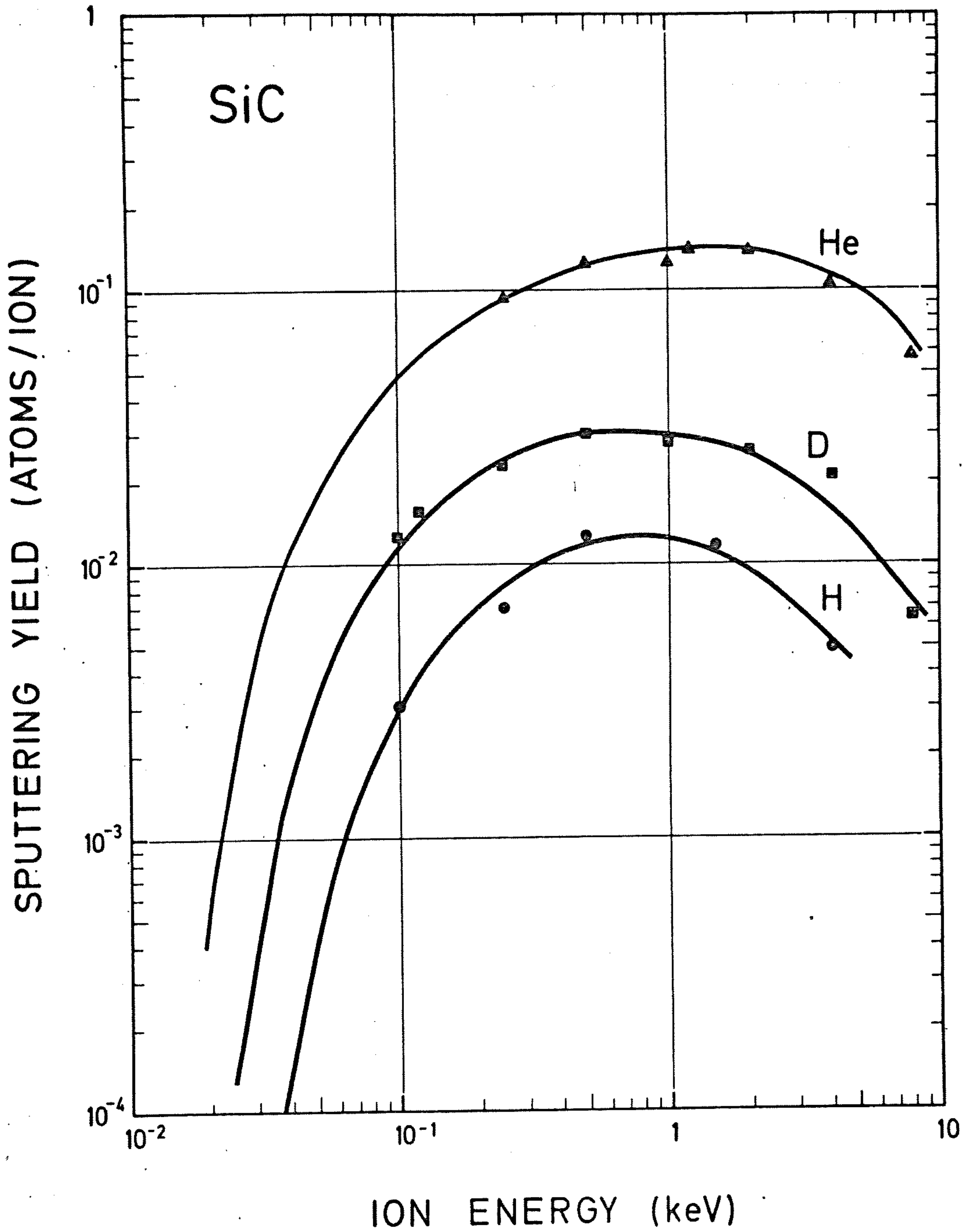

Fig. 20: Energy dependence of the sputtering yield of SiC with H, D and ^{4}He. The solid curves are fits to the data using the energy dependence of eq. (7) for energies below the maximum.
The data are published in /27 and /15/.

Table 21 SiO_2

Energy (eV)	Yields H	D	He
60	$2.28 \cdot 10^{-3}$	$7 \cdot 10^{-3}$	
100	$6.5 \cdot 10^{-3}$	$1.1 \cdot 10^{-2}$	
250			$5.05 \cdot 10^{-2}$
300	$1.6 \cdot 10^{-2}$	$3.65 \cdot 10^{-2}$	
500			$1.12 \cdot 10^{-1}$
1000		$3.7 \cdot 10^{-2}$	$1.48 \cdot 10^{-1}$
2000	$2.3 \cdot 10^{-2}$	$3.36 \cdot 10^{-2}$	$1.50 \cdot 10^{-1}$
4000			$9.44 \cdot 10^{-2}$
8000	$5.6 \cdot 10^{-3}$	$2.34 \cdot 10^{-2}$	$7.9 \cdot 10^{-2}$

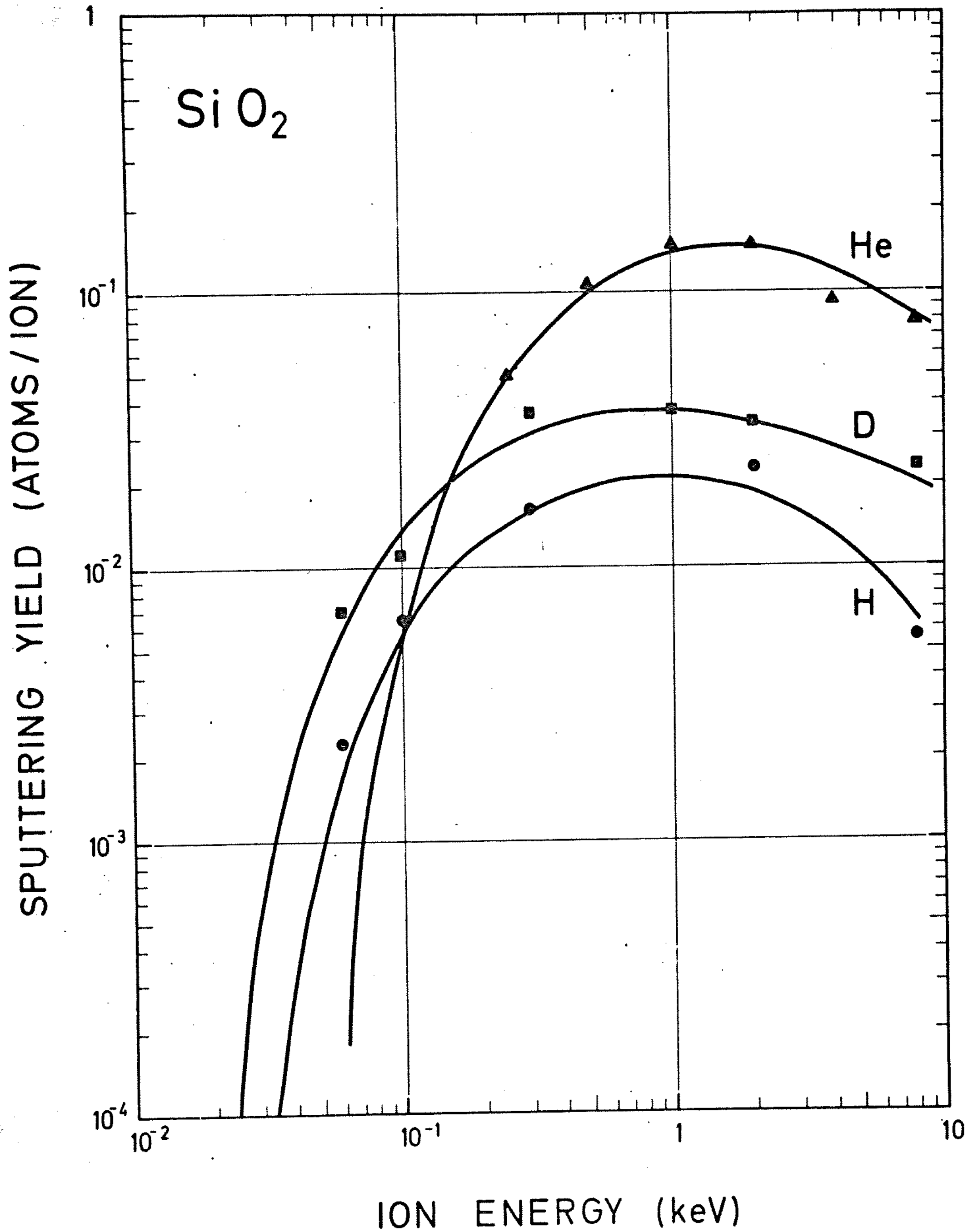

Fig. 21: Energy dependence of the sputtering yield of SiO_2 with H, D and ^4He. The curves are fits to the experimental points using the energy dependence of eq. (7) at energies below the maximum. The lower threshold energy for H and D compared to He might be due to reduction of the SiO_2 surface to pure Si metal, thus reducing the surface binding energy /28/.

The data are unpublished /28/.

Table 22 SS

Energy (eV)	Yields H	Yields D	Yields He
100		$3.35 \cdot 10^{-3}$	
150		$7.85 \cdot 10^{-3}$	$6.95 \cdot 10^{-2}$
150			$4.84 \cdot 10^{-2}$
200	$2.73 \cdot 10^{-3}$		
250			$7.09 \cdot 10^{-2}$
300	$3.64 \cdot 10^{-3}$	$1.72 \cdot 10^{-2}$	
330	$4.72 \cdot 10^{-3}$		
350	$5.05 \cdot 10^{-3}$		
400	$5.5 \cdot 10^{-3}$		
500	$8.67 \cdot 10^{-3}$	$1.98 \cdot 10^{-2}$	$9.3 \cdot 10^{-2}$
500		$2.53 \cdot 10^{-2}$	$7.25 \cdot 10^{-2}$
500			$9.29 \cdot 10^{-2}$
670	$6.57 \cdot 10^{-3}$		
1000	$9.77 \cdot 10^{-3}$	$2.60 \cdot 10^{-2}$	$8.5 \cdot 10^{-2}$
1000			$1.25 \cdot 10^{-1}$
2000	$8.02 \cdot 10^{-3}$	$2.66 \cdot 10^{-2}$	$1.59 \cdot 10^{-1}$
2000	$9.16 \cdot 10^{-3}$	$2.9 \cdot 10^{-2}$	$1.23 \cdot 10^{-1}$
2000	$9.26 \cdot 10^{-2}$	$2.15 \cdot 10^{-2}$	$1.55 \cdot 10^{-1}$
3000	$9.45 \cdot 10^{-3}$	$2.13 \cdot 10^{-2}$	
3000	$8.8 \cdot 10^{-3}$	$2.89 \cdot 10^{-2}$	
4000	$7.83 \cdot 10^{-3}$	$2.18 \cdot 10^{-2}$	$1.33 \cdot 10^{-1}$
4000			$1.4 \cdot 10^{-1}$
6000	$5.36 \cdot 10^{-3}$	$1.55 \cdot 10^{-2}$	
6000	$4.69 \cdot 10^{-3}$	$1.33 \cdot 10^{-2}$	
8000	$1.60 \cdot 10^{-3}$		$8.7 \cdot 10^{-2}$
8000			$8.03 \cdot 10^{-2}$
8000			$9.0 \cdot 10^{-2}$

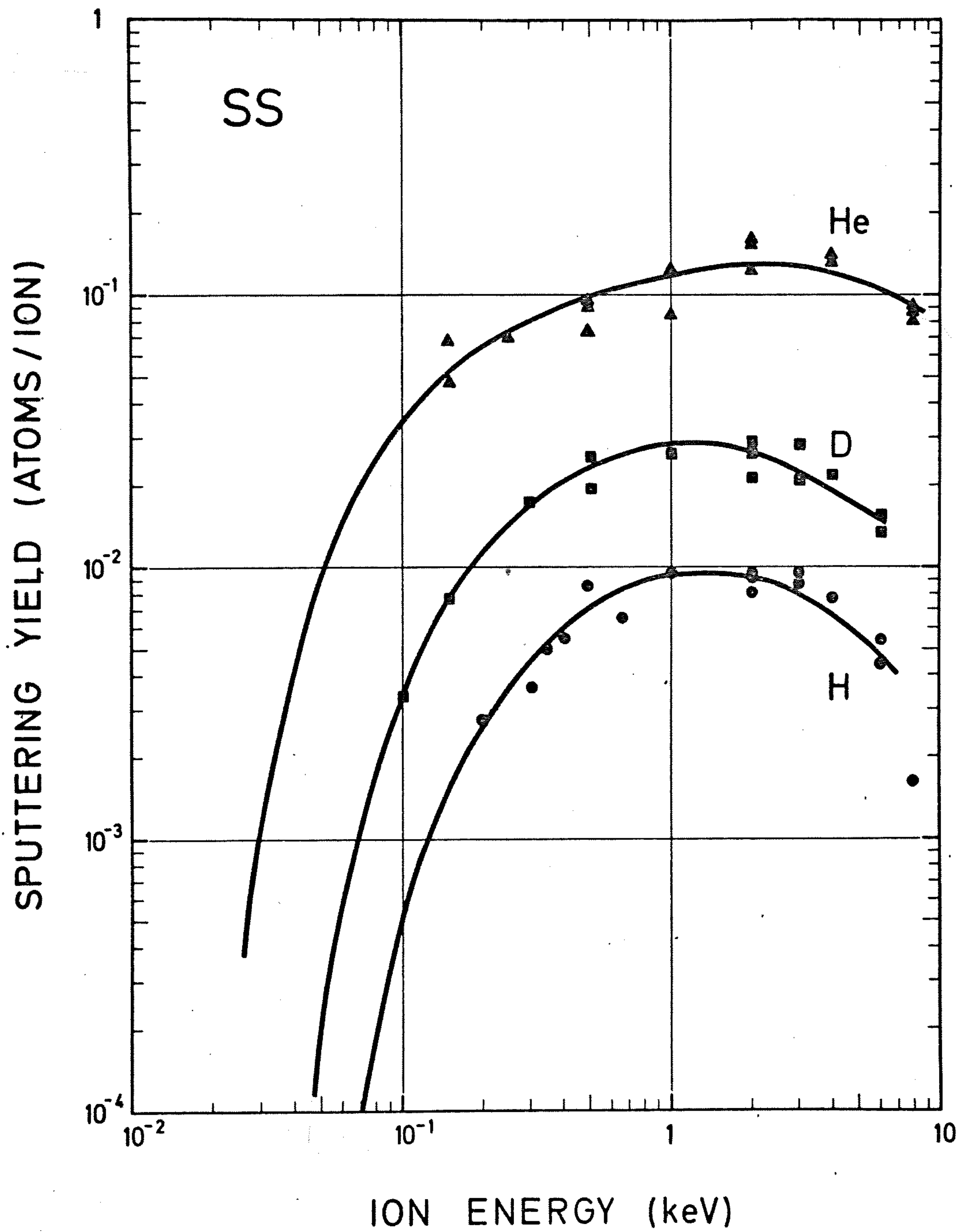

Fig. 22: Energy dependence of the sputtering yield of SS (SS 316, SS 304) with H, D and ^4He. The curves are fits to the data using the energy dependence of eq.(7) for energies below the maximum. Older data from /1/ with weight loss less than 10 μg have been omitted.

The data are published in /1, 16/.

Table 23 TaC

Energy (eV)	Yields H	Yields D	Yields He
400		$5.06 \cdot 10^{-4}$	
500		$1.12 \cdot 10^{-3}$	$9.42 \cdot 10^{-3}$
1000	$4.12 \cdot 10^{-4}$	$4.12 \cdot 10^{-3}$	$3.25 \cdot 10^{-2}$
1000		$3.78 \cdot 10^{-3}$	
2000	$1.75 \cdot 10^{-3}$	$8.39 \cdot 10^{-3}$	$3.63 \cdot 10^{-2}$
2000			$3.32 \cdot 10^{-2}$
3000	$1.9 \cdot 10^{-3}$	$8.9 \cdot 10^{-3}$	
4000	$2.49 \cdot 10^{-3}$		
4000	$3.19 \cdot 10^{-3}$		
5000	$1.75 \cdot 10^{-3}$	$6.55 \cdot 10^{-3}$	
6000			$5.6 \cdot 10^{-2}$
8000	$2.12 \cdot 10^{-3}$	$6.48 \cdot 10^{-3}$	
8000		$7.34 \cdot 10^{-3}$	$5.6 \cdot 10^{-2}$

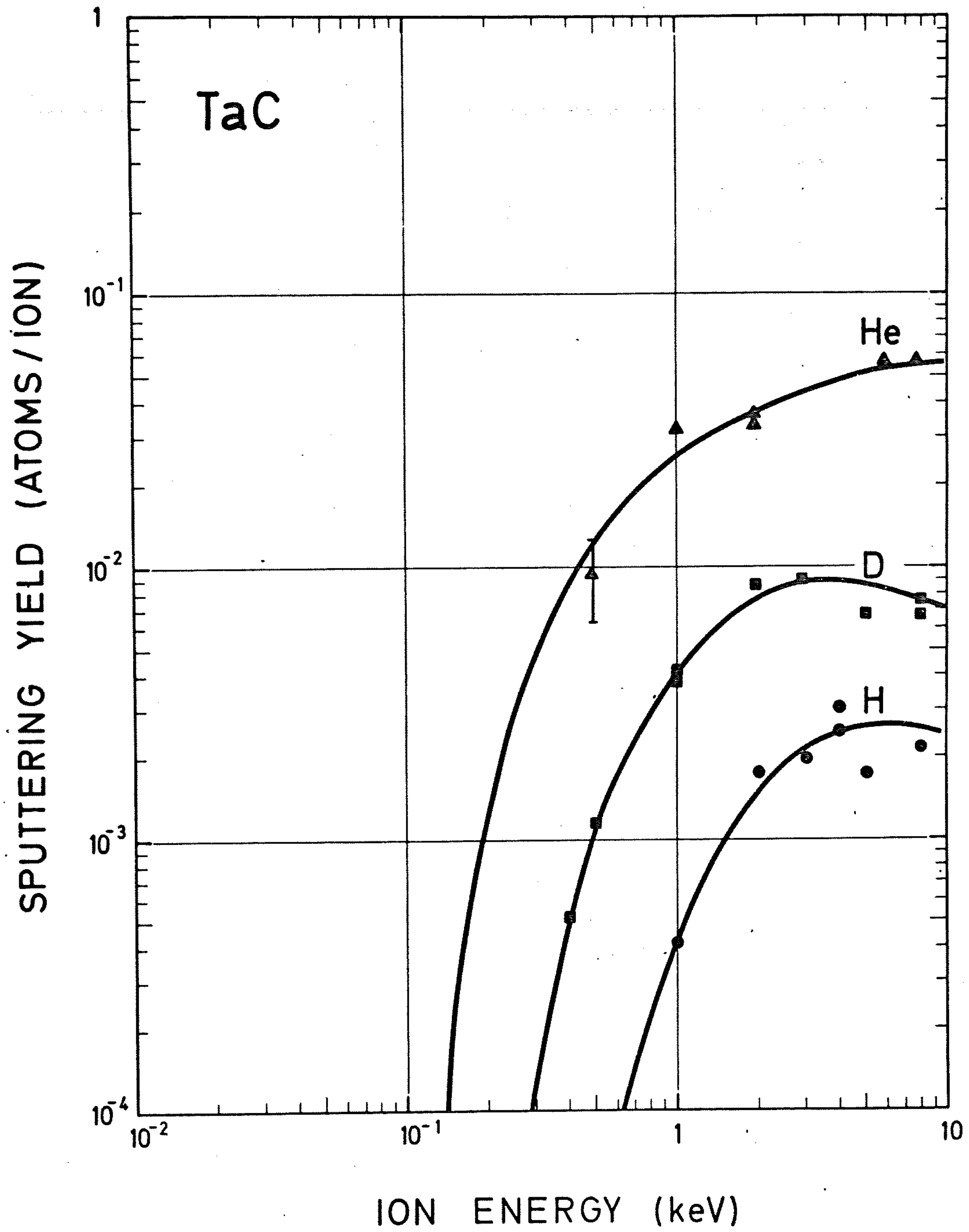

Fig. 23: Energy dependence of the sputtering yield of TaC with H, D and ^{4}He. The curves are best fits to the experimental points using the energy dependence of eq. (7) at energies below the maximum.
The data are mostly published in /15/.

Table 24 Ta_2O_5

Energy (eV)	Yields H	D	He
500		$2.18 \cdot 10^{-3}$	$3.37 \cdot 10^{-2}$
1000	$7.48 \cdot 10^{-4}$		$4.61 \cdot 10^{-2}$
1200		$1.12 \cdot 10^{-2}$	
2000		$1.3 \cdot 10^{-2}$	$7.45 \cdot 10^{-2}$
4000	$4.7 \cdot 10^{-3}$	$1.76 \cdot 10^{-2}$	$8.55 \cdot 10^{-2}$
8000	$4.92 \cdot 10^{-3}$	$1.62 \cdot 10^{-2}$	$9.62 \cdot 10^{-2}$

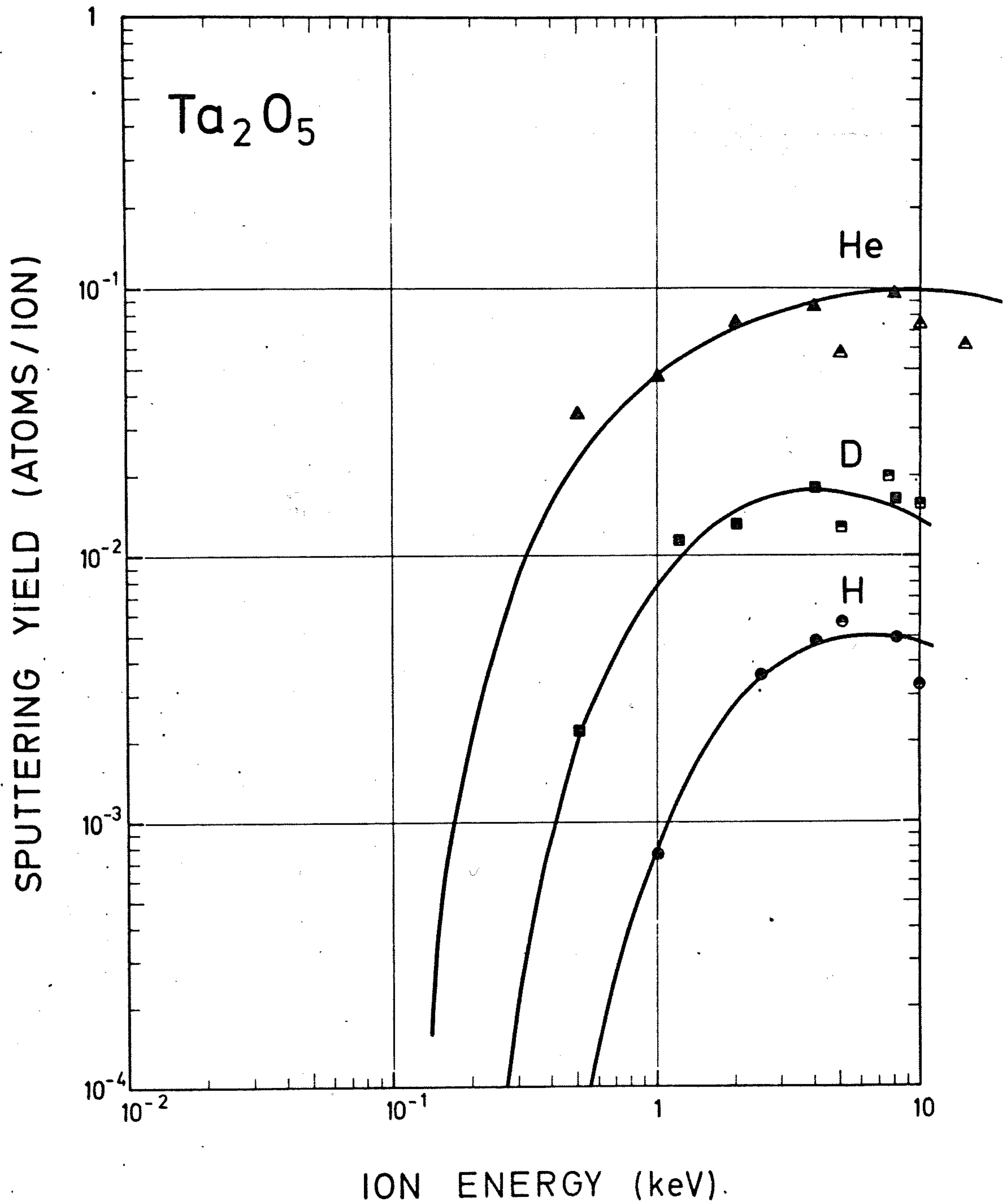

Fig. 24: Energy distribution of the sputtering yield of Ta_2O_5 with H, D and ^4He. The sputtering yield was measured on anodic oxidised films on Ta_2O_5 using the weight loss method /29/ (full point) and RBS /30/ (open points). The solid curves are fits to the experimental points using the energy dependence of eq. (7) at energies below the maximum.

Table 25 TiC

Energy (eV)	Yields H	Yields D	Yields He
120		$3.15 \cdot 10^{-3}$	
200		$4.14 \cdot 10^{-3}$	$2.84 \cdot 10^{-2}$
250	$1.85 \cdot 10^{-3}$		$5.01 \cdot 10^{-2}$
350		$1.30 \cdot 10^{-2}$	
500	$5.75 \cdot 10^{-3}$	$1.52 \cdot 10^{-2}$	$5.40 \cdot 10^{-2}$
600		$1.57 \cdot 10^{-2}$	
1000	$6.32 \cdot 10^{-3}$		$6.81 \cdot 10^{-2}$
2000	$6.82 \cdot 10^{-3}$	$1.68 \cdot 10^{-2}$	$8.0 \cdot 10^{-2}$
4000	$7.6 \cdot 10^{-3}$	$1.92 \cdot 10^{-2}$	$7.24 \cdot 10^{-2}$
8000		$1.43 \cdot 10^{-2}$	$6.06 \cdot 10^{-2}$

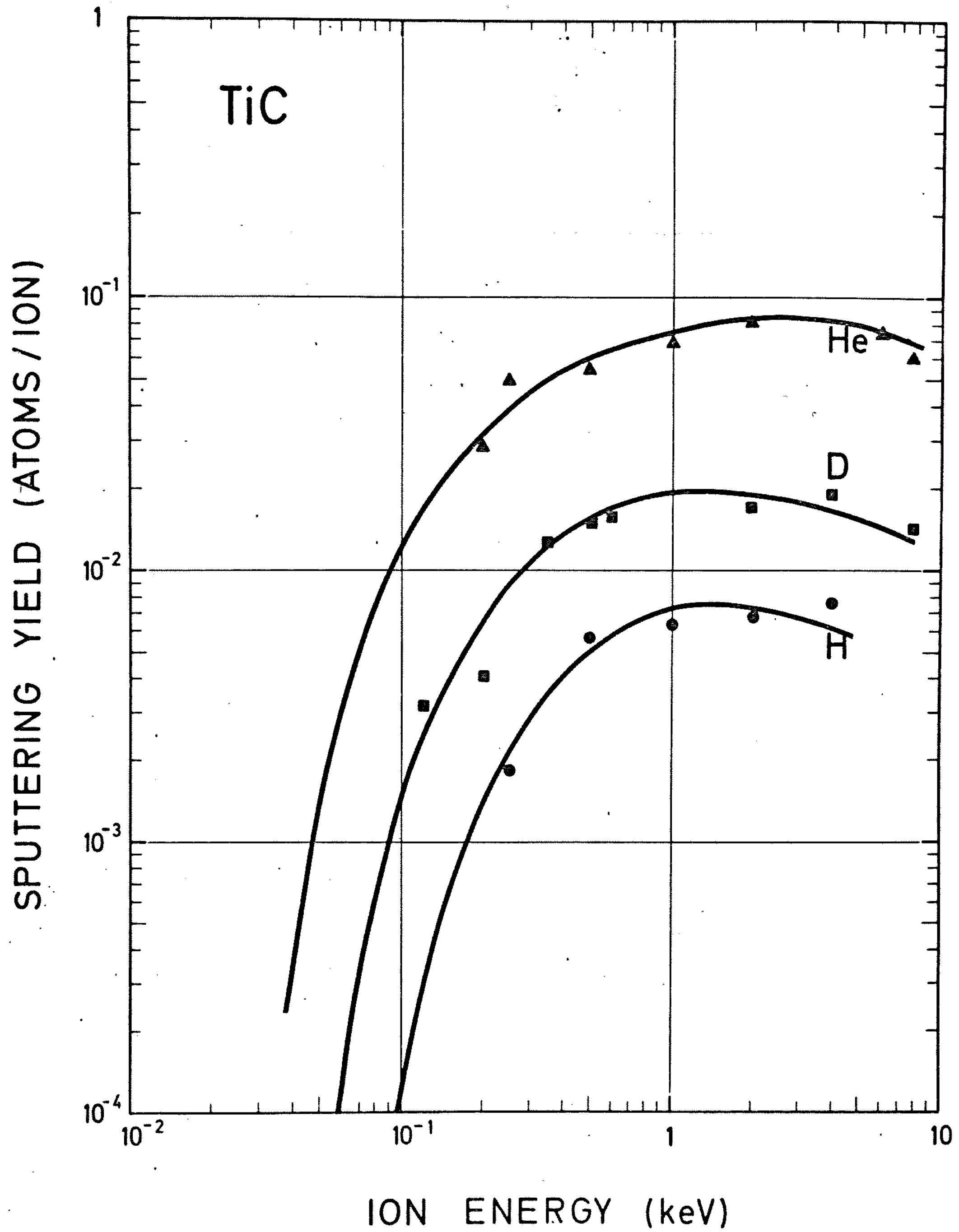

Fig. 25: Energy dependence of the sputtering yield of TiC with H, D and ^4He. The solid curves are fits to the data using the energy dependence of eq. (7) at energies below the maximum.

The data are published in /27, 15/.

Table 26

WC

Energy (eV)	Yields H	Yields D	Yields He
250		$4.0 \cdot 10^{-4}$	$6.8 \cdot 10^{-3}$
500		$2.2 \cdot 10^{-3}$	
1000	$8.1 \cdot 10^{-4}$	$4.8 \cdot 10^{-3}$	$3.68 \cdot 10^{-2}$
2000	$2.31 \cdot 10^{-3}$	$1 \cdot 10^{-2}$	
4000	$5 \cdot 10^{-3}$	$1.71 \cdot 10^{-2}$	
8000	$5.55 \cdot 10^{-3}$	$1.62 \cdot 10^{-2}$	$7.0 \cdot 10^{-2}$
15000		$1.6 \cdot 10^{-2}$	

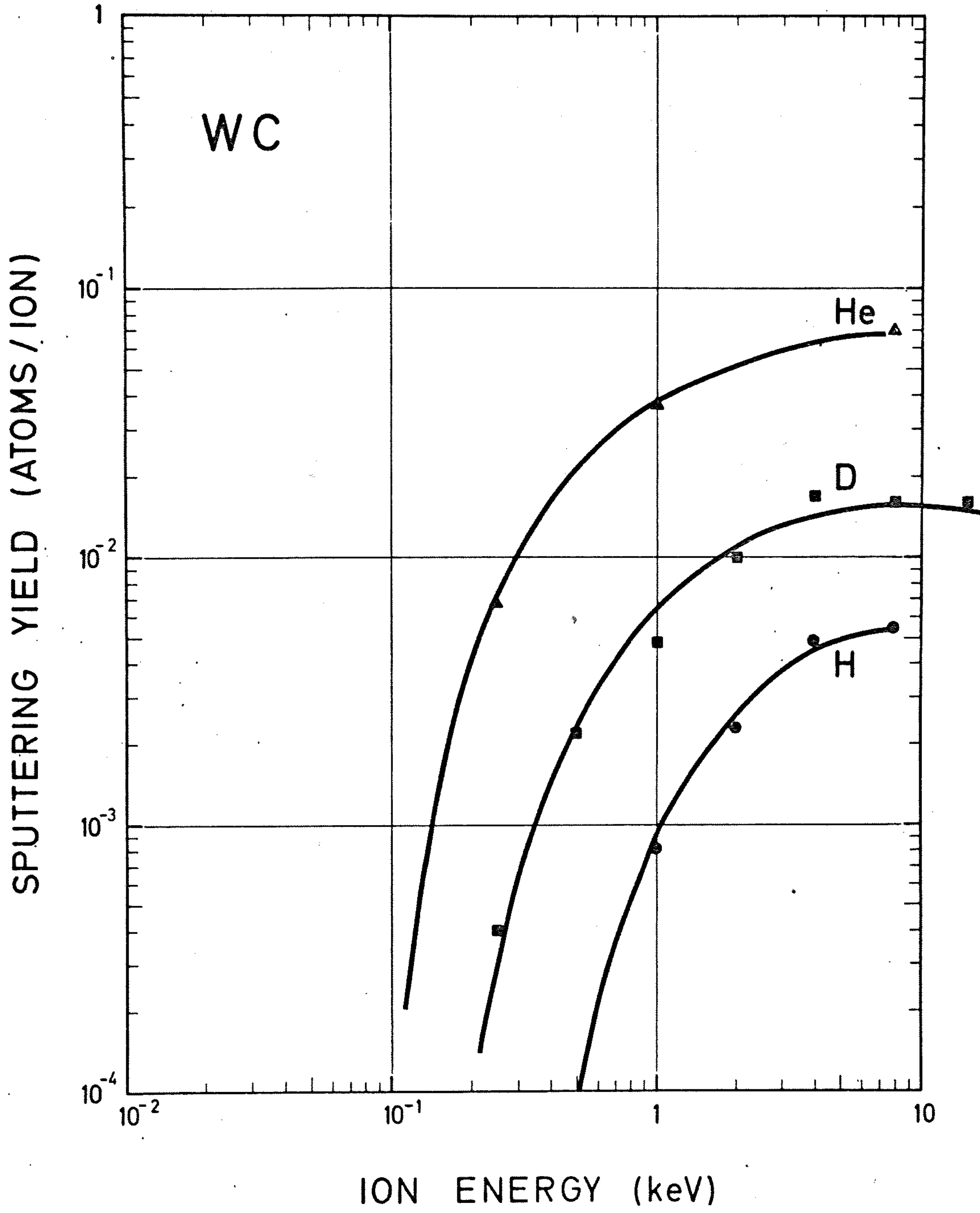

Fig. 26: Energy dependence of the sputtering yield of WC with H, D and He. The solid curves are fits to the experimental points using the energy dependence of eq. (7). The data are published in /15/.

Table 27 Zr C

Energy (eV)	Yields H	Yields D	Yields He
120		$3.94 \cdot 10^{-4}$	
150			$4.36 \cdot 10^{-3}$
250	$1.96 \cdot 10^{-4}$	$1.05 \cdot 10^{-3}$	$1.95 \cdot 10^{-2}$
500	$6.6 \cdot 10^{-4}$	$2.63 \cdot 10^{-3}$	$3.26 \cdot 10^{-2}$
1000	$1.05 \cdot 10^{-3}$	$6.3 \cdot 10^{-3}$	
2000	$1.94 \cdot 10^{-3}$	$7.9 \cdot 10^{-3}$	$4.77 \cdot 10^{-2}$
4000	$1.16 \cdot 10^{-3}$	$5.44 \cdot 10^{-3}$	$4.8 \cdot 10^{-2}$
8000		$3.27 \cdot 10^{-3}$	$4.71 \cdot 10^{-2}$

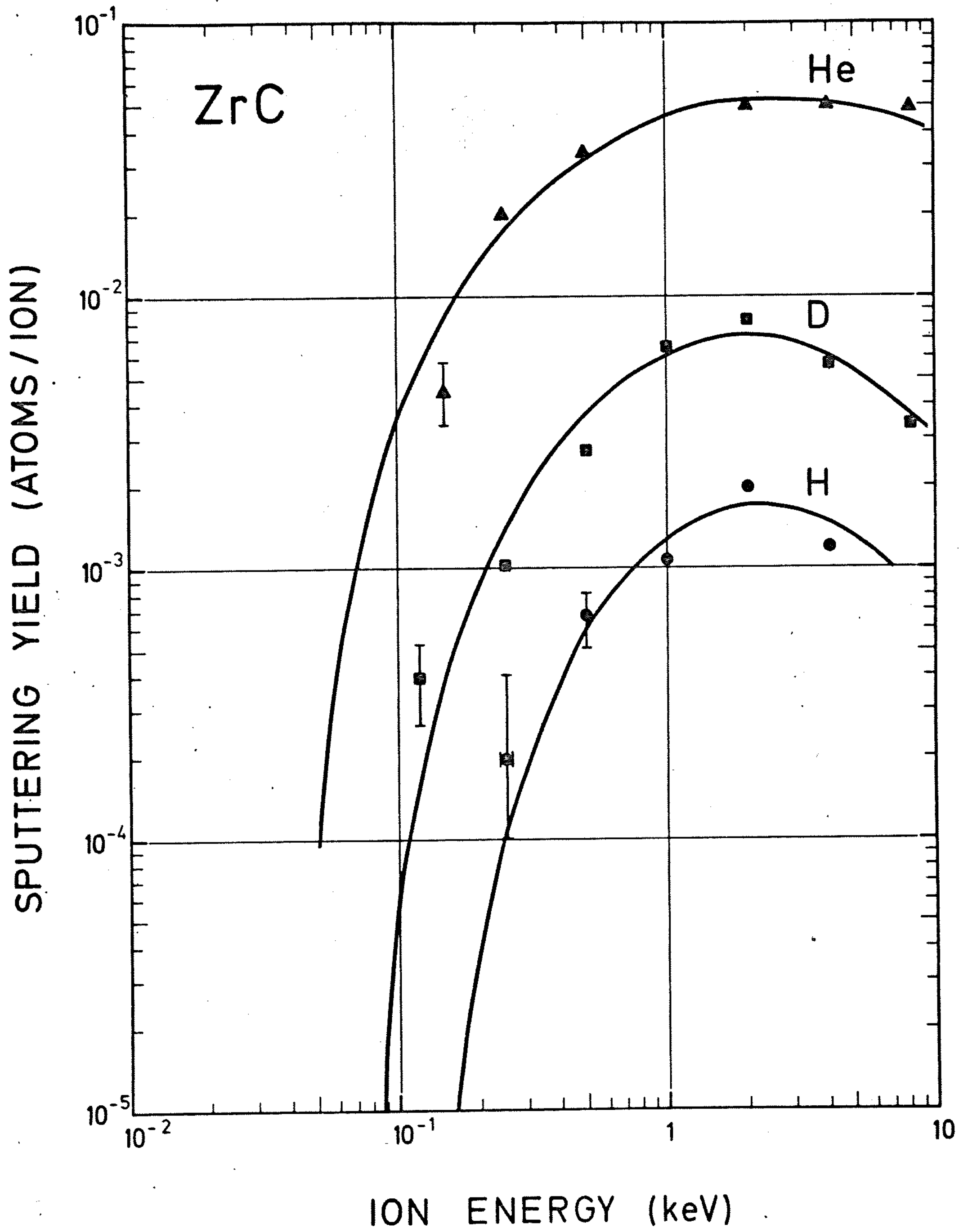

Fig. 27: Energy dependence of the sputtering yield of ZrC with H, D and ^{4}He. The solid curves are fits to the experimental data using the energy dependence of eq. (7) for energies below the maximum. Most of the data have been taken evaluating weight losses of less than 20 μg. The error introduced by $\pm$ 2 μg is indicated by error bars. The data are unpublished /31/.

2.) Angular dependence of the sputtering yield

The data for the angular dependence of the sputtering yield are given for the following ion target combinations and energies:

<u>Table 28:</u> Angular dependence of the sputtering yield

	H				D				He		ions
	1	2	4	8	1	2	4	8	4	8	energy (keV)
Au	x		x		x						
Mo		x	x	x		x		x	x	x	
Ni	x		x	x	x		x	x	x	x	
W		x									
TaC		x									

The results are presented in figs. 28 - 32 and Tables 29 - 33.

Table 29 Au

	Yields		
	H		D
Angle of incidence	1	4	1 keV
0°	$7.13 \cdot 10^{-3}$	$1.6 \cdot 10^{-2}$	$3.02 \cdot 10^{-2}$
15°	$7.28 \cdot 10^{-3}$		$3.0 \cdot 10^{-2}$
30°	$8.62 \cdot 10^{-3}$		$4.03 \cdot 10^{-2}$
45°	$1.15 \cdot 10^{-2}$	$2.36 \cdot 10^{-2}$	$4.35 \cdot 10^{-2}$
60°	$1.17 \cdot 10^{-2}$	$3.6 \cdot 10^{-2}$	$5.33 \cdot 10^{-2}$
60°	$1.22 \cdot 10^{-2}$		$5.74 \cdot 10^{-2}$
70°	$1.62 \cdot 10^{-2}$	$4.78 \cdot 10^{-2}$	$7.10 \cdot 10^{-2}$
75°	$1.75 \cdot 10^{-2}$	$5.68 \cdot 10^{-2}$	$7.94 \cdot 10^{-2}$
80°	$1.89 \cdot 10^{-2}$	$6.18 \cdot 10^{-2}$	$8.76 \cdot 10^{-2}$

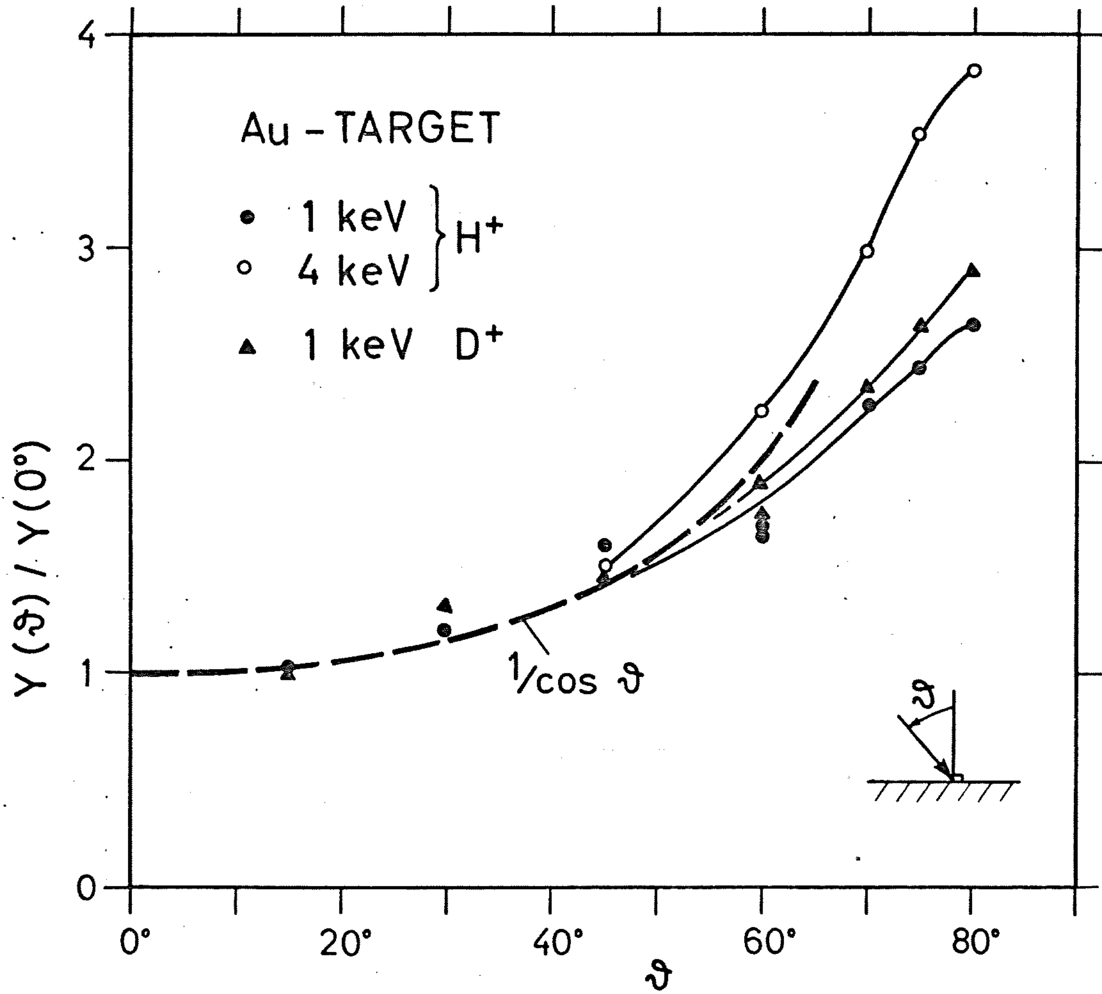

Fig. 28: Sputtering yield for Au with H and D as function of the angle of incidence. The yields are normalised to the value at 0° incidence. The broken curve indicates a 1/cos-dependence.
The data will be published /36 /.

Table 30 Mo

	Yields						
	H			D		He	
angle of incidence	2	4	8	2	8	4	8 keV
0°	$2.2\cdot10^{-3}$	$2.1\cdot10^{-3}$	$1.7\cdot10^{-3}$	$9.3\cdot10^{-3}$	$4.8\cdot10^{-3}$	$5.65\cdot10^{-2}$	$4.8\cdot10^{-2}$
30°	$3.87\cdot10^{-3}$			$1.37\cdot10^{-2}$		$9.3\cdot10^{-2}$	
45°	$4.78\cdot10^{-3}$			$1.89\cdot10^{-2}$		$1.1\cdot10^{-1}$	
60°	$8.95\cdot10^{-3}$		$1.13\cdot10^{-2}$	$2.99\cdot10^{-2}$		$1.53\cdot10^{-1}$	
70°	$1.55\cdot10^{-2}$	$1.84\cdot10^{-2}$	$1.56\cdot10^{-2}$	$4.69\cdot10^{-2}$	$4.52\cdot10^{-2}$	$2.4\cdot10^{-1}$	$2.27\cdot10^{-1}$
75°	$2.07\cdot10^{-2}$		$2.57\cdot10^{-2}$	$5.75\cdot10^{-2}$		$2.64\cdot10^{-1}$	
80°	$2.47\cdot10^{-1}$		$3.39\cdot10^{-2}$	$7.37\cdot10^{-2}$		$2.84\cdot10^{-1}$	
85°	$2.25\cdot10^{-2}$		$3.45\cdot10^{-2}$	$6.79\cdot10^{-2}$			

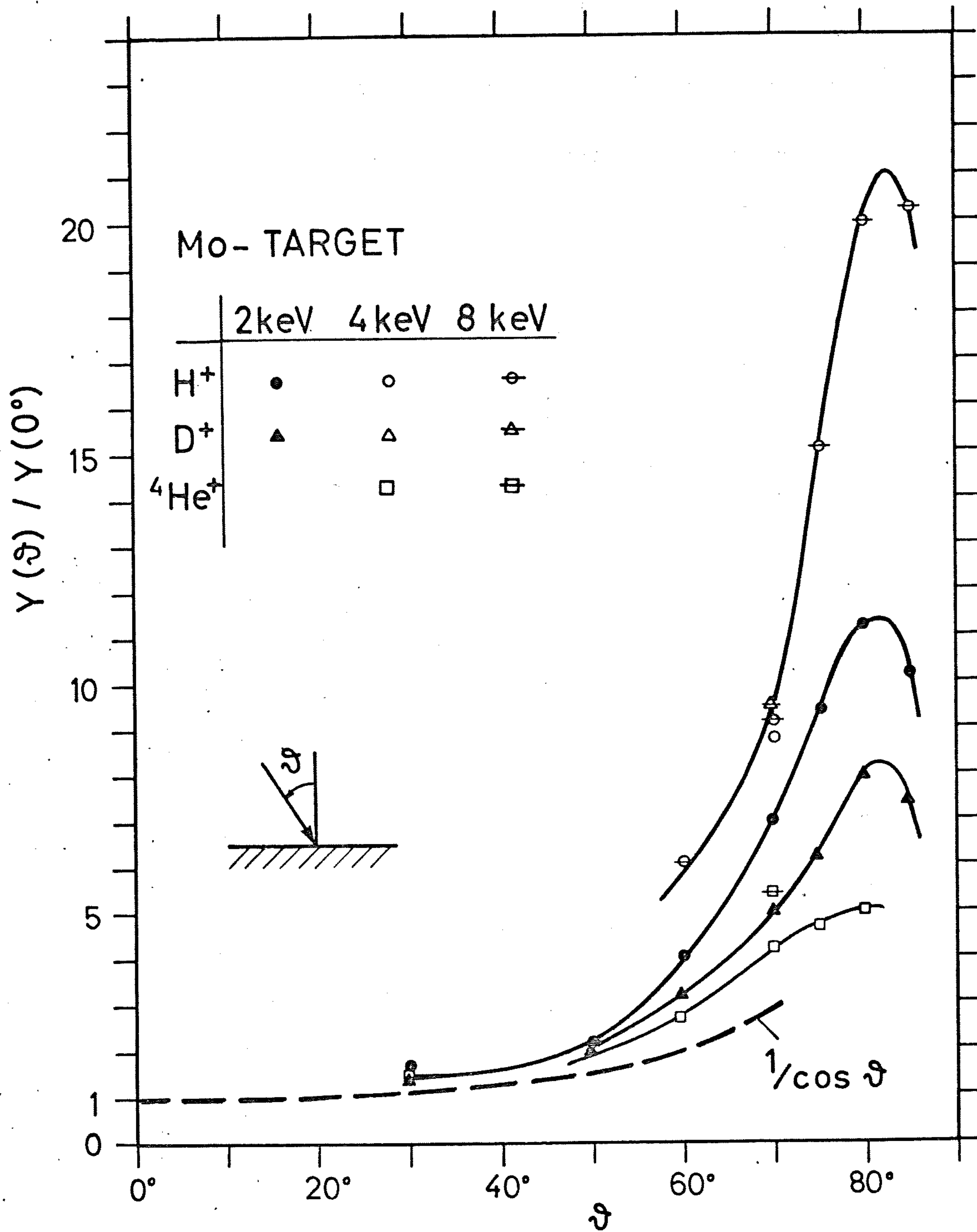

Fig. 29: Sputtering yield for Mo with H, D and ^{4}He as function of the angle of incidence. The yields are normalized to the value at 0° incidence. The broken curve indicates a 1/cos-dependence.
The data will be published in /36/.

Table 31 Ni

	Yields							
	H			D			He	
angle of incidence	1	4	8	1	4	8	4	8
0°	$1.55\cdot10^{-2}$	$1.22\cdot10^{-2}$	$8.22\cdot10^{-3}$	$4.25\cdot10^{-2}$	$3\cdot10^{-2}$	$2.28\cdot10^{-2}$	$1.97\cdot10^{-1}$	$1.73\cdot10^{-1}$
15°	$1.93\cdot10^{-2}$	$1.50\cdot10^{-2}$						
20°	$2.23\cdot10^{-2}$	$1.7\cdot10^{-2}$					$2.33\cdot10^{-1}$	
30°	$2.39\cdot10^{-2}$	$2.0\cdot10^{-2}$					$2.96\cdot10^{-1}$	
40°	$3.17\cdot10^{-2}$	$2.96\cdot10^{-2}$					$3.07\cdot10^{-1}$	
40°		$2.71\cdot10^{-2}$						
45°	$3.27\cdot10^{-2}$	$2.87\cdot10^{-2}$		$8.55\cdot10^{-2}$			$3.48\cdot10^{-1}$	
60°	$4.56\cdot10^{-2}$	$4.71\cdot10^{-2}$		$1.16\cdot10^{-1}$			$4.52\cdot10^{-1}$	
60°	$5.2\cdot10^{-2}$	$4.58\cdot10^{-2}$					$3.62\cdot10^{-1}$	
70°	$6.79\cdot10^{-2}$	$6.89\cdot10^{-2}$	$4.56\cdot10^{-2}$	$1.66\cdot10^{-1}$	$1.67\cdot10^{-1}$	$1.38\cdot10^{-1}$	$5.08\cdot10^{-1}$	$5.39\cdot10^{-1}$
70°	$7.58\cdot10^{-2}$	$8.57\cdot10^{-2}$					$6.41\cdot10^{-1}$	
75°	$8.25\cdot10^{-2}$	$9.29\cdot10^{-2}$		$1.96\cdot10^{-1}$			$8.11\cdot10^{-1}$	
80°	$1.01\cdot10^{-1}$	$1.25\cdot10^{-1}$	$8.77\cdot10^{-2}$	$2.76\cdot10^{-1}$				
80°	$9.7\cdot10^{-2}$	$1.43\cdot10^{-1}$					$8.22\cdot10^{-1}$	
80°	$1.03\cdot10^{-1}$							
85°	$6.35\cdot10^{-2}$	$1.43\cdot10^{-1}$		$1.58\cdot10^{-1}$			$7.69\cdot10^{-1}$	

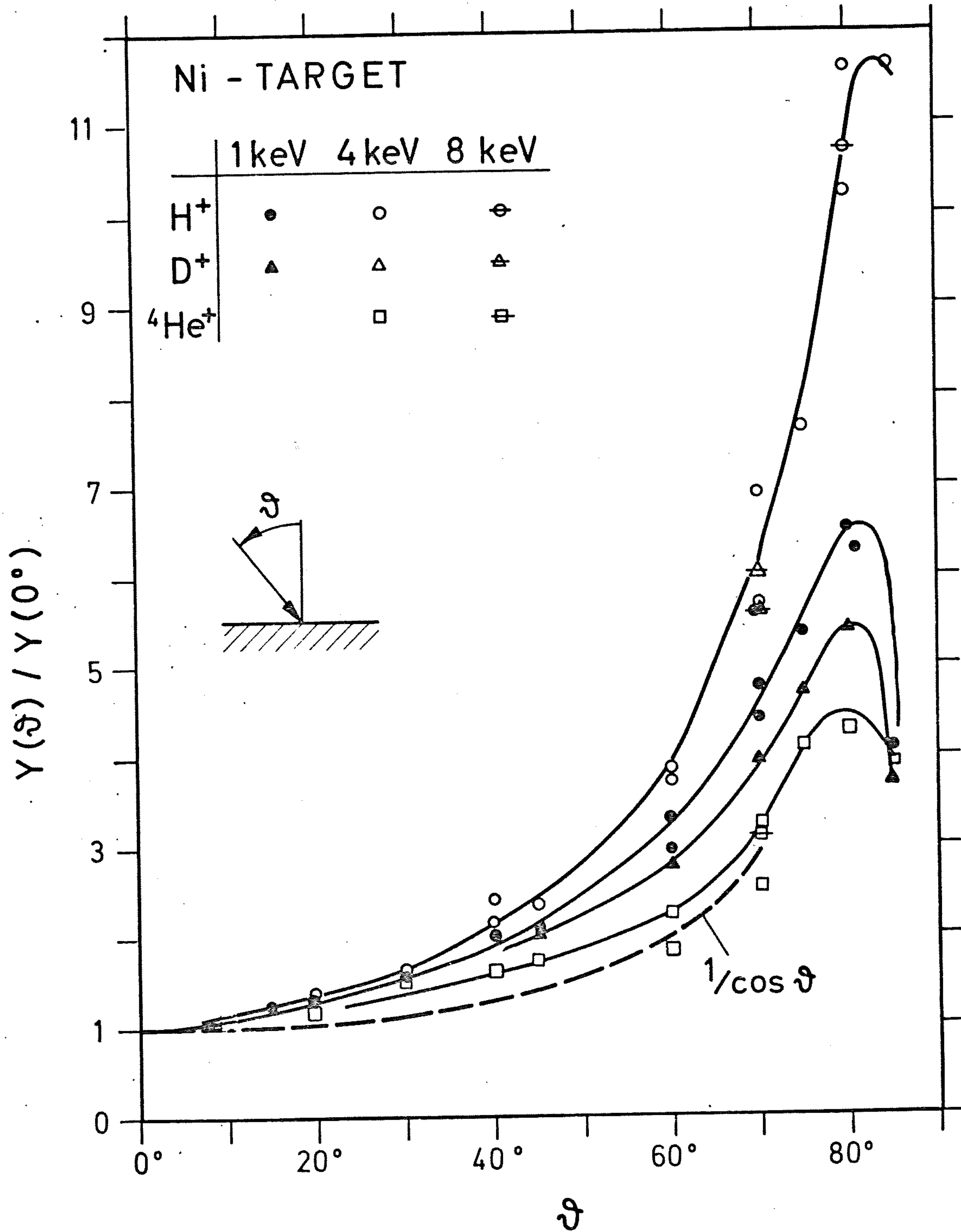

Fig. 30: Sputtering yield for Ni with H, D and ^{4}He as function of the angle of incidence. The yields are normalised to the value at 0° incidence. The broken curve indicates a 1/cos-dependence.
The data will be published in /36/ and /32 /.

Table 32 W

Yields

Angle of incidence	4 keV H
0°	$2.09 \cdot 10^{-3}$
60°	$9.61 \cdot 10^{-3}$
80°	$3.26 \cdot 10^{-2}$

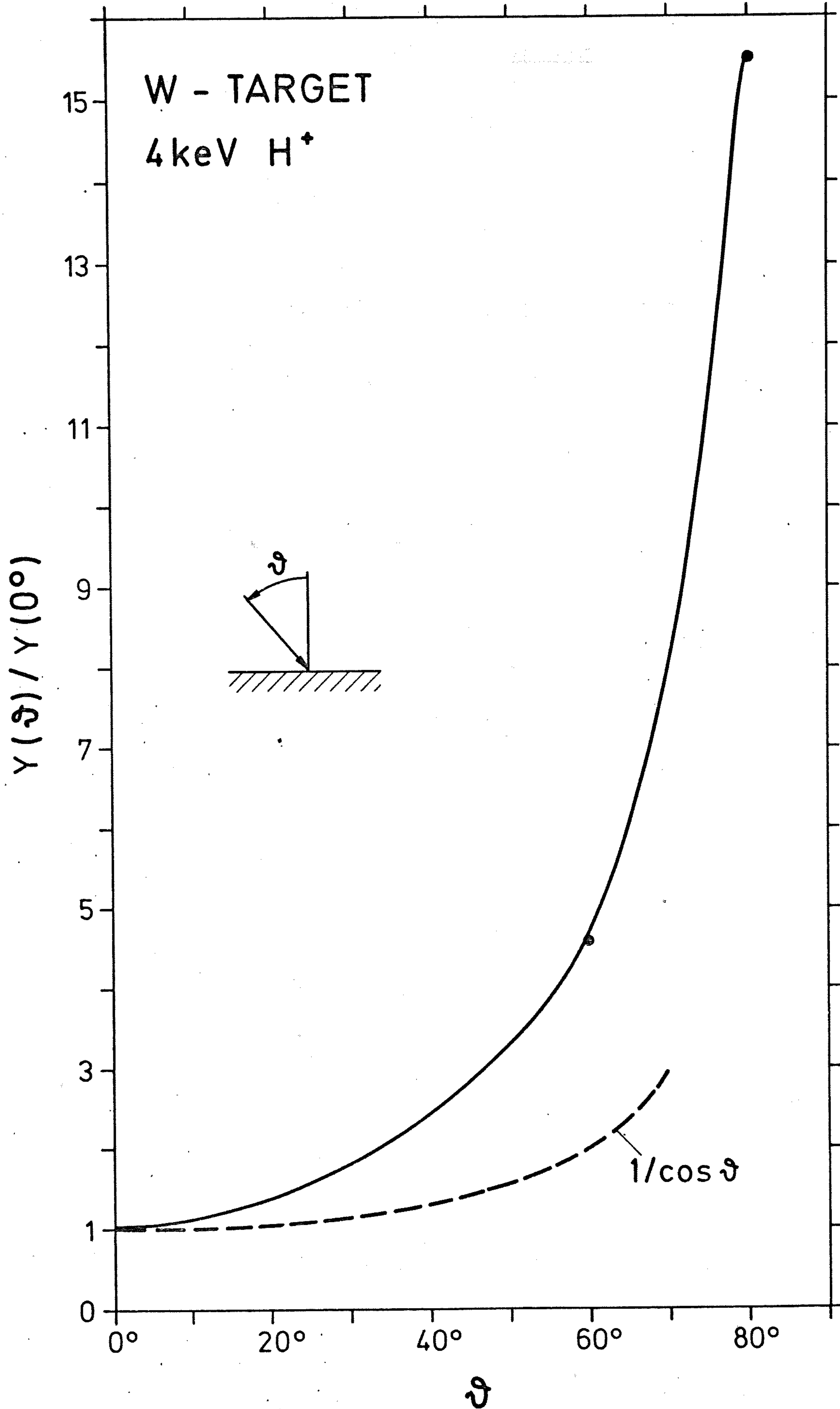

Fig. 31: Sputtering yield of W for 4 keV H for different angles of incidence. The yields are normalized to the value of 0° incidence. The broken curve indicates a 1/cos-dependence.
The data will be published in /32/.

Table 33 TaC

Yields

Angle of incidence	4 keV H
0°	$3.19 \cdot 10^{-3}$
60°	$7.14 \cdot 10^{-3}$
80°	$2.04 \cdot 10^{-2}$

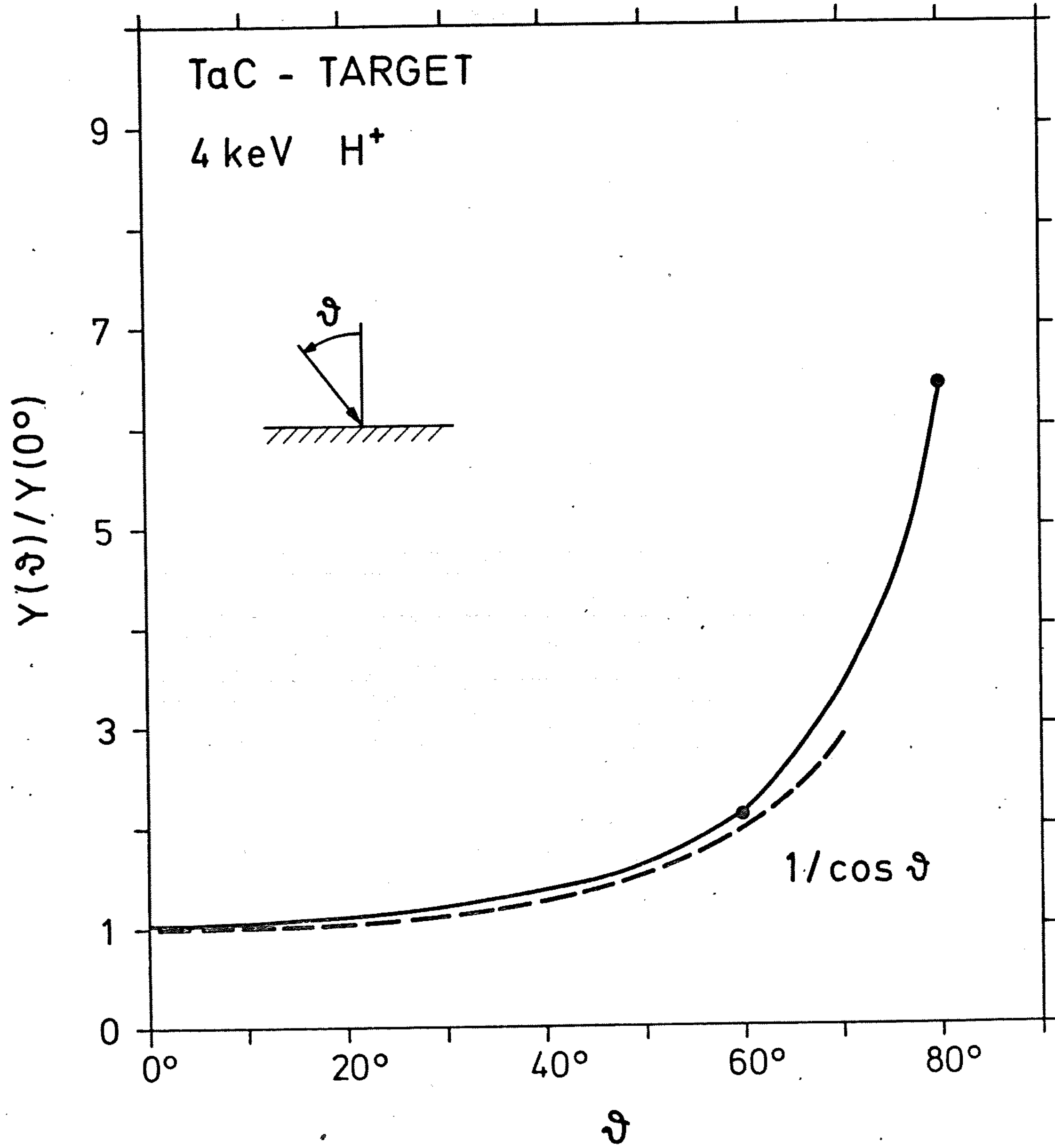

Fig. 32: Sputtering yield of TaC with 4 keV H for different angles of incidence. The yields are normalized to the value at 0° incidence. The broken curve indicates a 1/cos-dependence.
The data are unpublished /33/.

3.) Angular distribution of sputtered particles

For Ni, W, and TaC angular distributions of the sputtered particles have been measured. Ni, W and Ta have been analyzed by Rutherford backscattering on the collector. For the analysis of C the $^{12}C(d,p)^{13}C$ reaction has been used. Due to a carbon contamination of the collector foils the data for C show larger scattering and have to be considered as preliminary.
Table 34 shows the ion-target combinations, the energies and angles of incidence.

Table 34 Angular distribution of sputtered particles.

	H												He			ions
	1						4						4			keV
	0	20	40	60	70	80	0	20	40	60	70	80	0	40	60	80°
Ni	x	x	x	x	x	x	x	x	x	x	x	x	x	x	x	x
W							x		x			x				
TaC							x		x			x				

The results are presented in Figs. 33 - 39.

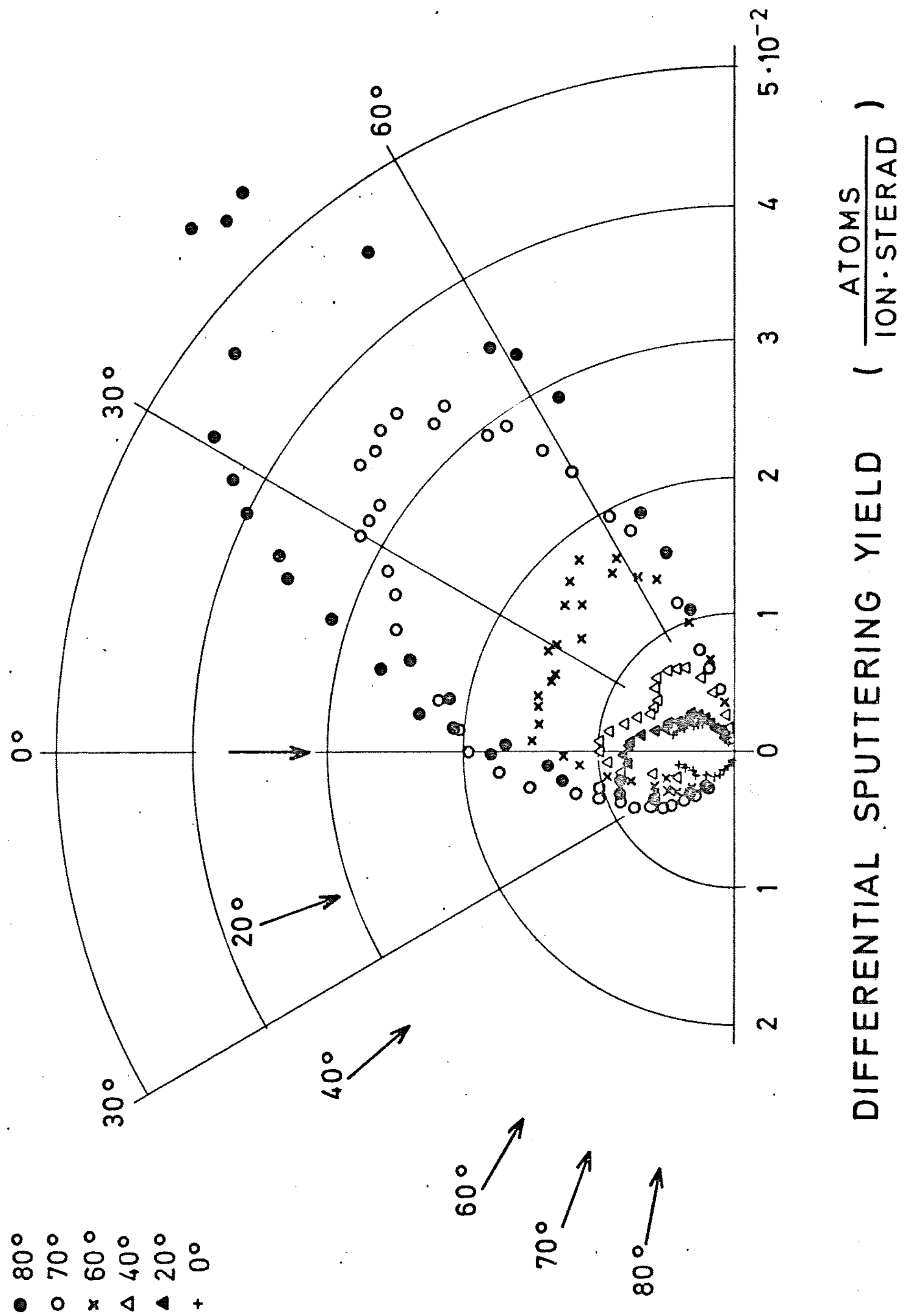

Fig. 33: Angular distribution of sputtered Ni atoms for 3 keV H_3^+ and different angles of incidence. The data have been calibrated with the weight loss method for normal incidence assuming rotational symmetry around the target normal. The results will be published in /32/.

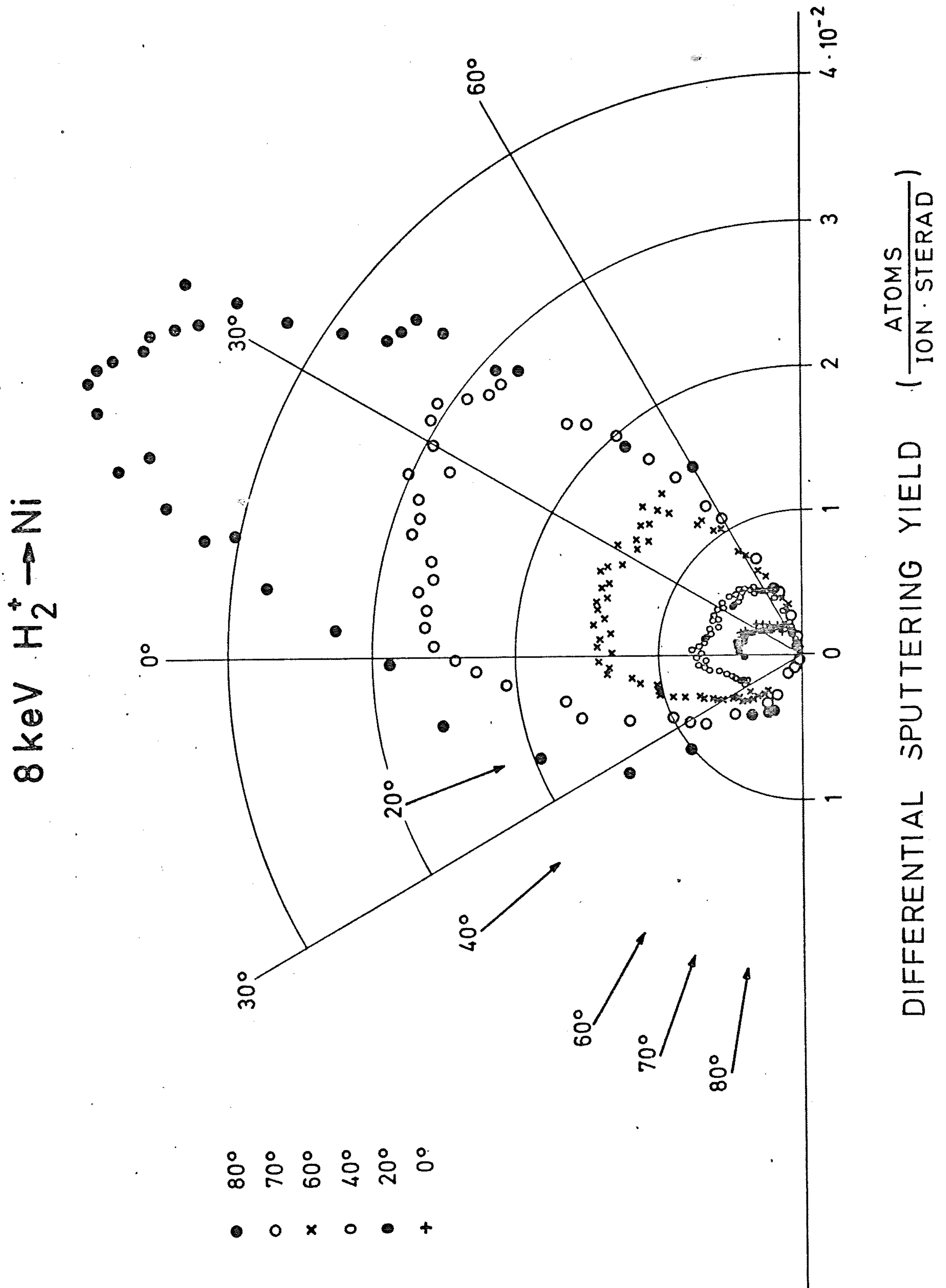

Fig. 34: Angular distribution of sputtered Ni atoms for 8 keV H_2^+ and different angles of incidence. The data have been calibrated with the weight loss method for normal incidence assuming rotational symmetry around the target normal.

The results will be published in /32/.

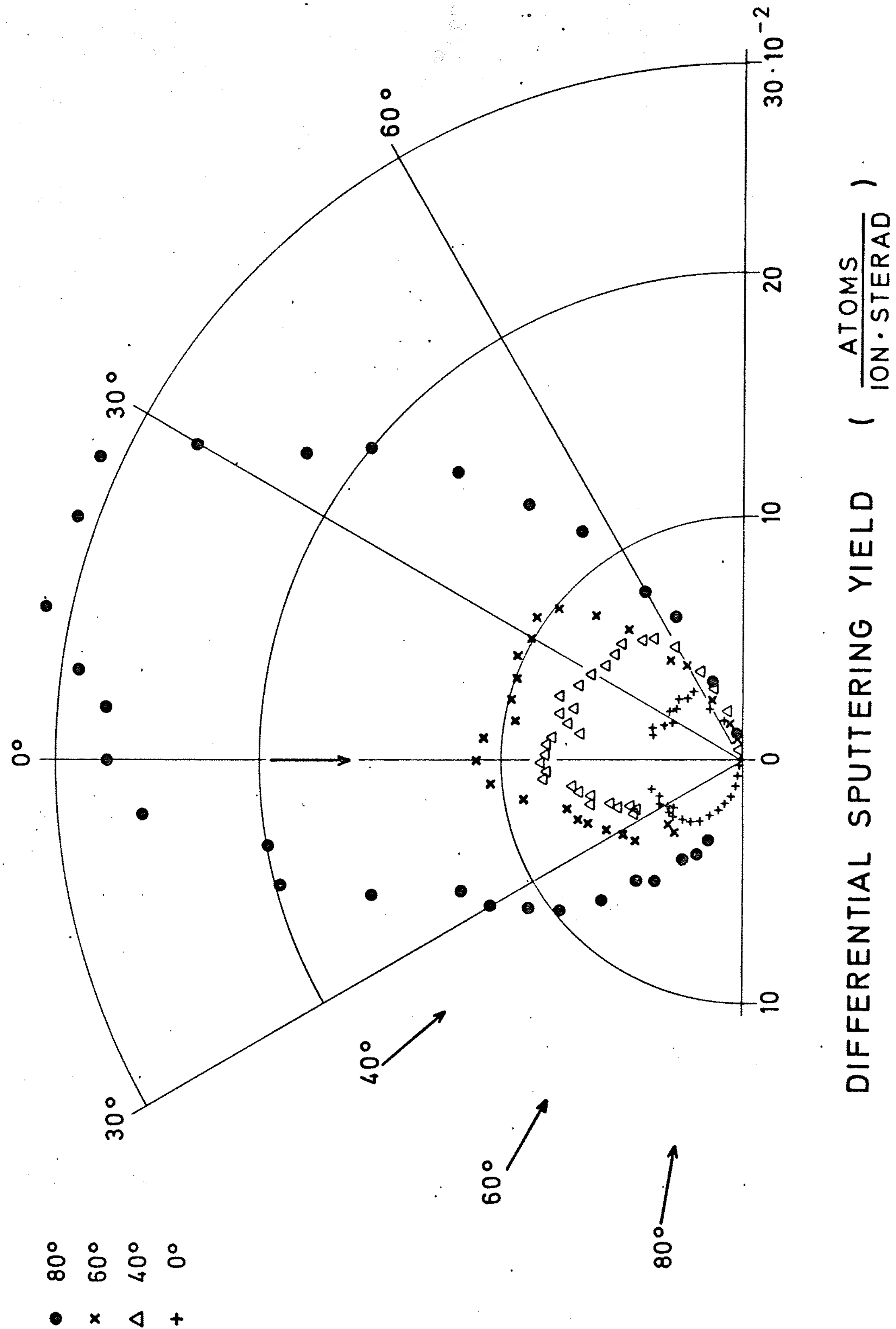

Fig. 35: Angular distribution of sputtered Ni atoms for 4 keV He^+ and different angles of incidence. The data have been calibrated with the weight loss method for normal incidence assuming rotational symmetry around the target normal.

The results will be published in /32/.

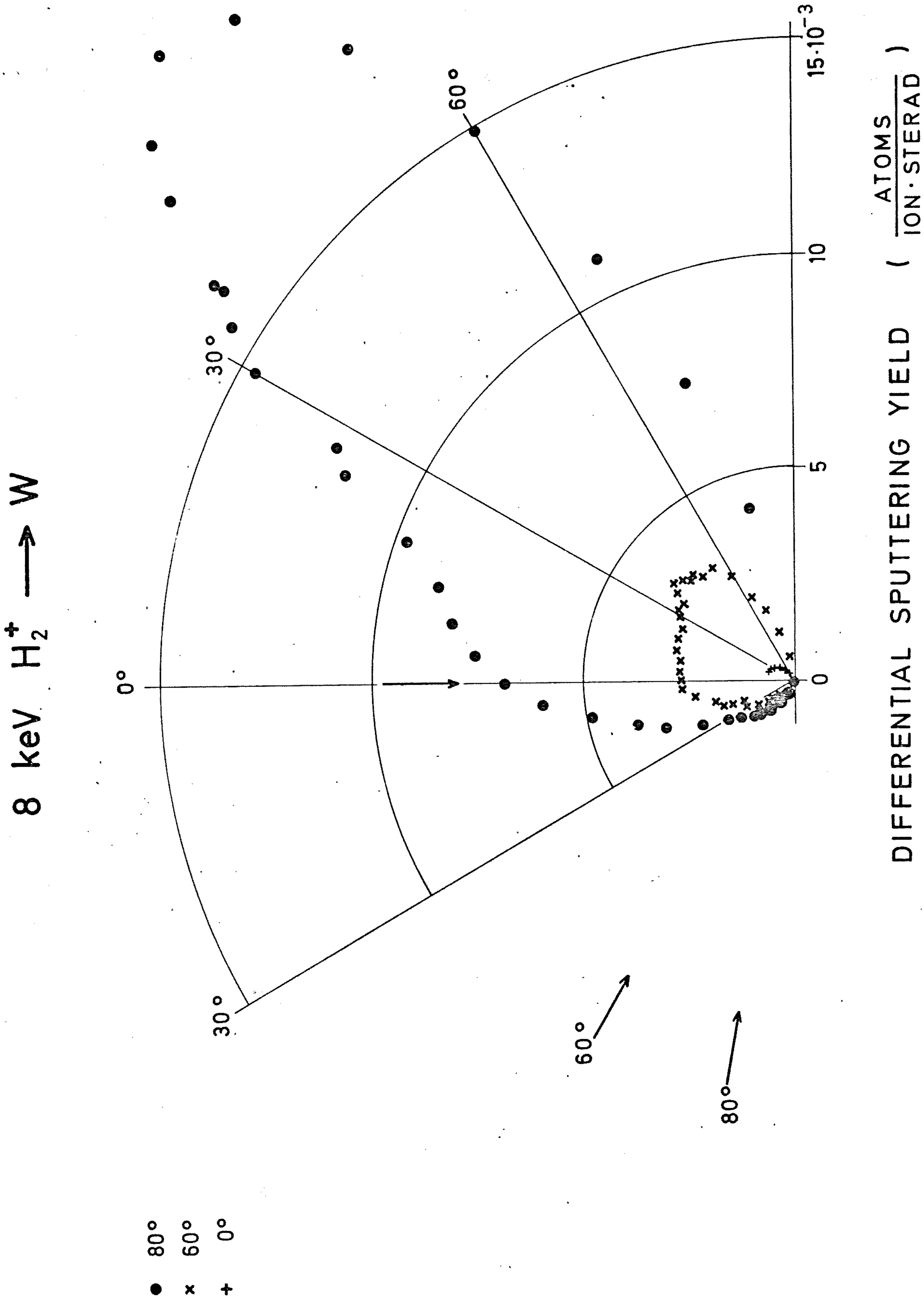

Fig. 36: Angular distribution of sputtered W atoms for 8 keV H_2^+ and different angles of incidence. The data have been calibrated with the weight loss method for normal incidence assuming rotational symmetry around the target normal. The results will be published in /32/.

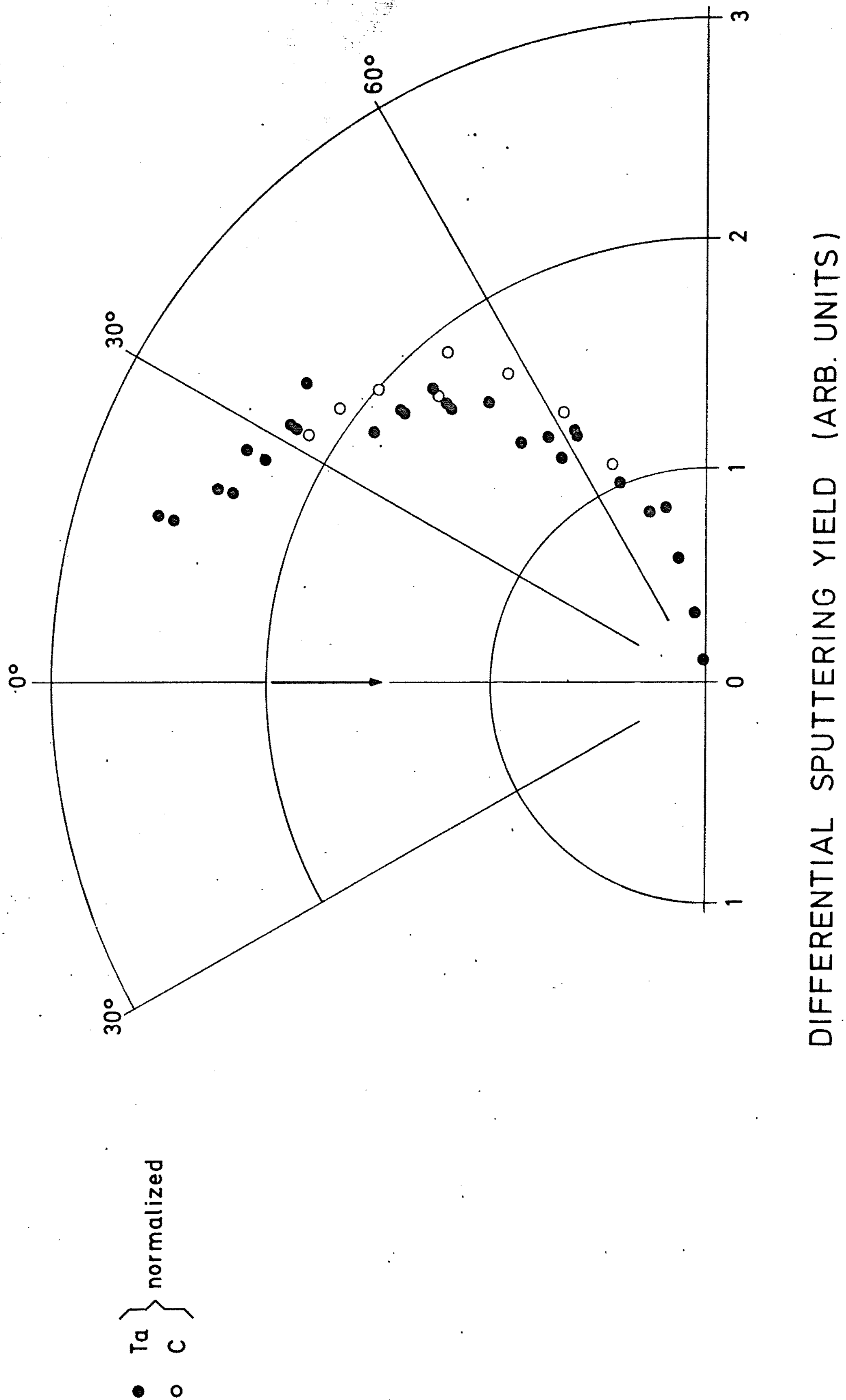

Fig. 37: Angular distribution of sputtered Ta and C atoms from TaC for 8 keV H_2^+ at 0° incidence. The data are normalized. The atoms have been collected on an Al-foil and analyzed with 1.2 MeV D^+ using RBS in the case of Ta and the $^{12}C(d,p)^{13}C$ nuclear reaction. The scatter in the C data is mostly due to the carbon background in the Al foil. The data and the method will be published in /33/.

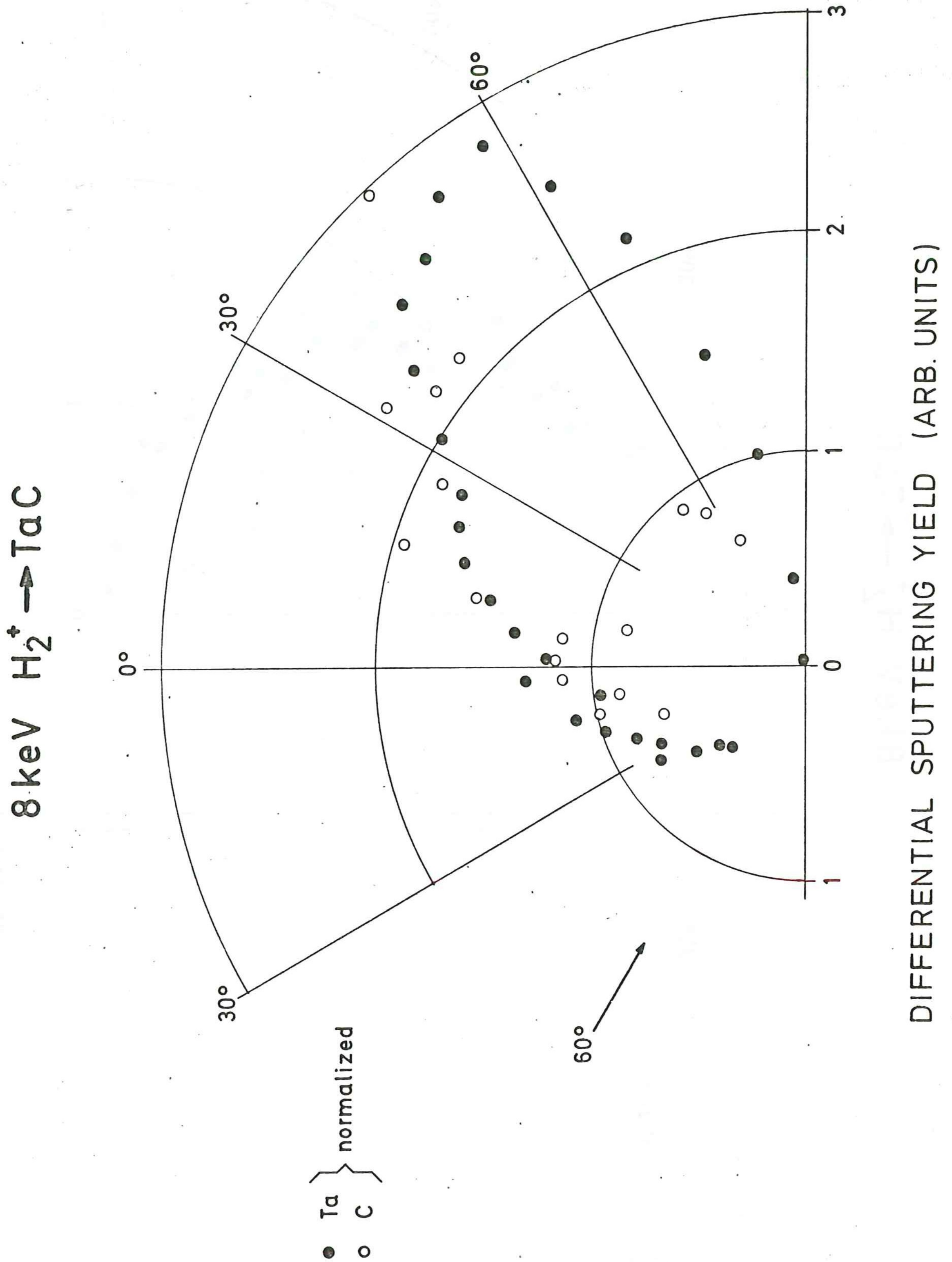

Fig. 38: Angular distribution of sputtered Ta and C atoms from TaC for 8 keV H_2^+ at 60° incidence. The data are normalized. The atoms have been collected on an Al-foil and analyzed with 1.2 MeV D^+ using RBS in the case of Ta and the $^{12}C(d,p)^{13}C$ nuclear reaction. The scatter in the C data is mostly due to the carbon background in the Al foil.
The data and the method will be published in /33/.

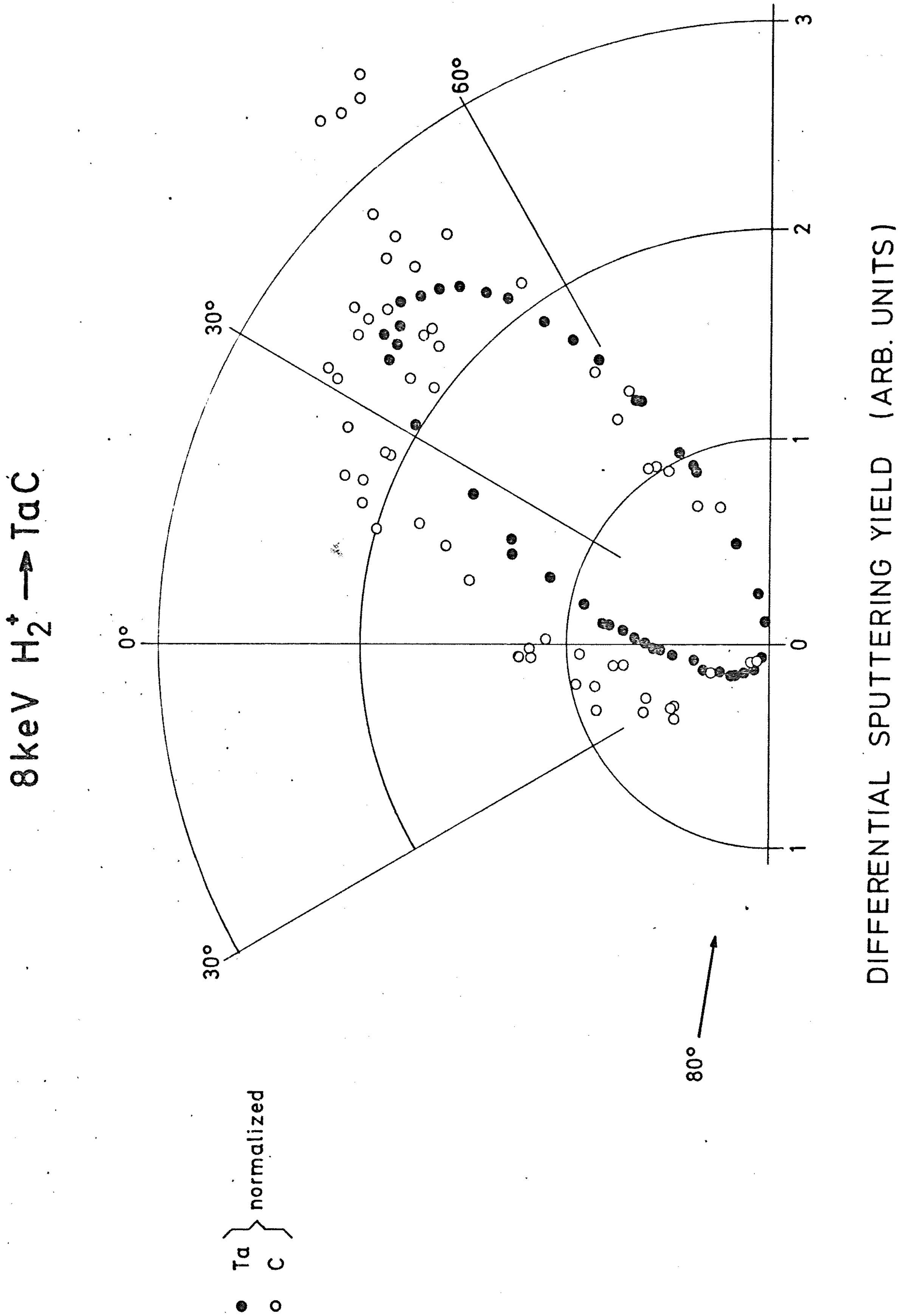

Fig. 39: Angular distribution of sputtered Ta and C atoms from TaC for 8 keV H_2^+ at incidence. The data are normalized. The atoms have been collected on an Al-foil and analyzed with 1.2 MeV D^+ using RBS in the case of Ta and the $^{12}C(d,p)^{13}C$ nuclear reaction. The scatter in the C data is mostly due to the carbon background in the Al foil. The data and the method will bepublished in /33/.

Discussion

In this report, which should mainly give the data obtained during four years of measurement on light ion sputtering, only a short derivation of an universal formula for sputtering will be given. More detailed discussion of the data will be found in the literature on the energy dependence of sputtering near the threshold energy /3, 35/ and on the mechanism of sputtering at grazing angles of incidence /32, 36/.

It has been found /3, 35/ that the energy dependence of the sputtering yield with light ions for normal incidence can be written as

$$Y = Q(M_1, M_2, E_B)\ f(E') \tag{3}$$

The energy dependence of the sputtering yield is contained in the function $f(E')$ with $E' = \frac{E}{E_{th}}$. The fitting factor Q is independent of energy and depends only on the atomic masses of the target and projectile and on the surface binding energy E_B.

Using the two fitting parameters Q and E_{th}, all yield data can be plotted on one single curve (fig. 40). The agreement of over 250 data point is striking and as a good approximation for E' up to 20 the function

$$f(E') = 8.5 \cdot 10^{-3}\ E'^{1/4}\ (1 - \frac{1}{E'})^{7/2} \tag{4}$$

can be used.

The fitting factors also show single analytic behaviour. In fig. 41 E_{th}/E_B is plotted against the mass ratio M_1/M_2 Up to a mean ratio of 0.4, E_{th} can be expressed as

$$E_{th} = \frac{E_B}{\gamma\ (1-\gamma\ )} \tag{5}$$

with

$$\gamma = \frac{4\ M_1 M_2}{(M_1+M_2)^2}.$$

This formula has been proposed for the threshold energy for sputtering for light ions and low energies /35, 37/. More detailed calculation by Harrison /41/ for the threshold energy using a binary collision model are also introduced in fig. 41 and show again that the fitting factor E_{th} can indeed be understood as the threshold energy for sputtering. The rather low values for C indicate, that E_B taken from

tables for the sublimation energy /38/ is too high. A lower binding energy seems to be reasonable as the ion bombardment destroys the crystalline structure and creates an amorphous surface layer /39/. Table 34 gives the values for E_{th} for the elements.

The factor Q/M_2 is plotted in fig. 42 against γ . It can be seen, that a fair approximation to Q can be made by the formula

$$Q = 0{,}75\ M_2\ \gamma^{5/3} \qquad (6)$$

Combining (3), (4) and (6) we get an universal function for the sputtering yield of light ions at low energies.

$$Y = 6.4 \cdot 10^{-3}\ M_2 \gamma^{5/3}\ E'^{1/4}\ (1 - \frac{1}{E'})^{7/2} \qquad (7)$$

This formula together with the simple expression for the threshold energy (5) should describe the sputtering yield for mass ratio $M_1/M_2 \leq 0.4$ and $1 < E' < 20$ within a factor of 2.

A more detailed discussion of the sputtering yield at normal incidence will be given in /35/.

To determine the wall erosion due to sputtering in fusion reactor devices, where the bombarding particles impinge with an energy distribution rather than monoenergetically, eq. (7) can be integrated for the energy distribution. Using a Maxwellian velocity distribution for the velocity component perpendicular to the wall, eq. (7) has been integrated and is plotted in fig. 43 (insert in back cover). It can be seen that the sputtering yield is increased to low energies and no threshold occurs. Using fig. 43, all given curves can be transferred to the sputtering yield curves for particles with Maxwellian energy distributions. The derivation of the sputtering yield curve for Maxwellian particle energy distribution is described in detail in /42/.

From the data for oblique incidence it may be seen that, generally, the normalized yield at the maximum $Y(\vartheta_{max})/Y(0^o)$ is increasing with increasing surface binding energy of the target material /38/ and is the higher the lighter the primary ion. Furthermore, a series of measurements at $\Theta = 70^o$ indicates that $Y(\vartheta_{max})/Y(0^o)$ is increasing with increasing ion energy in the energy region investigated, except for nickel between 4 keV and 8 keV, where a constant level seems to be reached.

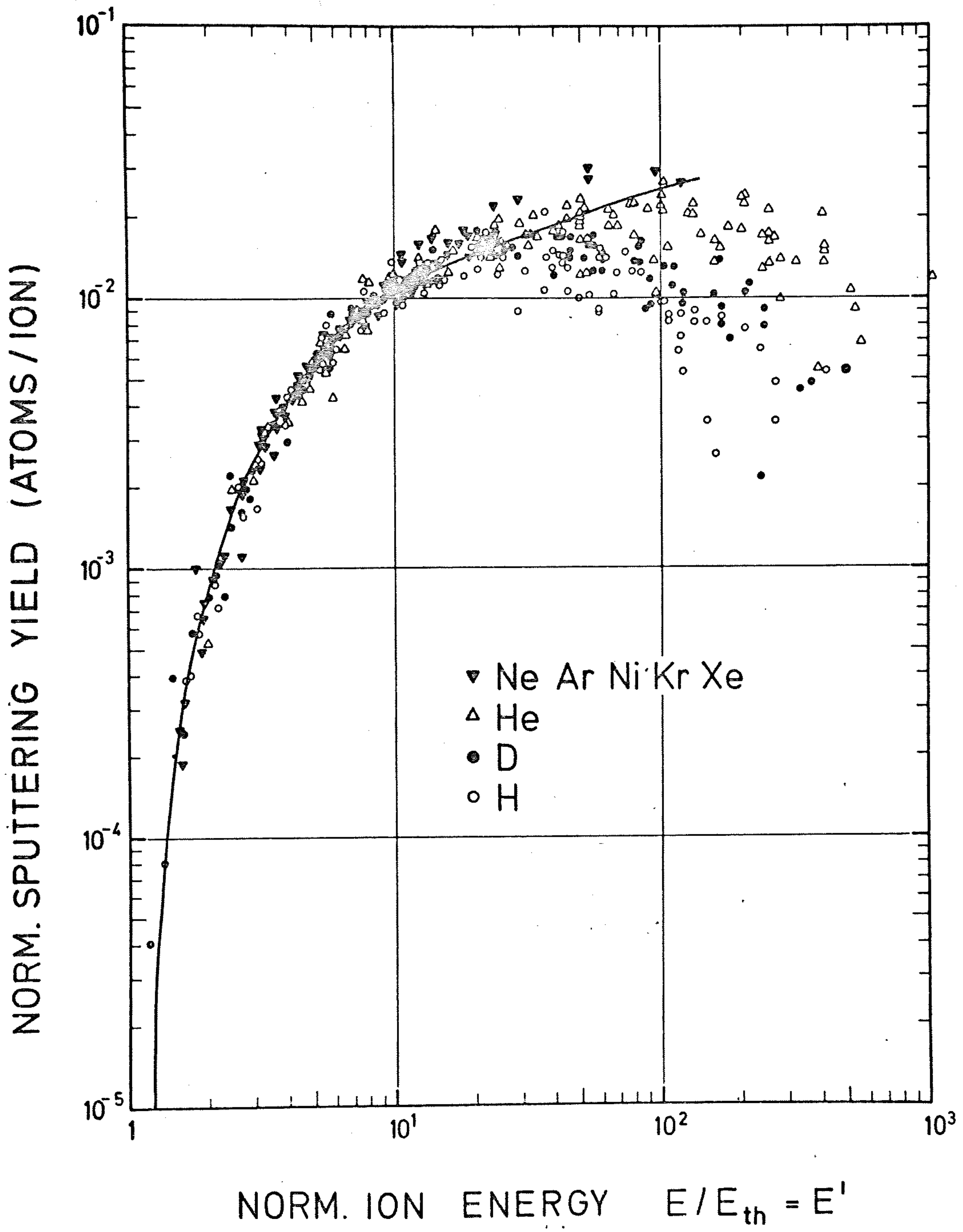

Fig. 40: Universal plot for the normalized sputtering yield. The curve gives the empirical formula for energy dependence of the sputtering yield (eq. 4).

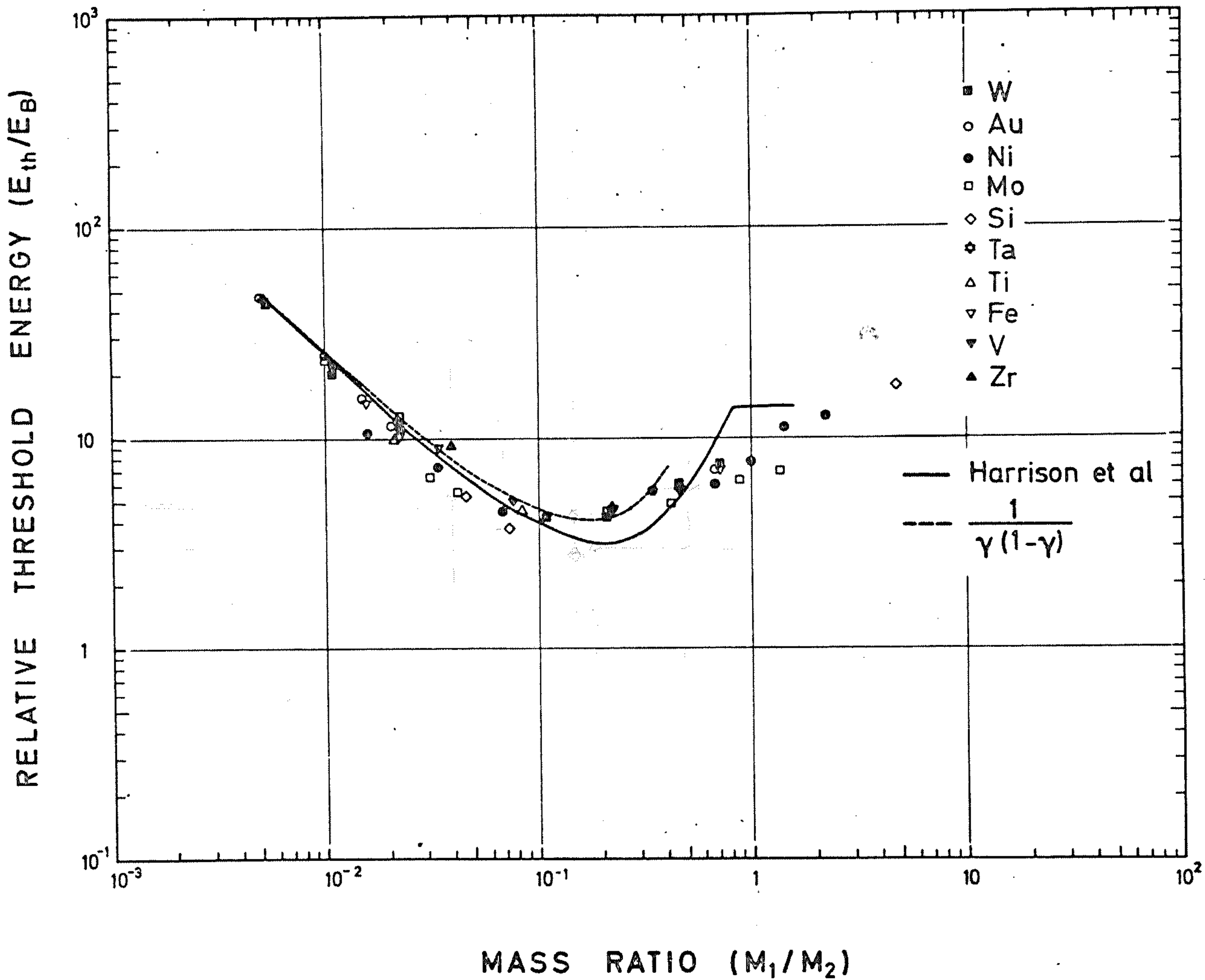

Fig. 41: Dependence of the relative threshold energy E_{th}/E_b for different elements on the mean ratio M_1/M_2. The curves give theoretical estimate for the threshold energy.

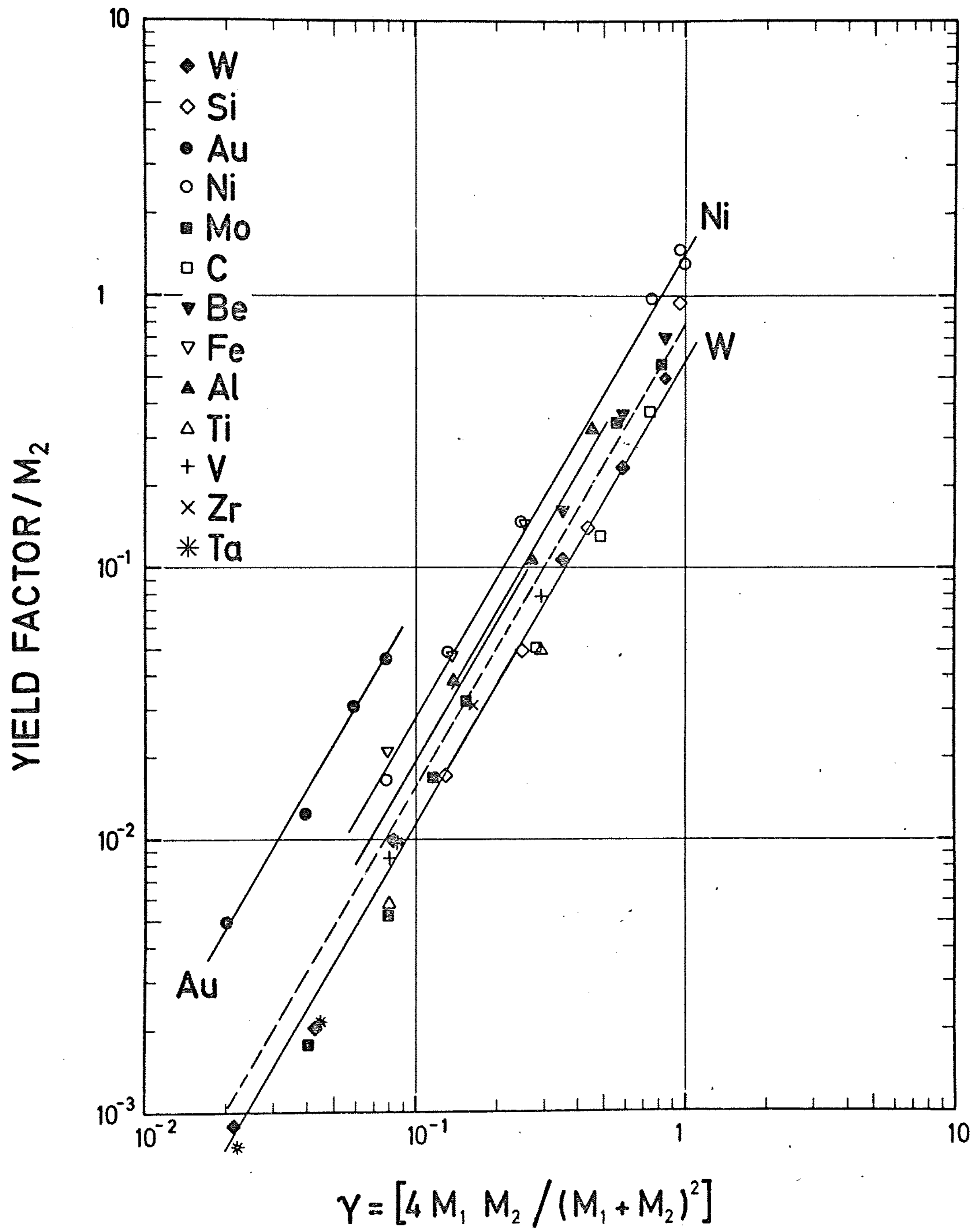

Fig. 42: Dependence of the yield factor Q/M_2 on γ for different elements. The dashed line gives the eq. (6).

TABLE 34 Threshold energy in eV

Target \ Ion	H	D	He^3	He^4
Al	53	34		20.5
Au	184	94	60	44
Be	27.5	24		33
C	9.9	11		16
Fe	64	40		35
Mo	164	86	45	39
Ni	47	32.5		20
Si	24.5	17.5		14
Ta	460	235		100
Ti	43.5			22
V	76			27
W	400	175		100
Zr				60

According to the Sigmund theory of heavy-ion sputtering /40/ the dependence of the sputtering yield on angle of incidence is given by $1/\cos^f \vartheta$ up to about the maximum in the yield (i.e. $\vartheta \sim 60^o$) and with $1 < f < 2$. It has been shown, however, that the Sigmund theory cannot be extrapolated to low-energy, light-ion sputtering, the theoretical yields being from one to several orders of magnitude too high for energies of < 10 keV /3/. In an atomistic model of sputtering the sputtering yield has been split into two components /36/

$$Y(E, \vartheta) = Y_I(E, \vartheta) + Y_{II}(E, \vartheta) \tag{8}$$

where Y_I and Y_{II} are the sputtering yields from two different sputtering mechanisms I and II (Fig. 44). Mechanism I is the sputtering caused by the interaction of the incoming ion with the target atoms at the surface. Mechanism II is sputtering initiated by primary ions which are reflected in the interior of the target, and which on their way out again suffer a heavy collision near the surface, causing ejection of a surface atom. In a simple model assuming binary collisions it can be shown that a stronger enhancement over a $1/\cos\vartheta$ -dependence of the sputtering yield for higher surface binding energies occurs in agreement with the experimental finding. For a detailed derivation it is referred here to ref. /36/.

The large increase in sputtering yield over the $1/\cos\vartheta$ dependence at grazing angles of incidence is due to sputtering events in direct collisions as shown in mechanism I. From binary collision calculation it can easily be shown, that for the emitted particles only angles of θ within a well defined cone are possible. The transferred energy in a binary collision must be larger than the surface binding energy. Assuming a planar surface potential minimum and maximum angles of ejection can be calculated. The exact value of the maximum angle of emergence might additionally be restricted by surface scattering of the ejected particles. The large enhancement of the sputtering yield measured at grazing angles of incidence due to mechanism I must therefore be observed in an anisotropic cone in forward direction, whereas the isotropic part due to mechanism II should remain unchanged. This expected behaviour is well reproduced in the actual data (Fig. 33-39). A more detailed examination of the distribution will be given in ref. /32/.

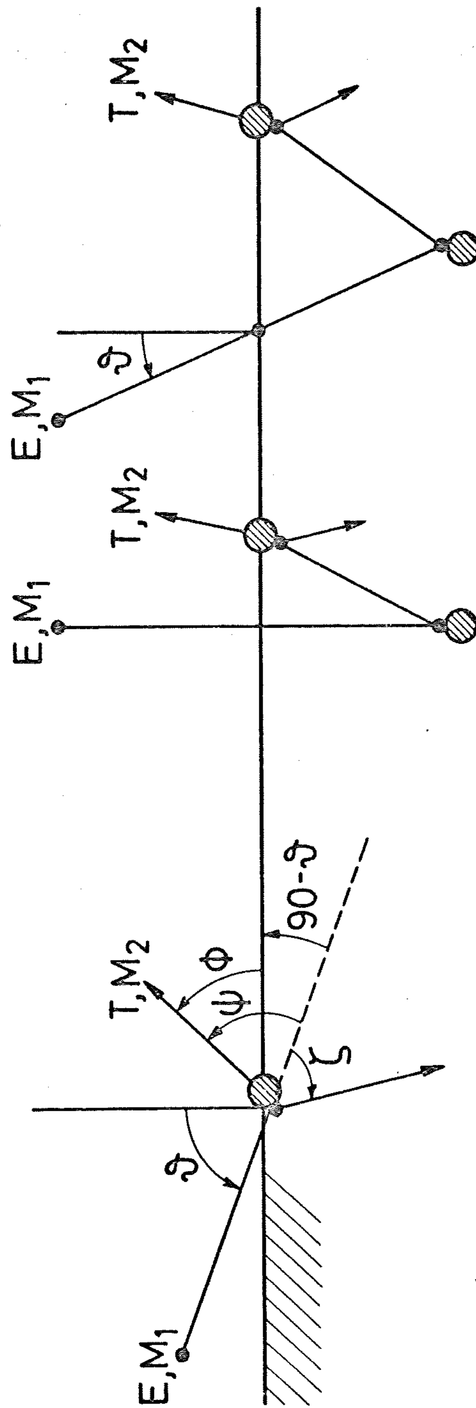

Fig.43

Conclusion

The data on sputtering of materials with light ions gathered in the years 1974 to 1978 are presented. The choice of materials has been made in most cases by their relevance in fusion technology. As new materials will become interesting, further erosion data will be needed. In the near future especially low-Z coatings will be examined.

For normal incidence the data show a strong similarity for all materials. Most important is the threshold energy for sputtering, which can be estimated by simple arguments (eq. (5)). For the energy dependence of the sputtering yield between E_{th} and 20 x E_{th} an empirical formula can be given (eq. (7)).

The model for sputtering near the threshold energy with light ions includes the reflection of the primary particle and subsequent sputtering of a surface atom. For oblique angle of incidence an additional mechanism becomes possible. The projectile ions can directly knock out a target atom (see fig. 42, mech. I). This mechanism is demonstrated for grazing angle of incidence ϑ as a strong increase of the sputtering yield over the $1/\cos\vartheta$ dependence especially at high surface binding energies as well as in a very anisotropic distribution of sputtered particles in a narrow cone at forward direction.

REFERENCES

/1/ R. Behrisch, J. Bohdansky, G.H. Oetjen, J.Roth, G. Schilling, H. Verbeek, J. Nucl. Mat. 60, 321 (1976).

/2/ G.Schilling, Kerntechnik 16, 309 (1974)

/3/ H.L. Bay, J. Roth, J. Bohdansky, J. Appl.Phys. 48, 4722 (1977).

/4/ G. Staudenmaier, J.Roth, R. Behrisch, J. Bohdansky, Ph.Staib, S.K. Erents, accepted for publication in J. Nucl. Mat.

/5/ M.K. Sinha, J. Roth, J. Bohdansky, Proc. 9th Symp. Fus. Technol., Garmisch, p. 41 (1976).

/6/ E. Hechtl, H.L. Bay, J. Bohdansky, Appl.Phys. 16, 147 (1978)

/7/ B.M.U. Scherzer, R. Behrisch, R.S. Blewer, H. Schmidl and TFR-group, Proc. 10th Symp. Fus. Technol. Padova, Italy (1978).

/8/ R.Behrisch, R.S. Blewer, H. Kukral, B.M.U. Scherzer, H. Schmidl, Ph. Staib, G. Staudenmaier and Groupe de TFR, J.Nucl. Mat. 76 & 77, 437 (1978).

/9/ R.Behrisch, Vak.Technik 10, 250 (1967)

/10/ E. Hechtl, Nucl. Instr.Meth. 139, 79 (1976).

/11/ Institut Dr. Klingele, München, Adelgundenstr. 8

/12/ J. Bohdansky, J. Roth, J. Brossa, First Topical Meeting on Fusion Reactor Material, Miami, Jan. 1979. To be published in J.Nucl. Mat.

/13/ J. Bohdansky, J. Roth, W. Ottenberger, R.S. Blewer, J. Borders, see /12/.

/14/ J. Roth, J. Bohdansky, W.Poschenrieder, M.K. Sinha, J.Nucl. Mat. 63, 222 (1976).

/15/ J. Roth, J. Bohdansky, P.A. Martinelli, Proc. Int. Conf. on Ion Beam Modification of Materials, Budapest, Sept. 1969.

/16/ J. Bohdansky, H.L. Bay, J. Roth, Proc.7th Int. Vacuum Congress and 3rd Int. Conf. on Solid Surfaces, Vienna, p. 1509 (1977).

/17/ H.L. Bay, J. Bohdansky, E. Hechtl, to be published.

/18/ E. Hechtl, H.L. Bay, J. Bohdansky, Rad. Effects 41, 77 (1979).

/19/ J. Roth, "Sputtering by ion bombardment", R.Behrisch (ed.), to be published in Topics of Applied Physics., Springer-Verlag, Heidelberg.

/20/ J. Bohdansky, J. Roth, M.K. Sinha, W. Ottenberger, J.Nucl.Mat. 63, 115 (1976).

/21/ H.L. Bay, W. Hofer, J. Bohdansky, unpublished.

/22/ C.H. Kenknight, G.K. Wehner, J. Appl.Phys. 35, 322 (1964)

/23/ J. Rosenberg, G.K. Wehner, J. Appl.Phys. 33, 1842 (1962).

/24/ E. Hechtl, J. Roth, J. Bohdansky, unpublished data.

/25/ J. Bohdansky, J. Roth,W.P. Poschenrieder, Inst. Phys.Conf. Ser. 28, 307 (1976).

/26/ J. Roth, J. Bohdansky, unpublished.

/27/ J. Bohdansky, H.L. Bay, W. Ottenberger, J. Nucl. Mat. 76 & 77 , 163 (1978)

/28/ J. Roth, J. Bohdansky, to be published.

/29/ J. Bohdansky, J. Roth, to be published.

/30/ H.v. Seefeld, R. Behrisch, B.M.U. Scherzer, Ph. Staib, H. Schmidl, Proc.7th Int. Conf. Atomic Coll. in Solids, Moscow (1977) to be published.

/31/ A.P. Martinelli, J.Roth, J. Bohdansky, unpublished.

/32/ H.L. Bay, J. Bohdansky, W.O. Hofer, J. Roth, to be published.

/33/ J. Roth, J. Bohdansky, unpublished.

/34/ B. Schweer, D. Rüsbuldt, P.A. Martinelli, J. Bohdansky, J. Roth, to be published.

/35/ J. Bohdansky, J. Roth, H.L. Bay, to be published.

/36/ H.L. Bay, J. Bohdansky, accepted for publication in Applied Physics.

/37/ R. Behrisch, G. Maderlechner, B.M.U. Scherzer, M.T. Robinson, submitted to Appl.Physics.

/38/ JANAF Thermo-Chemical Tables, ed. D.R. Stull, H. Prophet, NSRDS-NBS 37

/39/ R.B. Wright, R.Varma, D.M. Gruen, J.Nucl. Mat. 63, 415 (1976)

/40/ P. Sigmund, Phys. Rev. 184, 383 (1969).

/41/ D.E. Harrison, G.D. Magnuson, Phys.Rev. 122, 1421 (1961)

/42/ J. Bohdansky, J. Roth, H. Vernickel, Proc.10Th Symp.Fus. Technol. Padova, Italy (1978).

/43/ J. Borders, R.A. Langley, K.L. Wilson, J.Nucl. Mat 76 & 77, 168 (1978).